UTS UNIVERSITY OF TECHNOLOGY SYDNEY

Spiking Neural Network Framework for Brain Computer Interfaces

by Sai Kalyan Ranga Singanamalla

Thesis submitted in fulfilment of the requirements for the degree of

Doctor of Philosophy

under the supervision of Professor Chin-Teng Lin

University of Technology Sydney
Faculty of Engineering and Information Technology

September 2022

Certificate of Original Authorship

I, Sai Kalyan Ranga Singanamalla declare that this thesis, is submitted in fulfilment of the requirements for the award of Doctor of Philosophy, in the School of Computer Science, Faculty of Engineering and Information Technology at the University of Technology Sydney.

This thesis is wholly my own work unless otherwise referenced or acknowledged. In addition, I certify that all information sources and literature used are indicated in the thesis.

This document has not been submitted for qualifications at any other academic institution.

This research is supported by the Australian Government Research Training Program.

Signature: Production Note:
Signature removed prior to publication.

Date: 06/09/2022

ABSTRACT

Spiking Neural Network Framework for Brain Computer Interfaces

by

Sai Kalyan Ranga Singanamalla

In the field of Brain-computer interfaces (BCI), the majority of studies often rely on electroencephalography (EEG) over invasive methods despite the influence of noise and insufficient spatial resolution due to EEG's simplicity for practical usage. However, with EEG being an accumulation of spiking neural activity, reverse engineering it to a spiking version could establish new directions in improving BCI systems, which is the focus of this thesis. Spiking neural network (SNN) communicates via spikes and is a suitable model to study the spiking aspect of EEG-based BCI systems.

Electroencephalography recordings are often time consuming, and artifacts cause further rejection of these recorded samples. To overcome this, a few studies have developed generative models based on deep neural network (DNN) to create artificial EEG samples, but these models still require a huge number of samples which is counter-intuitive. Therefore, in this study, an SNN-based method was developed that can reconstruct EEG and generate synthetic samples with few original samples. These synthetic samples improved the motor imagery (MI) performance. To further explore the utility of SNN, it was trained to learn the template of an EEG signal and in turn obtain an approximated spike representation of the EEG samples. This significantly enhanced the classification performance in comparison to the baseline EEG-based performance of P300 and error-related negativity (ERN). The efficacy of the SNN depended on the neuron properties to an extent, and leveraging the heterogeneity of the properties could provide a better spike representation of the EEG. For ease of computation, the majority of past studies relied on a simplified spiking

neuron model that could only produce tonic spiking. Therefore, we introduced a new spiking model termed the burst spiking neural unit (BSNU) that could produce both tonic spiking and bursting signals. The BSNU model was initially validated on different machine learning benchmark tests to assess the efficacy of bursting and then the model was explored towards its ability for spike-representation. The BSNU-based SNN model outperformed SNU on the benchmark tests and has also been shown to further improve spike representation of EEG signals. This resulted in further enhancing the classification performance of P300 and MI datasets. In summary, this thesis is a consolidation of the SNN's role in improving different aspects of BCI paradigms, from data augmentation, and feature extraction to classification performance.

Dissertation directed by Professor Chin-Teng Lin
Australian Artificial Intelligence Institute (AAII)
School of Computer Science
University of Technology Sydney

To my family and friends

Acknowledgments

I would like to sincerely thank my supervisors Prof. Chin-Teng Lin and Dr. Yu-Kai Wang for their continuous academic and moral support during my PhD journey at the University of Technology Sydney. It was a great pleasure working alongside my supervisors and learning from them. Their guidance and critical thinking enabled me to become a better researcher. I would also like to thank my colleagues at Computational Intelligence and Brain-Computer Interface Lab for their help in overcoming the challenges of PhD life.

I would like to thank the Australian Research Council (ARC) for its financial support. In addition, I want to extend my gratitude to the Research Training via Program (RTP) scheme from the Department of Education and Training for funding my stipend.

Finally, I would like to express my gratitude to my mother Jayalakshmi, and my father Jagannatham for their love and immense support on all fronts of life.

Sai Kalyan Ranga Singanamalla

Sydney, Australia, 2022.

List of Publications

Journal

J-1. **Singanamalla, S.K.R.** and Lin, C.T., 2021. "Spiking Neural Network for Augmenting Electroencephalographic Data for Brain Computer Interfaces." *Frontiers in neuroscience*, 15, p.248.

J-2. **Singanamalla, S.K.R.** and Lin, C.T., 2022. "Spike-representation of EEG Signals for Performance Enhancement of Brain-Computer Interfaces." *Frontiers in neuroscience*.

J-3. **Singanamalla, S.K.R.**, Akella, A., and Lin, C.T., 2022. "Burst Spiking Neural Unit." (under review)

Conference

C-1. **Singanamalla, S.K.R.** ,A kella, A.,and Lin, C.T., 2021. "Optimal Stimulation of Spiking Neuron using Reinforcement Learning: Single Neuron Study". *30th Annual Computational Neuroscience Meeting: CNS*2021*, P101.

C-2. Akella, A., **Singanamalla, S.K.R.** and Lin, C.T., 2021. "A reinforcement learning approach to model evidence accumulation of decision making". *30th Annual Computational Neuroscience Meeting: CNS*2021*, P102.

C-3. Akella, A., **Singanamalla, S.K.R.** and Lin, C.T., 2021, May. "Reward based Hebbian Learning in Direct Feedback Alignment (Student Abstract)". *In Proceedings of the AAAI Conference on Artificial Intelligence*, (Vol. 35, No. 18, pp. 15749-15750).

Contents

Certificate i

Abstract ii

Dedication iv

Acknowledgments v

List of Publications vi

List of Figures xi

List of Tables xv

Abbreviation xvii

1 Introduction 1

1.1 Brain Computer Interface 1

1.1.1 Types of BCI Paradigms 2

1.1.2 Limitation of EEG-based BCI Systems 3

1.1.3 Invasive Methods for BCI 4

1.2 Spiking Neural Network 5

1.2.1 SNN for EEG Modelling 9

1.3 Research Problems 10

1.3.1 EEG Data Augmentation using SNN 11

1.3.2 Spike-based Representation of EEG Signal 12

1.3.3 Burst Spiking Neural Unit 13

1.4 Thesis Organization 13

2 Methodology **16**

2.1 Spiking Neuron Model . . . 16

2.1.1 The LIF Model . . . 17

2.2 Spike Filtering . . . 18

2.3 Surrogate Gradient Descent . . . 19

2.4 Classification Algorithms . . . 20

2.4.1 Linear Discriminant Analysis . . . 21

2.4.2 Support Vector Machines . . . 22

2.4.3 Naive Bayes Classifier . . . 23

2.4.4 K-Nearest Neighbours . . . 23

2.4.5 Gradient boosting . . . 24

3 EEG Data Augmentation using SNN **26**

3.1 Abstract . . . 26

3.2 Background . . . 27

3.3 Methods . . . 31

3.3.1 EEG Datasets . . . 33

3.3.2 Classification . . . 34

3.3.3 Generative Adversarial Networks (GAN) . . . 35

3.3.4 Variational Autoencoder . . . 37

3.4 Results . . . 38

3.4.1 The SNN for MI . . . 38

3.4.2 The SNN for SSVEP . . . 41

3.4.3 Synthetic EEG Signal Validation . . . 43

3.4.4 Classification . . . 45

3.4.5 Comparing SNN and GAN . . . 46
3.5 Discussion . . . 48

4 Spike-based EEG Representation 54

4.1 Abstract . . . 54
4.2 Background . . . 54
4.3 Methods . . . 58
4.3.1 SNN Architecture . . . 58
4.3.2 EEG Processing . . . 59
4.3.3 Classification . . . 60
4.3.4 Explainability . . . 60
4.3.5 Contrastive learning . . . 60
4.4 Results . . . 61
4.4.1 SNN Training . . . 61
4.4.2 Classification . . . 64
4.4.3 Confusion Matrix . . . 67
4.4.4 Explainability . . . 70
4.4.5 Node Prioritisation . . . 72
4.4.6 Contrastive Learning . . . 73
4.5 Discussion . . . 73

5 Burst Spiking Neural Unit 80

5.1 Abstract . . . 80
5.2 Background . . . 80
5.3 Methods . . . 82
5.3.1 Spiking Neural Unit model . . . 82

5.3.2 BSNU Model 83
5.4 Results 85
5.4.1 BSNU Validation 85
5.4.2 EEG Classification 88
5.5 Discussion 91

6 Conclusion **93**

List of Figures

1.1 A flow chart of commonly followed steps in a standard BCI application from Mudgal et al. (2020). 2

1.2 A spiking neuron computing with both input signal and output signal as spike trains. 7

1.3 An SNN communicating via spikes. 9

1.4 A flowchart describing the overview of the proposed BCI protocol. . . 11

1.5 An overview of the research map of this thesis. 15

2.1 Surrogate derivatives of different function adapted from Neftci et al. (2019). SuperSpike and SLAYER use fast sigmoid and exponential functions. 20

3.1 Depiction of a three-layered feedforward spiking network mapping a random spike train to an EEG signal with additional neural perturbation layer of Poisson neurons distorting the information of Spike Output layer. 32

3.2 Overview of the steps involved in generating synthetic EEG samples using the SNN. 33

3.3 An overview of Generative Adversarial Network structure. 36

3.4 Encoder-decoder style architecture of Variational autoencoder. 38

3.5 The SNN for MI signal reconstruction showcasing the **(A)** template reconstruction, **(B)** randomly selected neuronal spike trains from the hidden layer, **(C)** power spectrum, and **(D)** mean square error loss. 40

3.6 The SNN for SSVEP signal reconstruction showcasing the **(A)** template reconstruction, **(B)** randomly selected neuronal spike trains from the hidden layer, **(C)** power spectrum, and **(D)** MSE loss. 42

3.7 Evaluating synthetic MI and SSVEP data generated from different combinations of the number of noise neurons and the firing frequency in the perturbation layer. 44

3.8 Pearson's correlation between the synthetic samples and the template signal. 45

3.9 **(A)** The reconstruction (orange line) of 12 Hz and 15 Hz SSVEP EEG signals using the QIF neuron model-based SNN based on original template signal (blue line). **(B)** The decrease in loss during the training period. 50

3.10 **(A)** The reconstruction (orange line) of 12 Hz and 15 Hz SSVEP EEG signals using the EIF neuron model-based SNN based on the original template signal (blue line). **(B)** The decrease in loss during the training period. 51

3.11 The robustness of the SNN model with random disconnection of synapses for MI reconstruction. 52

4.1 The RSNN model executing two stages: 1) the forward process in which the SNN generated template EEG signals and 2) the inverse process in which the non-template signals were transformed to spike representations for classification. 58

4.2 The SNN model training for P300 signal showcasing the **(A)** signal reconstruction, **(B)** spike trains of RSNN activity, and **(C)** MSE loss. 62

4.3 The SNN model training for the ERN signal showcasing the **(A)** signal reconstruction, **(B)** spike trains of RSNN activity, and **(C)** MSE loss. 63

4.4 Confusion matrix analysis of the **(A)** EEG signals and **(B)** spike representation of the ERN dataset. 69

4.5 Confusion matrix analysis of the **(A)** EEG signals and **(B)** spike representations of the P300 dataset. 69

4.6 The PCA-based variance explanation of the EEG signal (blue line) and its corresponding spike representation (red line) for the ERN dataset. 71

4.7 The PCA based variance explanation of the EEG signal (blue line) and its corresponding spike representation (red line) for the P300 dataset (S13). 71

4.8 The Pearson's correlation among all samples in the ERN dataset for both the EEG signal and its spike representation. 72

4.9 The Pearson's correlation among all samples in the P300 dataset for both the EEG signal and its spike representation. 72

5.1 The firing pattern of the SNU and BSNU model under constant input current. 84

5.2 The BSNU model flow diagram mimicking the structure by ref Woźniak et al. (2020). 84

5.3 Comparing the classification performance of the SNU and BSNU based SNN for image domain datasets. The top inset of each plot showcases a sample image, and the bottom image displays the average classification performance of multiple seeds. 87

5.4 Comparing the classification performance of the SNU and BSNU based SNN on an SHD audio dataset containing German digits. . . . 88

5.5 The Soli radar's gesture recognition performance with the SNU and BSNU based SNN. 89

5.6 The text domain analysis with a softer version of the BSNU model for (**A**) language translation and (**B**) sentiment analysis. 89

List of Tables

1.1 A brief overview on advantages and disadvantages of different neuro-imaging methods. 6

1.2 A brief comparison of ANN and SNN properties. 8

2.1 List of LIF spiking neuron and Adam optimiser properties. 19

3.1 Comparison of the classification performances with and without synthetic data for the MI datasets assessment using different classifiers. 47

3.2 Comparison of the MI artificial data performances obtained by the SNN and different generative models. 48

4.1 A brief list of recent P300 studies and their advised features and number of channels for classification. 57

4.2 Comparison of the classification performance of the P300 based EEG signals and their spike representations by the SNN using different classifiers. 65

4.3 Comparison of the classification performance of the ERN based EEG signals and their spike representations by the SNN using different classifiers. 67

4.4 Comparison of the classification performance of the ERN dataset via NVB for the transformed signal with random weight and LSM. . . 68

4.5 Comparison of the classification performance of the spike representation of the ERN datasets with xGboost under different prioritisation conditions. 74

4.6 Comparison of the classification performance of the spike representation of the P300 datasets with xGboost under different prioritisation conditions. 75

4.7 Comparison of classification performance of P300 dataset via xGboost for transformed signal with constrastive learning. 76

4.8 Comparison of classification performance of ERN dataset via NVB for transformed signal with constrastive learning. 77

4.9 Comparison of the classification performance of an MI EEG signal and its spike representation using MLP classifier. 78

5.1 List of SNU and BSNU model parameters. 85

5.2 The P300 classification performance comparison of the spike representations obtained by the SNU and BSNU based SNN with xGboost and a 5x10 fold CV. 90

5.3 Performance of the MI-EEG spike representations of the SNU and BSNU using the MLP and bagging classifier. For each dataset, a 5x10 fold CV was applied. 91

Abbreviation

EEG - Electroencephalography

BCI - Brain Computer Interface

ERN - Error Related Negativity

PCA - Principle Component Analysis

MI - Motor Imagery

CSP - Common Spatial Pattern

SSVEP - Steady State Visually Evoked Potential

LIF - Leaky Integrate and Fire

SNU - Spiking Neural Unit

SNN - Spiking Neural Network

BSNU - Burst Spiking Nueral Unit

SVM - Support Vector Machine

NVB - Naive Bayes

MLP - Multi Layer Perceptron

CV - Cross Validation

Chapter 1

Introduction

1.1 Brain Computer Interface

Human-computer interaction has substantially changed the way with which humans interact with digital and physical systems. A brain-Computer Interface (BCI) is one such technology that allows a user to communicate or interact with an external device or an application through their brain signals alone (Wolpaw et al. 2000). Various kinds of neuroimaging methods are used based on the requirements of different applications and are broadly divided into invasive and non-invasive methods. Electroencephalography (EEG), functional near-infrared spectroscopy (fNIRS), and functional magnetic resonance imaging (fMRI) are some of the most commonly used noninvasive neuroimaging techniques for BCI, whereas electrocorticography (ECoG) is categorized as invasive and requires a surgical process for electrode implantation (Degenhart et al. 2016). Of the different neuroimaging methods, EEG is the most adopted due to its high temporal resolution and portability for real-world applications. A majority of the BCI systems interacting with an external application or device, follows the following steps: (1) recording of brain activity, (2) signal preprocessing, (3) feature extraction, (4) command classification, and (5) feedback. An overview of this protocol as shown in the figure 1.1. Several research groups around the world have demonstrated the capabilities of BCI systems by designing and developing a plethora of applications such as brain-controlled gaming, robotic systems, and home automation (Khorshidtalab and Salami 2011). Over the last decade, BCI research has also made strides in the clinical sector. Cognitive enhancement (Thomas et al. 2013), neurofeedback training (Hwang et al. 2009), neuro-stimulation (Rothschild 2010), and prosthetics (Santhanam et al. 2006) are a few such applications.

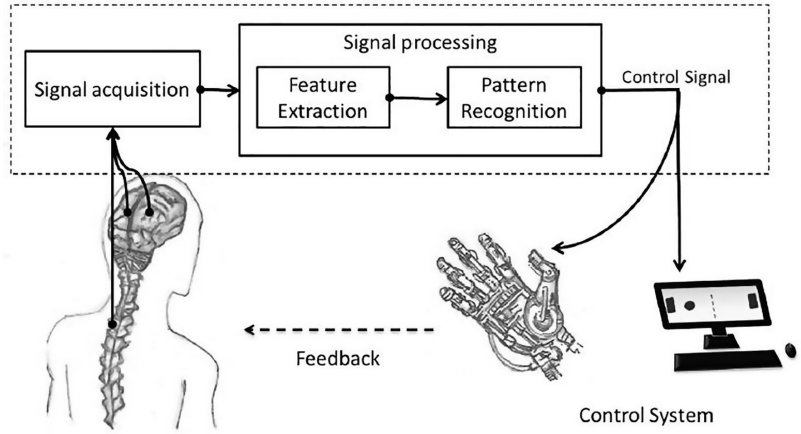

Figure 1.1 : A flow chart of commonly followed steps in a standard BCI application from Mudgal et al. (2020).

1.1.1 Types of BCI Paradigms

For a user to execute active brain-controlled action, the user performs certain tasks to elicit specific neural activity, which is later analysed for inference and command execution. These tasks often involve the paradigms motor imagery(MI) (Hwang et al. 2009; Aghaei et al. 2015), steady state visually evoked potential (SSVEP) (Müller et al. 2011), and event-related potential (ERP) (Yeom et al. 2014). Electrodes placed on the scalp surface according to 10–20 systems access the signal from different regions of the cortex spanning these paradigms. Motor imagery represents sensory-motor rhythms named event related synchronization (ERS) and event related de-synchronization (ERD) and are acquired from the central region over the motor cortex when the user is performing movement related imagined tasks such as left-hand & right-hand MI (Thomas et al. 2012). This kind of paradigm is commonly used in the situations that requires intuitive motion signal. For example, Reshmi and Amal (2013) developed a brain-controlled wheelchair with five classes, and Holm et al. (2019) designed a five class MI system for drone navigation. Steady state visually evoked potential is based on visual input in which the stimulus is a flickering object (such as a square block on a monitor or LED light) at a defined frequency and phase. This paradigm's relevant features are detected from electrodes placed over the visual cortex. Some prominent examples for this

paradigm include high-speed speller (Nakanishi et al. 2014), and exoskeleton control (Kwak et al. 2015). Event-related potential comprises a broad range of tasks such as P300 (Panicker et al. 2011), and error-related negativity (ERN) (Parra et al. 2003), whose biomarker is often analysed with the fluctuation of voltage in the EEG signal. This biomarker is observed from different brain regions depending on the kind of sensory input and the task of the user. P300 is indicated by the positive deflection (at approximately 300 ms of event onset) of the EEG signal in a situation such as oddball paradigm, where a user is attended to a target stimulus from a mix of non-target stimuli. Some popular use cases of P300 include speller (for character printing) and improving attention (Arvaneh et al. 2019). Error related negativity is depicted with a negative deflection in signal and occurs in response to an error and withholding of a response. This modality is commonly used in situations that require adaptive control mechanisms such as detecting unintended behaviour of a robot, and Go/No-Go inhibition tasks (Wang et al. 2020). Each of these paradigms offers different advantages and is used depending on the application requirements and physical abilities of the end user. Some studies have designed hybrid BCI systems, which are a combination of two or more BCI paradigms such as MI+SSVEP, and SSVEP+P300. These hybrid BCI systems provide a robust BCI performance and compensate for the drawbacks of each paradigm. For example, Ko et al. (2017) developed MI+SSVEP to enhance the performance of BCI system with a few EEG channels. Similarly, Bi et al. (2014) showcased a SSVEP+P300 based hybrid BCI system to control the speed and direction of the cursor.

1.1.2 Limitation of EEG-based BCI Systems

Despite the promising advantages of EEG-based BCI systems, the technology is still limited to laboratory settings due to several factors such as the non-stationary nature of an EEG signal, noise, artifacts, and insufficient information in the EEG signal. The signal acquires neural activity from the scalp surface and thereby fails to measure the activity of deeper regions. In addition, cognitive factors such as fatigue, attention, and drowsiness are prone to affecting BCI performance (Li et al. 2010). Also, studies have shown that a given task under new or complex environments

highly changes the brain dynamics in contrast to a given task under a standalone experimental constrained environment. Developments to improve EEG-based BCI performance have been targeted at specific stages of the control flow, ranging from better signal processing algorithms (Wierzgała et al. 2018), to novel feature extraction (Nakra and Duhan 2020), classification methods (Vishwakarma et al. 2020), real-time feedback (Saduanov et al. 2020), and adaptive measures (Guger et al. 2015). Clinical and indoor settings often resort to high density EEG systems, but outdoor real-world applications require the system to be lightweight with few channels. This further results in degraded performance with limited information and distortion of signal quality. Additionally, EEG data recording is a tedious process requiring equipment setup, and long duration of experiments, and the data can be contaminated by noise, leading to data rejection. In the case of invasive data recording, this data contamination is eliminated to an extent but requires the consumer to undergo a surgical process. At the basic level, EEG is the result of the accumulation of action potentials of spiking neurons, and reverse engineering EEG to its spike representation could open up new approaches towards BCI utility.

1.1.3 Invasive Methods for BCI

Apart from EEG, a non-invasive method, invasive neuroimaging methods are of interest in the BCI community. In invasive technologies, the electrodes are inserted directly into the cortex or placed on the direct brain surface. Due to this reason, the invasive recordings are less prone to noise and obtain better spatial and temporal resolution. Since electrode implantation requires the user to undergo the surgical process, they are less preferred by a common use due to the risk associated with it and also these methods raise the cost of using BCI systems. ECoG and Multi-electrode array (MEA) devices are well-known common invasive systems (Cinel et al. 2019). In ECoG, the electrodes are placed over the surface of the cortex and in MEA, the electrode needles penetrate the surface. These invasive devices through sense high-resolution data can cover only a small region of the brain and are thereby used for targeted applications in clinical settings. For example, sensorimotor activity detection using ECoG for movement in patients with Locked-

In-Syndrome(Freudenburg et al. 2019), finger movement decoding using ECoG in epileptic patients Jubien et al. (2019), brain-to-text i.e., writing characters using MEA by paralyzed patient (Willett et al. 2021), control of a cursor on a monitor using MEA by non-human primates (Lansdell et al. 2019), speller for amyotrophic lateral sclerosis (ALS) patients using MEA (Milekovic et al. 2018) etc. Some of these invasive recording studies besides developing BCI application in clinical settings also tried to investigate the neural dynamics to identify the neural dynamics involved in the functional difference of patient and control participants. Table 1.1 from Cinel et al. (2019) showcases a brief overview of the advantages and disadvantages of EEG and invasive methods.

1.2 Spiking Neural Network

Artificial neural network (ANN) have established dominance in the field of artificial intelligence (AI). These networks are termed the second generation of neural networks. An artificial neuron abstracts the dynamic nature of biological neurons and computes a non-linear function on the summation of inputs. The output of this neuron is often considered as the effective firing rate (Maass 1997) over time. Studies have shown that in addition to the firing rate, the spike timing of a neuron encodes information too. In other words, a spike (i.e. pulse or action potential), represented by an increase of the voltage of a neuron, is the basis of communication between two neurons connected via a synapse. This has led to the genesis of the spiking neuron as a computing unit in a network, defining a third-generation neural network called spiking neural network (SNN) (Maass 1997). Contrary to artificial neurons, a spiking neuron computes as a time-dependent dynamical system and is more biologically realistic in nature (as shown in figure 1.2). Information in an SNN is encoded through the firing patterns (or spike trains) of the neurons and inter-spike intervals, i.e. the time intervals between consecutive spikes (Gerstner et al. 2014). The spike trains are traversed across the population of neurons and result in the basis of an animals' behavior.

Traditionally, SNNs have been employed towards modelling complex behaviours,

Imaging method	**Invasive**	**Advantages**	**Disadvantages**
EEG	No	• Cheap • Portable • Good temporal resolution	• Low spatial resolution • Neural activity near scalp surface • Low signal-to-noise ratio
ECoG	Yes	• High signal-to-noise ratio • Good temporal resolution • Good spatial resolution	• Require surgery • Measure activity near brain surface • Expensive
MEA	Yes	• High signal-to-noise ratio • Good temporal resolution • Good spatial resolution	• Require surgery • Limited coverage of brain region • Risk of infection

Table 1.1 : A brief overview on advantages and disadvantages of different neuroimaging methods.

information processing in the brain, and clinical disorder causes. For example, Kim and Sejnowski (2021) showcased the importance of inhibitory signals for stable working memory using SNNs. Similarly, Nicola and Clopath (2019) used SNN advancements to show how memory replay and one-shot learning could be executed in the hippocampus. In clinical studies, SNNs are often used to understand the cause and effect of particular disorders at the neuron and metabolic levels. For example,

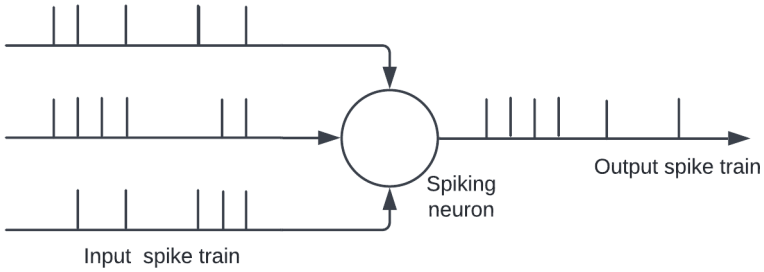

Figure 1.2 : A spiking neuron computing with both input signal and output signal as spike trains.

Muddapu et al. (2019) simulated the effects of energy deficiency due to glutamate in dopaminergic cells that lead to Parkinson's disease using SNNs and proposed stimulation strategies to overcome them.

In the last decade, deep neural networks (DNN) have achieved significant strides in AI and paved the way for models to achieve human-level performance. This has generated interest in incorporating SNN for AI applications. The immense achievements of DNNs suffer from computation costs and memory usage due to dense matrix operations, whereas SNNs impose biological realism. Their event-based communications have been shown to alleviate these issues and facilitate low-power consumption for on-chip neuromorphic computations, which often permit distributed and asynchronous processing (Diehl et al. 2015). A brief overview of the differences between ANN and SNN from computational perspective is shown in table 1.2 obtained from Xu et al. (2021). A wide range of spiking neuron models as computational units exist and the most commonly used models include leaky-integrate-and-fire (LIF) (Neftci et al. 2019), Izhikevich (Izhikevich 2003), and spike response model (SRM) (Jolivet et al. 2003). Each of these models encompasses advantages and disadvantages in terms of computational cost, biological realism, and the ability to produce different firing patterns. Some of the popular frameworks computational neuroscience groups commonly use to create architecture for SNNs include the Nest, Neuron, Nengo, and Brian framework (Jordan et al. 2019).

Spike events are discontinuous and therefore cannot use the standard gradient

	ANN	**SNN**
Generation	2nd generation NN	3rd generation NN
Biological brain mimicking	Abstraction	Better
Signal processing	Continuous multi-level value	Sparse and binary spike signals in time-domain. Event-driven information processing
Energy efficiency	General	Better
Neurons and Synapses	non-linear functions	LIF, Izhikevich, etc.
Training algorithms	Error-backpropagation	STDP, Surrogate-gradient, RLS etc.

Table 1.2 : A brief comparison of ANN and SNN properties.

descent back-propagation that the traditional ANNs use. Therefore, a few learning rules, such as Hebb's rule, Oja's rule, and spike time dependant plasticity (STDP) (Ferré et al. 2018), are commonly employed for simple learning tasks and modelling purposes. These rules are carried out based on the principle of long-term potentiation (LTP or an increase of synaptic weight) when a post-synaptic spike follows a pre-synaptic spike and long-term depression (LTD or a decrease of synaptic weight). Also, these rules do not account for errors like in ANN. This limits the applications plausible with SNNs. Some studies tried to introduce the error term to this plasticity rule resulting in a three-factor learning rule (Kuśmierz et al. 2017) but these methods enabled to customize error for synapses and as such still showcased lower performance. Indirect training approaches were developed to have efficient SNN. For example, ANNs were initially trained and were then converted to SNN for tasks like classification for event-based sensory input (Rueckauer et al. 2017). However, these approaches required fine-tuning of weights, architecture, and manual intervention. But, these converted networks are still behind conventional ANNs

in terms of classification performance. Recently, attempts have been made to adjust the backpropagation algorithm for SNNs, allowing them to train similar to ANN and achieved competitive performances (Lee et al. 2016). This also helped to take leverage of existing deep learning frameworks such as PyTorch, Tensorflow, and Keras (Vasilev et al. 2019) for fast prototyping and building complex models. This has also enabled SNNs to be compatible with different learning methodologies such as supervised, unsupervised, and reward-based learning. However, contradictory to DNNs, the spiking networks usually take input in the form of a spike train of a specific time window and outputs an encoded spike train, as shown in the figure 1.3.

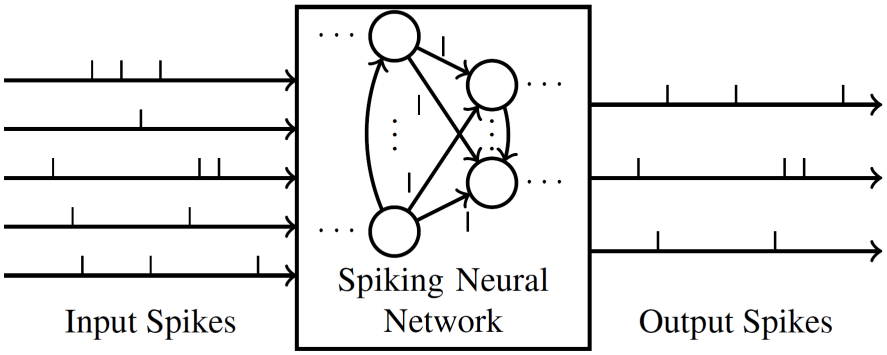

Figure 1.3 : An SNN communicating via spikes.

1.2.1 SNN for EEG Modelling

Regarding EEG-based studies, SNNs are primarily used for understanding the underlying cognitive process of a given task. A majority of these studies are implemented using NeuCube (Kasabov 2014; Tan et al. 2020), a three-dimensional SNN based tool designed for processing different spatio-temporal brain data. It has been widely used for EEG encoding and brain connectivity studies. For example, Doborjeh et al. (2019) encoded 62 channel EEG signal to study the effects of mindfulness training on brain connectivity changes from the EEG data of depressed and control participants. Similarly, Doborjeh et al. (2015) encoded EEG signals using SNNs to

study how the clusters of neurons interact in people with addiction. In conjunction with other signals such as electromyography (EMG) and Kinematic signals, SNNs have also been used in the functional structural organisation of neural activity in a grasp and list task (Kumarasinghe et al. 2020), which is useful for improving BCI utility. Leaving aside connectivity studies, NeuCube, an SNN based architecture, has been used for classification of EEG data for application such as emotion recognition (Alzhrani et al. 2021; Tan et al. 2021), sleep stage assessment (Budhraja et al. 2020), and depression (Shah et al. 2019).

From an AI point of view, SNNs have also been shown to classify classical MI-BCI paradigms with competent performance and can be structured in a multi-layer perceptron fashion similar to artificial feedforward neural network. Carino-Escobar et al. (2016) implemented particle swarm optimisation to train SNNs towards extracting channels and classify corresponding MI-EEG signals. Sossa et al. (2019) compared SNN-based classifier with different standard statistical machine learning classifiers for MI-EEG data and have shown that SNN resulted in better performance in most scenarios, e.g. the combination of different MI movements. In addition, a few previous studies implemented SNNs on neuromorphic hardware and validated them towards MI classification. Mashford et al. (2017) implemented a four-layer SNN for classifying two-channel MI-EEG signals on IBM TrueNorth neuromorphic chip. Similarly, Behrenbeck et al. (2019) implemented NeuCube style architecture on Spinnaker neuromorphic hardware to classify two class MI-EEG signals. These studies have shown the different ways in which SNN can be leveraged in a multitude of applications and analytical approaches towards EEG assessment.

1.3 Research Problems

The BCI systems have been following a generic protocols as shown in figure 1.1. Invasive methods recordings are better at signal quality than EEG but require surgical methods, making them undesirable to the common user. Therefore, in this thesis, we propose novel approaches that circumvent the standard EEG-based BCI protocols. In these approaches, the feature extraction happens on spiking

signal rather than on EEG signal. And, this spiking signal was obtained by reverse engineering the the EEG signals via SNN as shown in figure 1.4. To this end, different research problems have been formulated. And, each research problem addresses different issues of the BCI systems ranging from limited to feature extraction for better performance and further explore the impact of SNN model properties on the BCI performance.

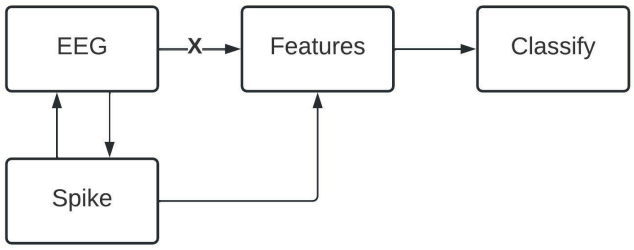

Figure 1.4 : A flowchart describing the overview of the proposed BCI protocol.

1.3.1 EEG Data Augmentation using SNN

Motivation

For practical application of a BCI system, EEG is the most commonly adopted neuroimaging method. As stated in Section 1.1.2, EEG data collection is time-consuming, and recorded data could have artifacts leading to data rejection. However, the recent trends in classification rely on deep learning models to obtain better performance (Altaheri et al. 2021), and these require large samples of data to obtain reliable classification outcomes. To this end, a few studies have produced techniques for data augmentation, i.e. to generate artificial samples for improving the classification performance (Zhang et al. 2022, 2019). However, the existing techniques pose unique problems, such as inconsistent signal generation or not being generalised enough for various kinds of paradigms (Lotte 2011; Dinarès-Ferran et al. 2018). Also, deep generative models require a huge number of samples to create synthetic samples, which are contrary in nature because data generation is usually required when there is no sufficient sample for better training. This calls for novel approaches that can generate artificial samples with a few available original samples.

Problem statement

This research question addresses the data augmentation issues by leveraging SNN to create synthetic MI signals with a few samples. In addition, the artificial data are validated and assessed to enhance the classification performance.

1.3.2 Spike-based Representation of EEG Signal

Motivation

It is well known that invasive signals such as ECoG are often cleaner and more informative than non-invasive EEG signals, but the surgical process requirement is impractical for a common user. As such, many studies have focused on improving EEG-based systems primarily with signal processing techniques or novel classification methods. If an EEG signal can be reverse engineered to its primal level, i.e. its approximated spike-train level, then we hypothesise that novel features can be extracted from the data.

Problem statement

To Transform EEG signals to their approximated spike representation via SNN. And validate the approach towards extraction of additional features and in turn enhance the classification performance in various BCI paradigms.

Representation learning, a sub-domain of deep learning, focuses on how well different categories of data can be discriminated in their latent representation (Le-Khac et al. 2020). It has garnered prominence due to its ability in improving the latent information of the data, which results in providing insights into data distribution and contributes to significant improvements in classification performance. Among the different methods, a family of contrastive learning has gained prominence due to its ability in learning invariant representation (Le-Khac et al. 2020). However, such methods have yet to be tested for SNN based applications. We hypothesise that incorporating contrastive learning into SNN could potentially help improve the spike representation of EEG signals and in turn improve the classification performance of BCI.

1.3.3 Burst Spiking Neural Unit

Motivation

Unlike DNNs, SNNs are known for their biological realism. However, for ease of complexity and computation purposes, simplified neuron models are often used to construct SNN architectures. These neuron models often produce tonic spiking patterns under constant input. Recent studies on SNN-based AI applications have tried to incorporate simple spiking neuron properties, such as heterogeneity (Perez-Nieves et al. 2021), and adaptive threshold (Shaban et al. 2021), to evaluate their effect on classification performance in standard machine learning benchmark tests. They have been shown to positively improve the performance of SNN and achieve competing performance compared to their DNN counterpart. However, bursting, a phenomenon of high density spiking patterns observed predominantly during various cognitive tasks, is ignored due to the complex mathematical nature of the model. Therefore, this calls for a new and simple spiking neuron model with a bursting phenomenon.

Problem Statement

To address this problem, we have formulated a new and simple spiking neuron model with bursting ability, termed the burst spiking neural unit (BSNU). We hypothesise that bursting, being very common in the cortex, could help improve the spike representation and outperform standard AI benchmark tasks.

1.4 Thesis Organization

To address the previously mentioned research problems (from Section 1.3), this thesis has dedicated a chapter to each question that discusses necessary methods used and its corresponding analysis and results, as listed below:

Chapter 1: Provides an introduction to the fundamentals of BCI, and SNN, and a brief overview of the research problems addressed in this thesis.

Chapter 2: Discusses the different methods and tools adopted. Additional tech-

niques targeting a specific research problem are discussed in detail in their respective chapters.

Chapter 3: Explores the problem of EEG data augmentation using SNN in detail and showcases that SNN can be leveraged to create synthetic EEG samples, which in turn lead to the improvement of MI-BCI classification performance.

Chapter 4: Discloses the approach and outcomes for the spike representation of EEG signals. In addition, this chapter also reveals insights as to why such improvements occur.

Chapter 5: Introduces a novel BSNU model and its ability for spike representation and other benchmark tests.

Chapter 6: Presents conclusions on the outcomes of this thesis and possible future directions.

Figure 1.5 below provides an overview of the research map of this thesis.

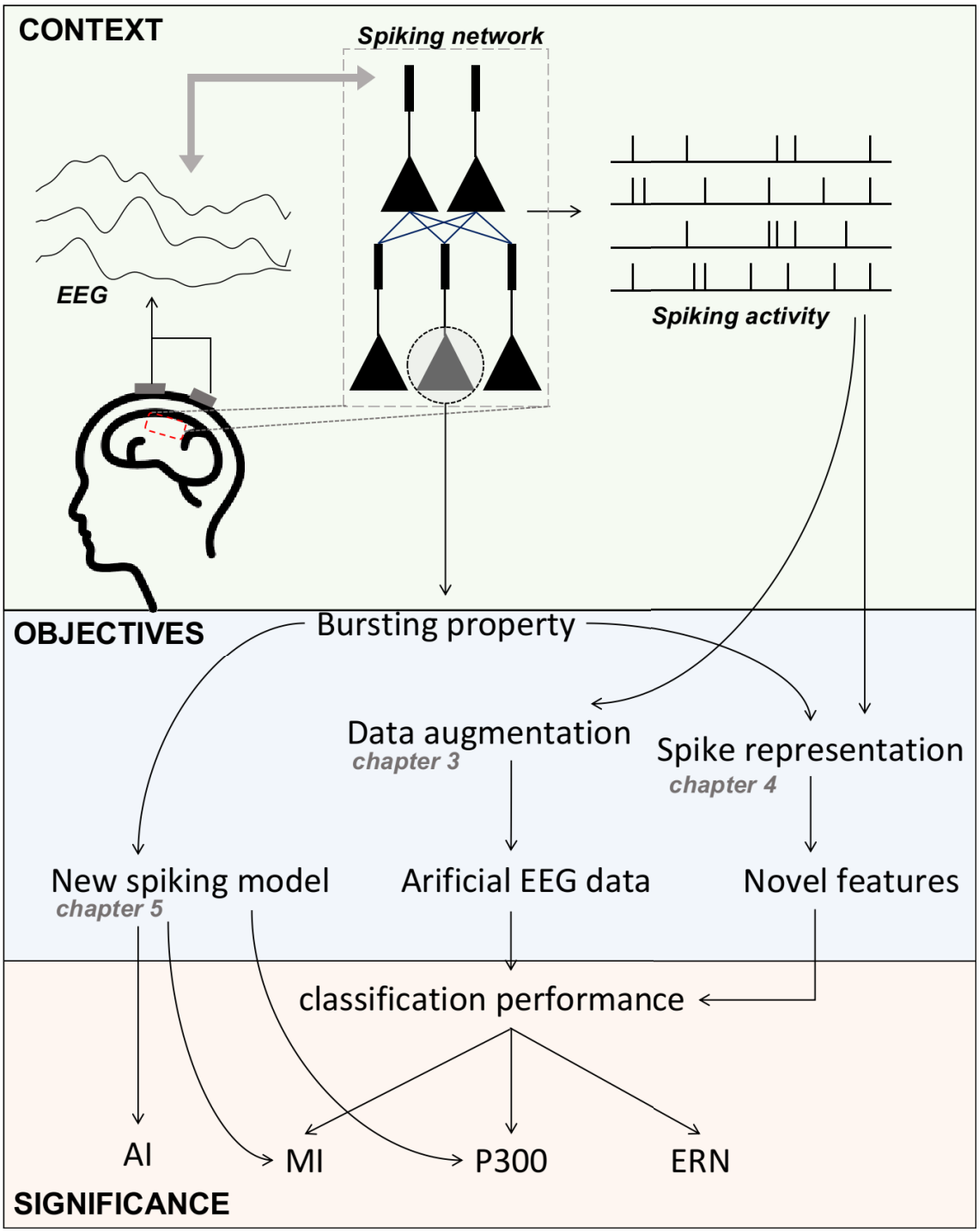

Figure 1.5 : An overview of the research map of this thesis.

Chapter 2

Methodology

A spiking neuron model is a basic unit (or node) in SNN architecture. An artificial neuron performs non-linear computation with real-valued inputs. However, owing to biological realism, the spiking neurons compute with spikes (via differential equations), and therefore, the SNN-based network layer also takes spike trains as input and output spike trains as well. The weight factor is then multiplied with these output spikes before progressing to the next layers. Human brain regions form complex network architectures, such as synapses extending from one layer to multiple hierarchical layers as in cortical columns (Kerdels and Peters 2018), small-world connectivity (Stam et al. 2007) with clusters of interconnected sub-networks, and long-range connections connecting distant regions. However, for simplicity, SNNs (especially for AI applications) are often structured in different fashions, such as feedforward, recurrent, and convolution, similar to DNN architectures.

2.1 Spiking Neuron Model

Among the different neuron models, LIF is the most commonly used model in the field of AI due to its computational simplicity and compatibility with the majority of learning algorithms. It has been successfully applied for AI tasks such as gesture recognition (Arsalan et al. 2021), object recognition (Cheng et al. 2020), and lane keeping of a vehicle (Bing et al. 2018). Additionally, deep learning technique adaptations to SNN have heavily relied on the LIF neuron model. Therefore, to build SNN we resort to the LIF model to address the majority of the research questions (see Section 1.3).

2.1.1 The LIF Model

The LIF neuron model is depicted with the abstract dynamics of a neuron's membrane voltage via first-order differential equations over time, as shown in equation 2.1.

$$\tau_{\mathrm{m}} \frac{\mathrm{d}u_i}{\mathrm{d}t} = -\left(u_i - u_{\mathrm{rest}}\right) + RI_i \tag{2.1}$$

where $u_i(t)$ is the membrane potential of a neuron i, u_{rest} is the resting potential, τ_m is the membrane time constant, R is the input resistance, u_{rest} is the resting potential and $I_i(t)$ is the input current. The input current is also commonly estimated with a first-order differential form with an exponentially decaying properties with input spike according to equation 2.2.

$$\frac{\mathrm{d}I_i}{\mathrm{d}t} = -\frac{I_i(t)}{\tau_{\mathrm{s}}} + \sum_j W_{ij} S_j(t) \tag{2.2}$$

Here, τ_s is the synaptic time constant, W is the input weight matrix and S_j is the spike train coming from neuron j. The membrane potential increases with the input current, and after reaching a threshold ϑ, the neuron emits a spike and resets its potential to u_{rest}. This process is repeats again with the incoming spike trains.

This reset property can be incorporated into equation 2.1 to simplify the essence of the dynamics of membrane voltage by a factor of $(\vartheta - u_{rest})$ when a spike is emitted, resulting in equation 2.3.

$$\frac{\mathrm{d}u_i}{\mathrm{d}t} = -\frac{1}{\tau_{\mathrm{m}}}\left(u_i - u_{\mathrm{rest}}\right) + RI_i + S_i(t)\left(u_{\mathrm{rest}} - \vartheta\right) \tag{2.3}$$

$$S_i(t) = \sum_k \delta\left(t - t_i^k\right) \tag{2.4}$$

Here, $S_i(t)$ is the spike train (sum of a Dirac delta function, δ) of a neuron and t_i^k is the kth firing time of the corresponding neuron (see equation 2.4). As suggested by Neftci et al. (2019), it is common in simulations to discretise dynamical systems and implement an approximated version of the LIF membrane potential for a small simulation time step $\Delta_t > 0$, as shown in equation 2.5. Similarly, the input current dynamics are also discretised according to equation 2.6.

$$u_i[n+1] = \beta u_i[n] + I_i[n] - S_i[n] \tag{2.5}$$

$$I_i[n+1] = \alpha I_i[n] + \sum_j W_{ij} S_j[n] \tag{2.6}$$

Here, n is the stimulation time step, $\alpha \equiv \exp\left(-\frac{\Delta_t}{\tau_s}\right)$, and $\beta \equiv \exp\left(-\frac{\Delta_t}{\tau_m}\right)$ acts as decay strength. These values are constant and fall in the range $(0, 1)$. The output spike train of neuron i at given time step n is described according to equation 2.7 and $S_i[n] \in \{0, 1\}$.

$$S_i[n] = \Theta(u_i[n] - \vartheta) \tag{2.7}$$

Here, Θ is a Heaviside step activation function such that $\Theta(x) = 1$ or 0 for x for x $\geqslant 0$ or < 0, respectively. It is also commonly referred to as a threshold activation function in SNN studies. Refer to table 2.1 for the list of LIF parameter values.

Two other neuron models, the quadratic integrate-and-fire (QIF) model (equation 2.8) and the exponential integrate-and-fire (EIF) model (equation 2.9), have also been tested for EEG reconstruction.

$$\tau_m \frac{\mathrm{d}}{\mathrm{d}t} u_i = a_0 \left(u_i - u_{\text{rest}}\right)\left(u_i - u_c\right) + RI_i \tag{2.8}$$

$$\tau_m \frac{\mathrm{d}}{\mathrm{d}t} u_i = -\left(u_i - u_{\text{rest}}\right) + \Delta_T \exp\left(\frac{u_i - \vartheta}{\Delta_T}\right) + RI_i \tag{2.9}$$

Here, $a_0 > 0$, $u_c > u_{\text{rest}}$, and sharpness parameter $\Delta_T > 0$. And, I_i follows the same dynamics as equation 2.2.

2.2 Spike Filtering

Spike trains are discreet in nature and represented by 0 or 1 at a given time point. To observe the neural dynamics of smoother outputs, filtering is applied to the spike trains to obtain a continuous signal. For example, filters have been used to enable the output of SNN to fit different oscillatory signals (Nicola and Clopath 2017), human motion capture data (Alemi et al. 2018), and study Go-NoGo tasks (Kim et al. 2019). These studies commonly used single-exponential filters and double-exponential filters, each offering a different level of smoothness. A single-exponential synaptic filter is described according to equation 2.10.

$$\dot{r}_j = -\frac{r_j}{\tau_s} + \frac{1}{\tau_s} \sum_{t_{jk}<t} \delta\left(t - t_{jk}\right) \tag{2.10}$$

where r_j is the filtered output neuron of the jth neuron, τ_s represents the synaptic time constant, δ is the spike train, and t_{jk} is the kth spike emitted. The double-exponential filter is described according to equations 2.11 - 2.12.

$$\dot{r}_j = -\frac{r_j}{\tau_d} + h_j \tag{2.11}$$

$$\dot{h}_j = -\frac{h_j}{\tau_r} + \frac{1}{\tau_r \tau_d} \sum_{t_{jk}<t} \delta\left(t - t_{jk}\right) \tag{2.12}$$

where τ_r is the synaptic rise time, and τ_d is the synaptic decay time.

Table 2.1 : List of LIF spiking neuron and Adam optimiser properties.

Spiking Neuron	**Value**
dt	1 ms
u_{rest}	0 mv
τ_m	10 ms
τ_s	5 ms
R	1 M
ϑ	1 mv
τ_d	2 ms
τ_r	3 ms
$l(\tau)$	0.8

2.3 Surrogate Gradient Descent

A spike is emitted when the membrane voltage exceeds pre-defined membrane voltage threshold ϑ and the voltage resets back to its resting potential. This behaviour mimics the Heaviside step activation function (Θ in equation 2.7). This threshold activation function of the spiking neuron is non-differentiable, and therefore, earlier studies often use learning algorithms such as STDP and its variants to

train SNN with a side-effect of lower performance. This is because due to the non-differentiability, training the synaptic weights is challenging as the traditional gradient descent algorithm commonly used for training DNNs is not applicable since the gradient calculation is zero everywhere except at the time event of spike emissions, where the gradient becomes undefined. Recently, techniques have been formulated to overcome this issue by eliminating the non-differentiability during backpropagation. Surrogate gradient descent is one such approach proposed by Zenke and Ganguli (2018), and Neftci et al. (2019). Here, a continuous relaxation on the gradient estimation that does not affect the forward pass of spike trains is made possible using pseudo-derivatives. The step nature of spike emission $S_i[n] \propto \Theta(u_i[n] - \vartheta)$ from forward propagation is replaced with $\sigma(u_i[n] - \vartheta)$ during backpropagation, where $\sigma(x) = 1/(1 + exp(-x))$ is called the *Sigmoid* activation function. An overview of surrogate derivatives from different studies is shown in figure 2.1 adapted from Neftci et al. (2019). For optimisation purposes, Adam (Kingma and Ba 2014) is used for training the SNN using surrogate derivatives.

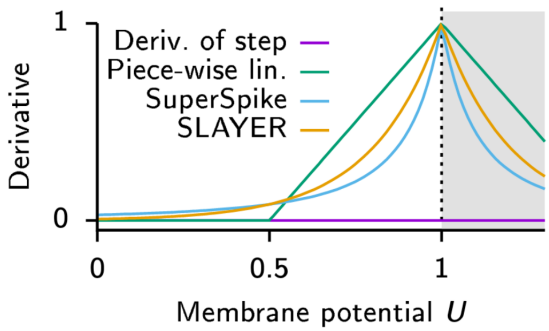

Figure 2.1 : Surrogate derivatives of different function adapted from Neftci et al. (2019). SuperSpike and SLAYER use fast sigmoid and exponential functions.

2.4 Classification Algorithms

In BCI applications, classification is a mandatory step for measuring human intention for controlling an application. To validate the outcome of each research problem, we applied different commonly used classification methods for supervised

learning for BCI paradigms. Some of these algorithms include Linear discriminant analysis (LDA), Support vector machines (SVM), Gaussian classifier, k-Nearest Neighbour (KNN), and boosting algorithms. Described below are the details of these algorithms.

2.4.1 Linear Discriminant Analysis

LDA, a method derived from Fisher's discriminant (Mika et al. 1999), is a linear transformation technique commonly used for dimensionality reduction and classification for different BCI paradigms (Zhang et al. 2013b; Varsehi and Firoozabadi 2021). This algorithm is a supervised technique and computes axes or linear discriminants that maximise the separation between classes and minimise within-class distance. For a given dataset with features $\mathbf{X}$, the objective of LDA is to project the data to low dimension space as shown in equation 2.13.

$$\mathrm{Y} = \mathbf{w}^{\mathrm{T}}\mathrm{X} \tag{2.13}$$

where Y is the projected data, and $\mathbf{w}$ is the projection vector defined according to equation 2.14.

$$\mathbf{w} = \boldsymbol{\Sigma}^{-1}\left(\boldsymbol{\mu}_2 - \boldsymbol{\mu}_1\right) \tag{2.14}$$

where μ_c is the mean of a given class c, and Σ is the common covariance. The mean and covariance are calculated as below:

$$\boldsymbol{\mu}_c = \frac{1}{N_c}\sum_{i\in\mathcal{I}_c}\mathbf{x}_i \tag{2.15}$$

$$\boldsymbol{\Sigma}_c = \frac{1}{N_c - 1}\sum_{i\in\mathcal{I}_c}\left(\mathbf{x}_i - \boldsymbol{\mu}_c\right)\left(\mathbf{x}_i - \boldsymbol{\mu}_c\right)^T, c = 1, 2 \tag{2.16}$$

$$\boldsymbol{\Sigma} = \left(N_1\right)/(N)\boldsymbol{\Sigma}_1 + \left(N_2\right)/(N)\boldsymbol{\Sigma}_2 \tag{2.17}$$

where N_c is the number of sample in a given class, and N is the total number of samples.

2.4.2 Support Vector Machines

The idea behind SVM is to identify a hyperplane in feature space that categorizes the data points of two classes. Theoretically, many such hyperplanes or decision boundaries are possible to distinguish the data points. However, the objective of SVM is to identify the hyperplane that can result in maximum margin or distance between samples of both classes. And, this is to ensure that test samples' classification outcomes are estimated with more confidence. The position and orientation of the hyperplane depend on support vectors, i.e., the data points closer to the margin. The hyperplane is described according to equation 2.18.

$$\mathbf{w}^T\mathbf{x} + b = 0 \tag{2.18}$$

where $\mathbf{w}$ is normal vector, b is the offset of plane from origin, and $\mathbf{x}$ represents a set of points. Consider a training dataset D with samples X_i, and the corresponding labels y_i in which $y_i = +1$ *or* -1 depending on the class as shown in equation 2.19.

$$\{\mathbf{x}_i, y_i\} \quad \text{where} \quad i = 1 \ldots L, y_i \in \{-1, 1\}, \mathbf{x} \in \Re^D \tag{2.19}$$

As hyperplanes are closest to the support vectors, these are formulated according to equation 2.20 in which, a hyperplane is obtained, one for each class.

$$\begin{aligned} w \cdot x_i + b &\geq 1 \quad \text{for } y_i = +1 \\ w \cdot x_i + b &\leq -1 \quad \text{for } y_i = -1 \end{aligned} \tag{2.20}$$

Here, w, and b are optimised by maximising the distance or margin (see equation 2.21) between the two hyperplanes.

$$M = max_w \frac{2}{\|w\|} \tag{2.21}$$

For optimisation purpose, the maximal distance formula defined above is modified to equation 2.22.

$$\min \frac{\|w\|^2}{2} \tag{2.22}$$

Therefore, the optimization problem for SVM is defined as follows:

$$\min \|w\|^2 \quad \text{such that } y_i \left(w \cdot x_i + b\right) - 1 \geq 0 \text{ for } i = 1..l \tag{2.23}$$

2.4.3 Naive Bayes Classifier

The NVB classifier is a probabilistic machine learning model based on the Bayes theorem. For hypothesis A and evidence B, the formula for Bayes theorem is as follows:

$$P(A \mid B) = \frac{P(B \mid A)P(A)}{P(B)} \tag{2.24}$$

This classifier assumes that the features are independent i.e. the presence of one feature does not affect the other. Also, it assumes that all the features have an equal effect on the outcome. For a feature vector X, and its class label, y, the Bayes theorem is written as equation 2.25.

$$P(y \mid X) = \frac{P(X \mid y)P(y)}{P(X)} \tag{2.25}$$

By incorporating the chain rule, the posterior probability from equation 2.25 is rewritten as 2.26, where $X = (x_1, x_2, x_3, \ldots, \ldots, x_n)$. Since X is static, the posterior probability takes simplified form as shown in 2.27.

$$P\left(y \mid x_1, \ldots, x_n\right) = \frac{P\left(x_1 \mid y\right) P\left(x_2 \mid y\right) \ldots P\left(x_n \mid y\right) P(y)}{P\left(x_1\right) P\left(x_2\right) \ldots P\left(x_n\right)} \tag{2.26}$$

$$P\left(y \mid x_1, \ldots, x_n\right) \propto P(y) \prod_{i=1}^{n} P\left(x_i \mid y\right) \tag{2.27}$$

Therefore, the objective of the NVB classifier is to increase the posterior probability of class label for a given sample and defined as follows:

$$y = \text{argmax}_y \, P(y) \prod_{i=1}^{n} P\left(x_i \mid y\right) \tag{2.28}$$

In this thesis, we adopted a Gaussian version of the Bayes classifier. Here, the condition probability $P\left(x_i \mid y\right)$ takes the Gaussian format (see equation 2.29.

$$P\left(x_i \mid y\right) = \frac{1}{\sqrt{2\pi\sigma_y^2}} \exp\left(-\frac{\left(x_i - \mu_y\right)^2}{2\sigma_y^2}\right) \tag{2.29}$$

2.4.4 K-Nearest Neighbours

K-Nearest neighbours is a supervised classification algorithm based on the principle that similar samples exist in closer proximity in the feature space. This is a

vote based classifier in which the distances between a given test sample and a set of training samples are estimated. Then, the majority training labels from K lowest distance or closer samples are assigned as the voted class of test sample. The term K in KNN is an integer value and is highly dependent on the dataset. This algorithm was also highly considered classifier for feature vectors obtained from various feature extraction methods across different BCI paradigms such wavelet features from MI (Mohdiwale et al. 2020), CSP features from MI (Dagdevir and Tokmakci 2021), features from xDAWN spatial filters on P300 (Miah et al. 2021), and time-series of error related potential (ErrP) (Zhang et al. 2018).

2.4.5 Gradient boosting

This is an ensemble learning in which weaker models (or base learners whose performance is marginally better than chance) are combined to form a stronger model. In this study, we used decision trees as the model. In particular, the strong model is built by iteratively learning from each of the weaker models to overcome bias-variance tradeoff, i.e. during the iterative process, a new tree is built to overcome the errors made by the previous tree. In an iterative step m, for a sample $\{x, y\}$, and model F_m, the residual to which a base learner is estimated according to equation 2.30.

$$h_m(x) = y - F_m(x) \tag{2.30}$$

In the following step, the model is updated to correct the errors from the previous step as follows:

$$F_{m+1}(x) = F_m(x) + h_m(x) \tag{2.31}$$

The objective of this classifiers is to find optimal model $\hat{F}$ as show in equation 2.32.

$$\hat{F} = \arg\min_{F} \mathbb{E}_{x,y}[L(y, F(x))] \tag{2.32}$$

The optimal model $\hat{F}$ then takes shape of an weighted sum of the base learners $h_i(x)$ according to equation 2.33.

$$\hat{F}(x) = \sum_{i=1}^{M} \gamma_i h_i(x) + \text{ constant} \tag{2.33}$$

For a dataset of n samples, the model is initialized to a constant value and incrementally updated in a specified number of stages (M) as described below:

step 1: Initialize the model with a constant output value.

$$F_0(x) = \min_{\gamma} \sum_{i=1}^{n} L\left(y_i, \gamma\right) \tag{2.34}$$

step 2: At a given stage $m = 1t0M$ in the iterative process, pseudo-residuals are calculated from the previous stage $m-1$. This is done for each sample in the dataset, and a new dataset (D_m) is obtained.

$$r_{im} = -\left.\frac{\partial L\left(y, F_{m-1}(x)\right)}{\partial F_{m-1}(x)}\right|_{x=x_i, y=y_i} \quad \forall\, i = 1, 2, \ldots, n \tag{2.35}$$

$$D_m = \{(x_i, r_{im}) : i = 1, 2, \ldots, n\} \tag{2.36}$$

step 3: The base learner h_m is trained with the new dataset, and then a new model F_m is derived as follows:

$$F_m(x) = F_{m-1}(x) + \gamma h_m(x) \tag{2.37}$$

step 4: To find the optimal γ (see equation 2.38), the loss from model predictions applied on the original dataset is minimised. Then the model from equation 2.37 is updated according to equation 2.39.

$$\gamma_{\text{opt}} = \underset{\gamma}{\operatorname{argmin}} \sum_{i=1}^{n} L\left(y_i, F_m\left(x_i\right)\right) = \underset{\gamma}{\operatorname{argmin}} \sum_{i=1}^{n} L\left(y_i, F_{m-1}\left(x_i\right) + \gamma h_m\left(x_i\right)\right) \tag{2.38}$$

$$F_m(x) = F_{m-1}(x) + \gamma_{\text{opt}}\, h_m(x) \tag{2.39}$$

Chapter 3

EEG Data Augmentation using SNN

3.1 Abstract

A generic BCI system is characterised by a tedious experimental setup, data loss due to various artifacts caused by motion and external factors, and the recording of a huge number of trials for deep learning based classification purposes, which is time-consuming. To address the limited data issues, a few studies have explored generating artificial EEG signals. However, some of the older data generation methods are inadequate to accommodate the prominent biomarkers of an EEG signal. With the advent of deep learning, DNN based generative models overcome this issue to an extent, but these models have an requirement of having huge number of samples for training. In addition, some of these models can only handle data augmentation for one category of a dataset in a given training session. Therefore, this calls for novel generative models that can generate artificial EEG samples with multiple classes without the side effect of feature loss from as few original samples as possible. An EEG signal is the result of the accumulation of a spiking signal from the neuronal populations beneath the scalp surface. And, studies have shown that spike train samples to a given stimuli are minor differences in the spike timing. Exploring spike-based EEG augmentation could help open up new possibilities. An SNN is the closest network model that can communicate via spikes and is a suitable replacement for a DNN. Therefore, in this chapter, we propose an SNN-based approach that initially maps the model to a template signal and generates multi-class artificial EEG signals from a few original samples. The approach is employed for data augmentation of MI and SSVEP. The artificial data are also validated with different classifiers and correlation metrics.

3.2 Background

With the advent of deep learning methods, there have been unprecedented improvements in the performance of different BCI paradigms (Zhang et al. 2017; Chiarelli et al. 2018; Schwemmer et al. 2018). For example, Schwemmer et al. (2018) implemented a combination of LSMT and convolution layers on high-dense intra-cortical recordings to classify different hand movements such as index and wrist's extension & flexion. Similarly, Lawhern et al. (2018) developed an EEG-Net model based on convolution layers and shown to efficiently work on a wide range of paradigms such as motor activity, P300, and ERN. Also, the deep learning models were accommodated to classify the hybrid recordings such as EEG + fNIRS (Chiarelli et al. 2018). However, the deep learning methods often require an abundant number of labelled samples to leverage its potential and to obtain better performance. However, the large scale EEG recordings is a tedious and time consuming experimental process. In addition, noise and artifacts due to motion, and other external factors often contaminate the samples. This leads to data rejection, i.e. these samples are discarded during the pre-processing steps of EEG signal.

To overcome the limited samples problem, data argumentation techniques plays a crucial role. By generating artificial EEG samples, the dataset size can be increased, and this in turn helps to better train the machine learning algorithms. Before the inception of deep learning based data augmentation methods, statistical methods were applied on EEG signals for generating artificial samples. For example, Lotte (2011) generated synthetic EEG sample by splitting each of the recorded original samples into different segments and randomly combining these segments to obtain a new different sample. But this process leads to the loss of temporal-domain features in the artificial signal. Similarly, Dinarès-Ferran et al. (2018) employed Empirical Mode Decomposition (EMD) which decomposes a given signal into a finite number of intrinsic mode functions (IMF), a nonlinear component of the EEG signal. The IMF components obtained from different original samples were then combined to create an artificial sample. However, the study stated that this approach generated irrelevant artificial samples and as such, the process could mislead the classification

algorithms.

In a recent trend, different versions of deep learning-based generative models were formulated to solve the data augmentation needs of various domains such as image, speech and text. Some of the well known deep generative models include generative adversarial networks (GAN) and their variants, and variational autoencoders (VAE). The details of these algorithms are presented in detail in Sections 3.3.3-3.3.4. For example, GAN was used to generate a realistic sample of medical imaging such as CT-scan for lymph node segmentation (Tang et al. 2019), retinal imaging (Iqbal and Ali 2018) etc. Apart from image datasets, biomedical time series data such as the electrocardiogram (ECG), and EMG were also under focus for data augmentation. For example, generation of artificial ECG samples using a deep convolution GAN (DCGAN) for improving the classification performance (Golany et al. 2020), and simulating Parkinson's tremor pattern on EMG for better diagnosis (Anicet Zanini and Luna Colombini 2020).

These models have also been explored to generate synthetic EEG samples with an aim to increase the performance of different BCI paradigms. For example, Aznan et al. (2019) focused on generating SSVEP data of 3 classes (10, 12, and 15 Hz) using a DCGAN, Wassertian GAN (W-GAN), and VAE. But, they have observed that a single generative model cannot improve the performance of all subject datasets, i.e. for each subject, a different generative model resulted in a better outcome. Similarly, Hartmann et al. (2018) generated left-hand motor imagery data using W-GANs and showcased that their approach could result in EEG realistic signals. But, this study performed classification between left-hand MI and resting signal rather than among different MI signals. Besides, these studies were able to produce only one class or category of the dataset at a time because of the choice of generative DNN model. In addition, few EEG studies adopted GAN variants to advance different BCI applications such as emotion recognition (Luo and Lu 2018), sleepiness detection in driving conditions (Jiao et al. 2020), improve rapid series visual presentation (RSVP) detection rate (Panwar et al. 2019), and seizure prediction (Truong et al. 2019). Apart from data augmentation, GAN was also shown to be efficient for EEG

denoising (An et al. 2022), increasing the resolution of signal (Corley and Huang 2018), removal of artifacts (Lin et al. 2020) etc. Although GAN-based models have resulted in promising performance, they are prone to instability, require fine-tuning of the hyperparameters, and need a large number of samples for the training purpose. This is counter-intuitive because they are used due to insufficient data but these generative models require a sufficient number of samples to function efficiently. This calls for a generative model that can generate data with few original samples, and at the same time, generate multi-class EEG samples without loss of bio-markers.

Information in the human brain is processed by an interconnected population of spiking neurons, and how the collective neuronal activity is responsible for anan-imal's behaviour or actions remains a highly explored neuroscience research topic (Sussillo and Abbott 2009; Churchland et al. 2012; Nicola and Clopath 2017; Gilra and Gerstner 2017). Spiking network are of importance in understanding these behaviours from a computational perspective. For example, Nicola and Clopath (2017) generated different signals such as sinusoidal waves, Lorenz attractor, Ode to Joy, bird song, and movie replay. This study explored the dynamics of net-works by building biologically similar network structures and trained the model in a supervised fashion using the FORCE algorithm. In another study, dynamically balanced recurrent spiking networks trained via bounded constrained coordinate descent optimisation were developed to can reconstruct motion tracking signals (In-grosso and Abbott 2019). Similarly, few studies explored information processing such as evaluating network coupling nonlinearities of brain signal using Izhikevich model (Nunes et al. 2019), a spontaneous cortical activity that occurs during sleep (Pena et al. 2018), the emergence of neural adaptation i.e., encoding of known stim-uli whilst adapting to novel stimulus (Gutierrez and Denève 2019), and adjustment of inhibitory/excitatory neural connections in the hippocampus to maintain stable dynamics (Sukenik et al. 2021).

Brain computer interface systems could potentially be enhanced by studying the underlying spiking dynamics responsible for an EEG signal oscillation and providing novel approaches to address EEG data augmentation problems. As stated in Section

1.2.1, few studies explored utility of SNN for EEG studies. However, these studies assume EEG as the input and SNN as the encoder. In practice, an EEG signal is the outcome of a spiking signal. A few SNN studies that tried to reconstruct different time-serial signals used recursive least square (RLS) for training the model. For efficient training several variants of RLS came into inception for such as FORCE (Nicola and Clopath 2017), full-Force (DePasquale et al. 2018; Ioannides et al. 2022), partial-Force (Tamura and Tanaka 2021a), and transfer-RLS method (Tamura and Tanaka 2021b). In addition, the RLS training algorithm was also shown to be compatible with tuning the target signal at neuron level (Kim and Chow 2018), and can accommodate constraints in the loss function such as ROWSUM constraint introduced by Kim and Chow (2021) to maintain Dale's law. Although these studies showcased better signal reconstruction, they were mainly applied on periodic signals, and also required independent set of hyperparameters for training different types of signals. In other words, reconstruction of different training signals required different set of hyperparameters. Unlike periodic signals, an EEG signal is non-stationary and has a high variance. Therefore, in this chapter, we adopted a feedforward SNN and trained the network via the surrogate gradient descent (Zenke and Ganguli 2018; Neftci et al. 2019) method to reconstruct the EEG template signal and in turn generate synthetic EEG signals.

Each recorded EEG trial is unique in a time-series for a given stimulus despite there being similar biomarkers (i.e., feature pattern such as peak in power spectrum for SSVEP, ERD/ERS featuer of MI) across multiple samples. Therefore, reconstructing an EEG signal and generating unique samples by a SNN with few samples poses a challenge and the existing signal generation methods from SNN models focus on one signal. A famous spike train repeatability study by Mainen and Sejnowski (1995) demonstrated that a neocortical population can produce different spike trains for repetitions of a given stimulus. Similar variability was observed in a single neuron recording of monkey's motor cortex during a reaching task (Nawrot et al. 2008), neurons from V1 visual cortex to naturalistic visual stimuli (Xia et al. 2021). Some plausible reasons for such variability include unknown information flow from other

populations, and intrinsic background noise in population. Taking the essence of this variability, we propose to add an external spiking perturbation layer that can induce background noise to a trained SNN model. By regulating the perturbation layer's properties, i.e. noise level, the proposed model can produce unique artificial samples. This perturbation results in adjustments of spike timing similar to the variability studies. The primary use for any artificial data in machine learning is to improve the classification performance. In this study, we explore the efficacy of synthetic MI-EEG data of two classes. The proposed approach is able to generate artificial MI-EEG data and enhanced the classification performance. There are three contributions in this chapter, as follows: (1) a developed SNN model that is immune to the BCI paradigm, i.e, a model that can be leveraged to augment different modalities such as MI and SSVEP without extensively changing the model hyperparameters, (2) the generation of multi class artificial MI samples from only a few original samples, and (3) extensive validation of artificial MI signals that have often been ignored in previous studies and enhanced the classification performance.

3.3 Methods

A feedforward style SNN, as illustrated in figure 3.1, was designed to produce EEG signals. Each node in a spiking layer was based on the LIF spiking neuron model (see Section 2.1.1). Since the ground truth spike train responsible for a given target EEG signal was inaccessible, a 10 Hz firing rate based Poisson spike train was used for the input layer. For MI and SSVEP reconstruction, the same architecture was used but with a different number of nodes or neurons in each layer during the training process. The spike train obtained from the output layer was then transformed into a continuous rate signal using a double exponential synaptic filter (see equation 2.9). This rate signal was converted to an output EEG signal via the weighted average. The weight matrices between all layers, except for the connection between the perturbation layer and hidden layer, were trained during the reconstruction process. In the EEG output layer, each node corresponded to one EEG channel from the target signal. The perturbation layer that acted as background noise, was composed of a different number of Poisson neurons with a

varying firing rate.

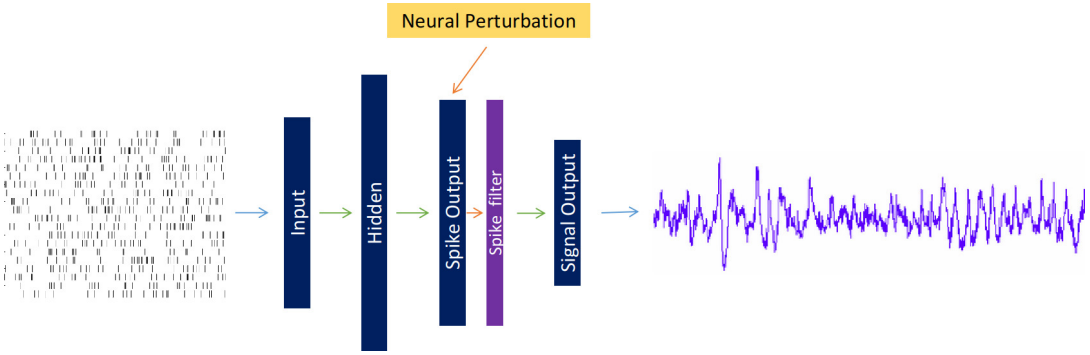

Figure 3.1 : Depiction of a three-layered feedforward spiking network mapping a random spike train to an EEG signal with additional neural perturbation layer of Poisson neurons distorting the information of Spike Output layer.

The data generation protocol shown in figure 3.2 was implemented in three stages: (1) obtaining reliable EEG templates of each class by averaging the original samples (in SSVEP) or selecting the best trial among all samples (in MI), (2) training the SNN model (without the active perturbation layer) to reproduce EEG templates of all classes, and (3) activating the perturbation layer of the trained model to generate artificial EEG samples. The multiple samples of EEG signals recorded from a given stimulus varied due to noise and artifacts, and the majority of the samples retained similar bio-marker.

For Stage 1 (i.e. template extraction), depending on the BCI paradigms we adopted different process. In the case of SSVEP, we averaged a few trials to obtain a clean signal containing a strong biomarker. For MI, the averaging process distorted the biomarker in its power spectrum (mu and beta bands) so we applied classification on the dataset to obtain a sample that had a high probability of being categorised into the correct class. Such best trial, one from each class, was considered as the template signal. For the weight optimisation, the surrogate gradient descent method was used for the SNN training process (second stage) to reconstruct the previously extracted EEG template samples. In the final stage, all weight matrices were fixed, and the neural perturbation layer was activated to generate artificial samples. For

each sample, a random spike train was generated by this perturbation layer that caused a pattern change in the hidden layer, which in turn resulted in a unique artificial sample. This background noise could also be controlled by modulating the layer with different numbers of Poisson neurons and their firing rates.

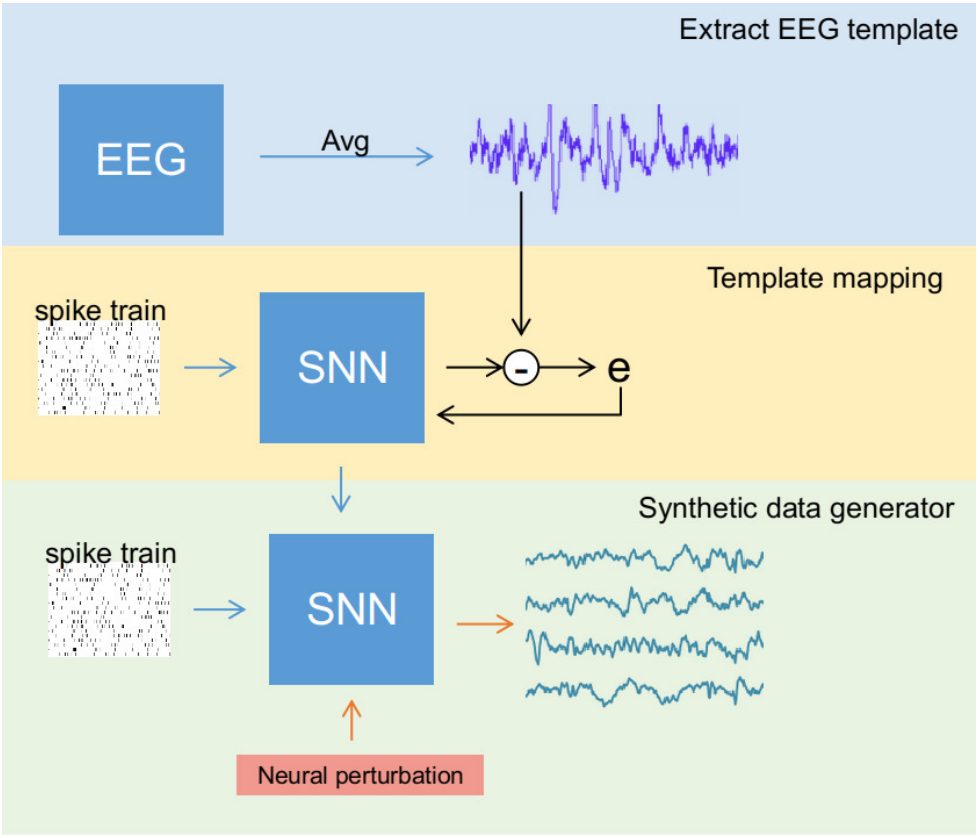

Figure 3.2 : Overview of the steps involved in generating synthetic EEG samples using the SNN.

3.3.1 EEG Datasets

In this study, publicly available datasets from various sources were used for both MI and SSVEP. For MI, BCI competition IV resources from Tangermann et al. (2012) and data previously recorded by our group from Ko et al. (2019) were used. From the entire MI dataset, three second trial durations were epoched and sampled to 250 Hz. Also, these datasets comprised two classes, i.e. left-hand MI and right-hand MI classes. Similarly, for SSVEP, the datasets from Wang et al. (2016) were

used, and only two second durations from stimulus onset were extracted and down-sampled to 250 Hz for further usage with the SNN model.

3.3.2 Classification

Among the different BCI paradigms, SSVEP is easy to detect and can obtain a high performance in comparison to MI. Therefore, the efficacy of data augmentation was assessed to enhance the MI classification performance. Different perturbation combinations (different number of noise neurons and their firing rate) in the perturbation layer were used to generate 100 samples (per combination) of artificial MI-EEG data. The artificial MI-EEG data were further assessed for classification performance by (1) comparing the cross-classification between the artificial and original data and (2) performing a correlation analysis to compare the similarity of the artificial data with the original data. Common spatial pattern (CSP), a widely adopted method for extracting MI-related features (Wang et al. 2006), was used to test the above assessment, and the details of the CSP algorithm are described in Section 3.3.2. Finally, the features obtained via CSP were classified using LDA, SVM with linear kernel, K-NN with K=5, and Gaussian classifier (Xygonakis et al. 2018; Mishuhina and Jiang 2018).

Common spatial pattern

The objective of CSP is to estimate spatial filters for maximal variance to discriminate two sets of data. With E as the EEG signal and W as the spatial filter, the transformed signal S is given by the following set of formulae:

$$S = W^T E \quad \text{or} \quad s(t) = W^T e(t) \tag{3.1}$$

The criteria for CSP is as follows:

$$\begin{aligned} &\text{maximize} && \operatorname{tr} W^T \Sigma_1 \boldsymbol{W} \\ &\text{subject to} && \boldsymbol{W}^T \left(\Sigma_1 + \Sigma_2\right) \boldsymbol{W} = \boldsymbol{I} \end{aligned} \tag{3.2}$$

where

$$\begin{aligned} \boldsymbol{\Sigma}_1 &= \underset{E_n \in \{\text{ class } 1\}}{\text{Exp}} \frac{\boldsymbol{E}_n \boldsymbol{E}_n^T}{\operatorname{tr} \boldsymbol{E}_n \boldsymbol{E}_n^T} \\ \boldsymbol{\Sigma}_2 &= \underset{E_n \in \{\text{ class } 2\}}{\text{Exp}} \frac{\boldsymbol{E}_n \boldsymbol{E}_n^T}{\operatorname{tr} \boldsymbol{E}_n \boldsymbol{E}_n^T} \end{aligned} \tag{3.3}$$

3.3.3 Generative Adversarial Networks (GAN)

GAN is a DNN-based deep generative neural network, which contains a discriminator network and a generator network. The discriminator takes true samples and samples generated by the generator network and tries to distinguish the artificial sample from true samples. The generator network is trained to generate samples that can be hard for the discriminator to classify. These two neural networks contest each other similar to that of a zero-sum game. This adversarial setting has been shown to produce more realistic data, especially with image datasets. Figure 3.3 depicts an overview of the interaction between generator and discriminator network.

Discriminator:

A discriminator is a classifier, which is usually based on a deep convolution neural network. It is a classifier used to distinguish between the real and the generated samples. The discriminator is penalized for misclassifying the sample and the weights of the discriminator are adjusted using backpropagation.

Generator:

The generator is a deep neural network that creates fake data. The generator is given a random input and the generator network learns to transform the random input into a fake data sample. The generator is penalized for failing with the discriminator. In other words, penalization occurs when the discriminator network can recognize a generated image as a fake image.

When given a random distribution as input, GANs should generate data with a distribution closer to the distribution of the real data. Therefore the loss functions should reduce the differences between these distributions. This can be achieved by training the GAN architecture using minmax loss and the training tries to minimize the objective function as shown in equation 3.4.

$$E_x[\log(D(x))] + E_z[\log(1 - D(G(z)))] \tag{3.4}$$

where $D(x)$ is the discriminator's output for the real sample, $D(G(z))$ is the discriminator's output for the generated sample, and E_x denotes expectation. The

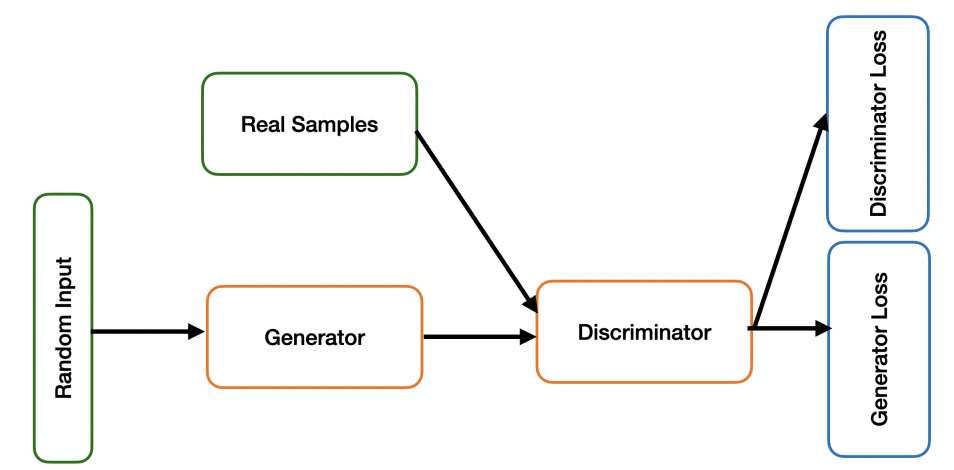

Figure 3.3 : An overview of Generative Adversarial Network structure.

discriminator tries to maximize this loss function while the generator learns to minimise the same.

The discriminator network is penalized for misclassifying the generated sample from the real samples. This is achieved by maximizing the function from equation 3.5.

$$\nabla_{\theta_d} \frac{1}{m} \sum_{i=1}^{m} \left[\log D\left(\boldsymbol{x}^{(i)}\right) + \log\left(1 - D\left(G\left(\boldsymbol{z}^{(i)}\right)\right)\right) \right] \tag{3.5}$$

$\log D\left(\boldsymbol{x}^{(i)}\right)$ represents the probability of correctly classifying the real image by the discriminator. Maximising $\left(1 - D\left(G\left(\boldsymbol{z}^{(i)}\right)\right)\right)$ will help the discriminator improve its performance on discriminating the fake samples from the real samples.

For training the generator network, the loss function from equation 3.6 should be minimised.

$$\nabla_{\theta_g} \frac{1}{m} \sum_{i=1}^{m} \log\left(1 - D\left(G\left(z^{(i)}\right)\right)\right) \tag{3.6}$$

This penalizes the generator network if the discriminator is able to correctly classify (or recognize) the generated samples from the real samples.

W-GAN, a variant of GAN, works similar to GAN but differs in the loss function. In W-GAN the discriminator is referred to as critic. $D(x) - D(G(z))$ is the critic loss and the objective of the critic network maximises this loss function. The nature

of this function is to maximise the difference or distance between the real sample and the generated sample. D(G(z)) is the generator loss and the generator learns to maximize this function. DCGAN is another variant of GAN that uses deep convolution neural networks for discriminator and convolution transpose layers for generator networks.

3.3.4 Variational Autoencoder

Variational autoencoder (VAE) is a DNN similar to Autoencoders (AE) with encoder-decoder structure (Zhai et al. 2018). While AE's encoder produces a vector of values, VAE describes an observation or input in latent space in a probabilistic manner. For instance, for an observation x, there exist some hidden variables z described according to equation 3.7 and the decoder maps this latent variable back to the input.

$$p(z \mid x) = \frac{p(x \mid z)p(z)}{p(x)} \tag{3.7}$$

A generative model ideally seeks to learn the distribution of existing data $p(x)$, but it is generally difficult to construct such distribution.

$$p(x) = \int p(x \mid z)p(z)dz \tag{3.8}$$

As shown in equation 3.8, it is an intractable distribution. Variational inference is usually adopted to obtain an approximated solution to this issue. To this end, the $p(z \mid x)$ is approximated using another distribution $q(z \mid x)$, where q is tractable. The aim is to make the parameters of $q(z \mid x)$ similar to $p(z \mid x)$. In other words, the objective is to minimize the distance between these two distributions, and this is achieved by minimizing the Kullback-Leibler divergence (KL divergence) measure between these distributions as shown in equation 3.9.

$$\min KL(q(z \mid x) \| p(z \mid x)) \tag{3.9}$$

where, for a probability space X, the KL divergence is defined as $\mathrm{KL}(P\|Q) = \sum_{x\in X} P(x) \log\left(\frac{P(x)}{Q(x)}\right)$.

The VAE model finds the distribution $q(z \mid x)$ by reconstructing the input through the decoder as shown in figure 3.4.

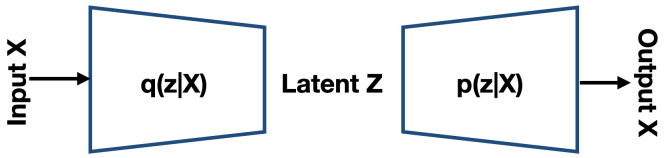

Figure 3.4 : Encoder-decoder style architecture of Variational autoencoder.

By combining the KL loss with the reconstruction of the likelihood, the overall loss function is described according to equation 3.10.

$$E_{q(z|x)} \log p(x \mid z) - KL(q(z \mid x)||p(z)) \tag{3.10}$$

The left part of figure 3.4 is the encoder ($q(z \mid x)$) and the right part is the decoder ($p(z \mid x)$). The encoder module will learn the parameters which describe the distribution of the data. Also, the loss function in equation 3.10 enables the output of encoder to resemble true prior $p(z)$. The VAE assumes that the prior follow a multivariate Gaussian distribution, and the encoder's output (the latent z) is mean and variance. The decoder module will then take samples from the multivariate Gaussian distribution of the latent z and learn to reconstruct the original input.

3.4 Results

3.4.1 The SNN for MI

Prominent MI features, such as ERS and ERD, are typically observed over the motor cortex and traced at central EEG electrodes (typically from the C3 and C4 channels) in the mu frequency range of 8-13 Hz (Thomas et al. 2009; Shahid et al. 2010). Therefore, in this study, C3 and C4 channel time-series EEG data of

two classes i.e. (1) left-hand MI (LH-MI) and (2) right-hand MI (RH-MI), were targeted for data augmentation. The data were bandpass filtered between 0.5-20 Hz and sampled at 250 Hz in the pre-processing. To extract the target template, CSP was used to find the best sample from this processed data based on the probability of each sample being classified accurately. As previously stated, a 10 Hz Poisson spike train matrix was provided as input, with one fixed input for each class, and the SNN was trained using surrogate gradient to produce the C3 and C4 channel template. However, during this training process, the perturbation layer (in figure 3.1) remained inactive.

Figure 3.5A–B shows the two-channel EEG reconstruction from the training (template) signal before and after the training process (according to the template matching step from Figure 3.2) and the corresponding reorganisation neuron's spiking information from the hidden layer (see the yellow box in figure 3.5B, indicating that the learning process was effective in reorganising the spike trains after training). As previously mentioned, for the MI reconstruction, the C3 and C4 channel data generated by the SNN (orange line in figure 3.5A) were initially random and eventually converged to the EEG template (blue line). The essence of the figure 3.5 is to showase that an SNN can accurately reconstruct a given EEG signal.

We further verified the similarity of the reconstructed power spectrum to the power spectrum of the training signals, as shown in figure 3.5C, where the bold lines present the original power spectrum and the dashed lines represent the reconstructed line for each channel i.e. C3 and C4, individually for the LH-MI (blue line) and RH-MI (red line). Figure 3.5D shows that the loss, i.e., the mean squared error (MSE) between the SNN generated signal and the template signal, converge quickly after a few iterations or epochs. This trained model was later used to generate multiple artificial signals by activating the perturbation layer.

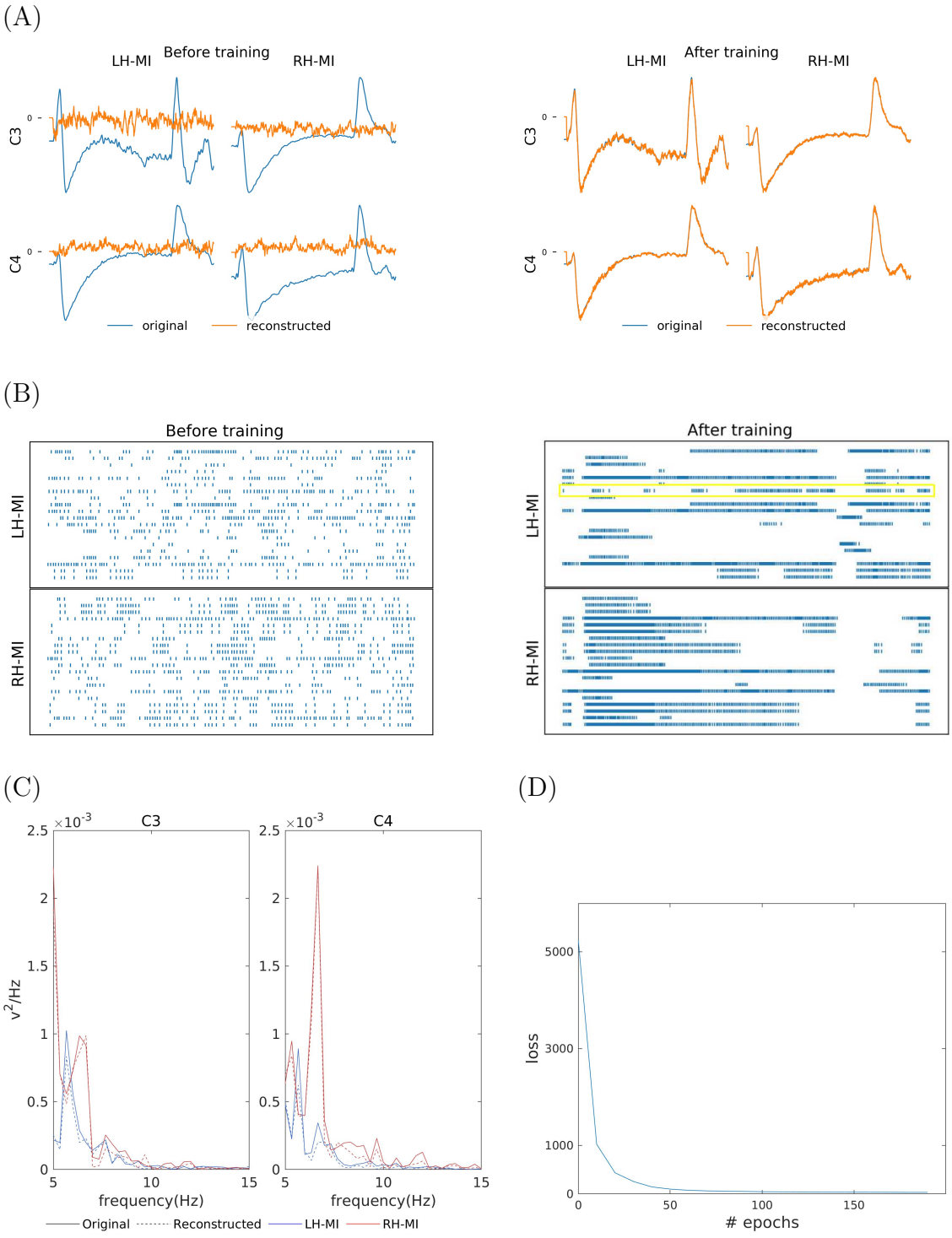

Figure 3.5 : The SNN for MI signal reconstruction showcasing the **(A)** template reconstruction, **(B)** randomly selected neuronal spike trains from the hidden layer, **(C)** power spectrum, and **(D)** mean square error loss.

3.4.2 The SNN for SSVEP

Steady state visually evoked potential is the other highly utilised modality for BCI communications. It is detected by the presence of high power at a frequency similar to the flickering stimulus visually focused on by a user. This signal is usually detected from the occipital region, and recordings are typically analysed from the O1, O2, and Oz electrodes (Zhang et al. 2013a). For example, if a user focuses on a 15 Hz flickering stimulus, the EEG signal from the occipital region displays high power at 15 Hz in the frequency domain. Since SSVEP has a high signal-to-noise ratio and is easily traceable with a single electrode, Oz channels data of 10 Hz and 11 Hz SSVEP were considered for the SNN-based reconstruction. Contrary to MI, the template signal from SSVEP data was extracted by averaging the available samples.

Similar to MI template reconstruction, one fixed 10 Hz Poisson spike train matrix for each class was used as the input to reconstruct the 10Hz and 11Hz Oz SSVEP signals. Since the targeted frequency lay in the low-frequency range, the dataset was band-pass filtered between 0.5 and 20 Hz and had a sampling rate of 250 Hz.

As shown in figure 3.6A–B, the original and reconstructed signal are similar. Also, the hidden layer's spike trains are reorganised after the SNN training process. The SNN training processes were able to successfully reproduce an EEG signal (orange line in figure 3.6A) closely matching the original template (blue line). Additionally, figure 3.6C shows the resemblance of the reconstructed signal's power spectrum (dashed line) to that of the training signal (bold line). For both the 10 Hz signal (blue line) and 11 Hz signal (red line), the reconstruction showed the presence of a strong peak (an SSVEP biomarker) at their respective frequencies in the power spectrum. According to figure3.6D, similar to MI, the loss (MSE) converged within a few epochs of the training process.

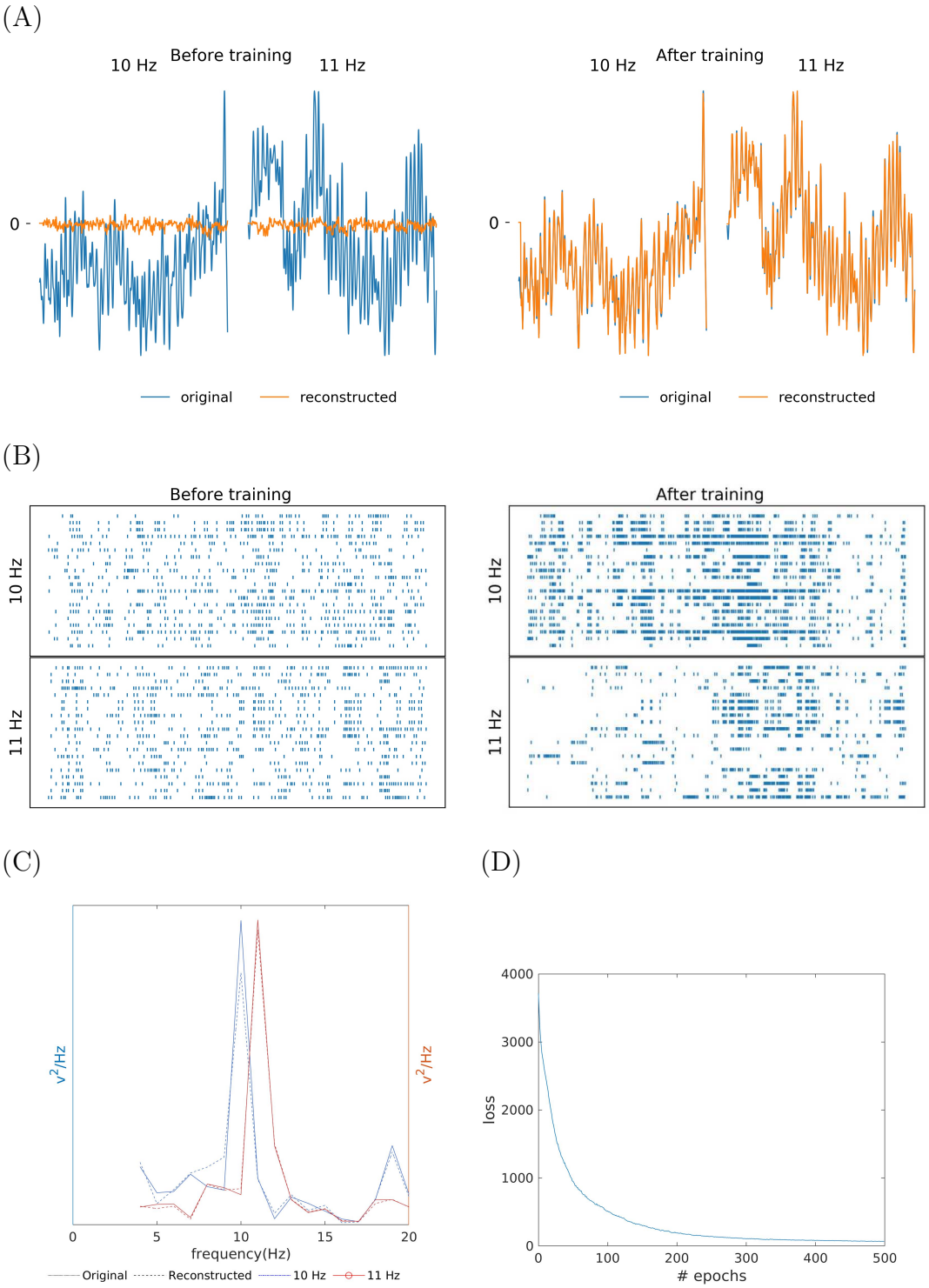

Figure 3.6 : The SNN for SSVEP signal reconstruction showcasing the **(A)** template reconstruction, **(B)** randomly selected neuronal spike trains from the hidden layer, **(C)** power spectrum, and **(D)** MSE loss.

3.4.3 Synthetic EEG Signal Validation

After successfully training the SNN to reconstruct an EEG signal, the neural perturbation layer was activated to generate synthetic EEG data. The number of Poisson neurons (or noise neurons) and the firing rate (or noise frequency) were varied to generate synthetic data in different variance levels. To validate the synthetic data, 100 samples per class were generated for a given combination of neurons and their firing frequency.

Two validation procedures were implemented, i.e. *validation-a*, wherein a classifier was trained with the original dataset and tested with the synthetic dataset, and *validation-b*, wherein a classifier was trained with the synthetic data and tested with the original data. These validations were performed independently, with the data generated by each perturbation combination (see figure 3.7). The classifiers used to validate the artificial MI and SSVEP data included CSP with LDA and multi-layer perceptron (MLP), respectively.

For MI, from figure 3.7A, it was observed that the synthetic EEG could be classified accurately when the classifier was trained with the original data (*validation-a*). Figure 3.7B shows that although the classification accuracies were not high for *validation-b*, the highest accuracy of approximately 80% was similar to the performance when the original dataset was used both for training and testing. These validations were done independently for each perturbation combination, ranging from 20- to 800-Hz noise frequencies and 10 to 220 noise neurons. This suggested that the generated synthetic data covered the broad variance of the EEG samples. Similarly, for SSVEP, figure 3.7C-D shows that the synthetic SSVEP passed the validation check with high accuracy. In addition to successful classification, the synthetic data yielded the highest accuracy of approximately 90% when used as a training dataset.

For SSVEP, the perturbation covered a range of 10-50 noise neurons and 10- to 850-Hz noise frequencies. Similar to that of MI, the SSVEP synthetic validation was done independently for each perturbation combination. Overall, these validation results showed that in addition to reconstructing the EEG signal, the SNN could

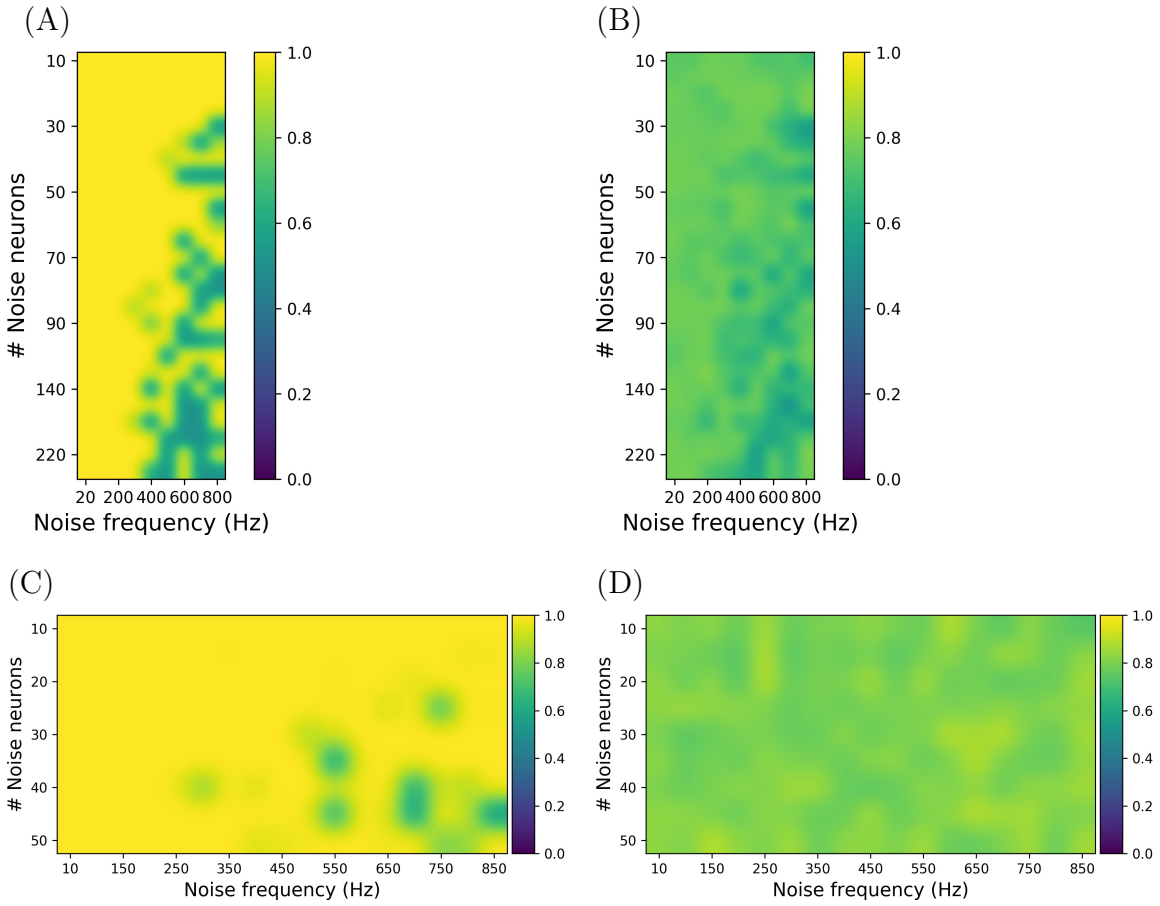

Figure 3.7 : Evaluating synthetic MI and SSVEP data generated from different combinations of the number of noise neurons and the firing frequency in the perturbation layer.

be used to generate synthetic EEG samples that are in agreement with the original samples.

The configuration of the perturbation layer (i.e. the combination of the number of noise neurons and their firing rate) could be changed to generate data at various scales (or different levels of noise) from the template. A small number of neurons with low firing rates tended to produce EEG trials that were highly similar to the template, while a perturbation layer with a huge number of neurons and a high firing rate completely distorted the synthetic samples of the template. To further check the effect of perturbation combination of artificial data, Pearson's correlation, a

metric for estimating the linear correlation between two variables was implemented. Figure 3.8 shows that for a given EEG channel of a given class (in this case, the RH-MI's C4 channel), the correlation between the averaged (100 samples) synthetic sample and the template was inversely proportional to the number of neurons and the firing rate of the perturbation layer.

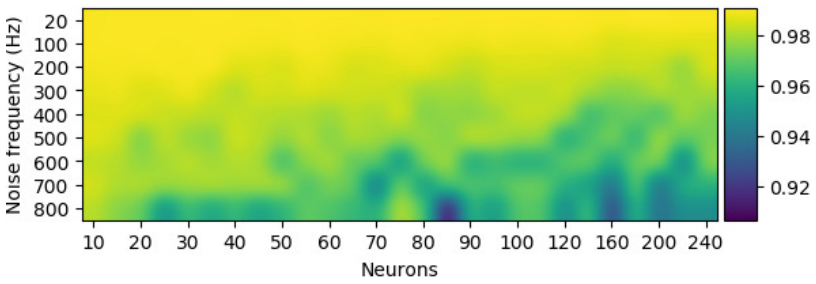

Figure 3.8 : Pearson's correlation between the synthetic samples and the template signal.

3.4.4 Classification

Since detecting reliable MI features is difficult in comparison to detecting SSVEP features, we focused on the classification efficacy of MI-BCI using artificial data. Therefore, to assess synthetic MI-EEG data, similar to *validation-b*, a classifier was trained with synthetic data (100 samples per class) and tested with the original data. For a baseline comparison, a 100-fold cross-validation process was applied for the original data, in which the original data were used for both training and testing. For each fold, 95% of the original data (samples were randomly selected) formed a training set, and the remaining 5% of the original data were labelled as a test set. This process was repeated for each fold and average accuracy across the fold is estimated to be the baseline accuracy. The synthetic data generated by the perturbation configuration that resulted in the highest accuracy during the validation process (from figure 3.7B) were used as the final artificial dataset. This process was verified with multiple publicly available datasets (see Section 3.3.1).

Table 3.1 showcases the accuracy obtained by the synthetic data with LDA, SVM, KNN, and Gaussian classifier. Each classifier was implemented on each dataset

and in total, 13 different datasets were used in this study. When trained with synthetic data, all classifiers were able to successfully predict the labels of the original samples, and the overall performance was comparable to the baseline performance. In particular, using LDA resulted in the highest baseline performance of 70.78%, as commonly stated in the literature, and the generated synthetic data enhanced the performance to 72.71% with LDA. Considering all classifiers, a given dataset showed enhanced performance with the synthetic data. Interestingly, for a few datasets, the synthetic data could enhance the classification performance up to 9% (e.g. dataset 4 with Gaussian classifier). As a cross-validation approach was used to obtain each dataset's baseline accuracy and the distribution of these accuracies across the datasets was unknown, a Wilcoxon signed-rank test was implemented for statistical significance analysis (between the performances with the synthetic data and original data) and obtained a p-value < 0.01 for all classifiers.

3.4.5 Comparing SNN and GAN

We compared recently published generative models and GAN variants, such as VAE, W-GAN, and DCGAN, and class-conditioned W-GAN (cc-WGAN) (Aznan et al. 2019; Panwar et al. 2020), with the SNN for the MI data generation and validation tests. The cc-WGAN model was used to generate MI data for a few datasets. Usually, GAN-based EEG synthesis normalises EEG data from 0 to 1 or -1 to 1, and the proposed SNN model can function at the original scales of the recorded data. Previous studies usually mixed the samples of original and artificial data for classification enhancement and often failed to perform *validation-b* (from Section 3.4.3). Any artificial data should pass this validation check to confirm that they represent the targeted data. To this end, in this study, for a fair comparison, data without normalisation from different generative models such as VAE, DCGAN, W-GAN, and cc-WGAN were considered for this check. From Table 3.2 below, it can be observed that the GAN variants, generated data performance was below the chance level and that the SNN generated data successfully passed this check.

Table 3.1 : Comparison of the classification performances with and without synthetic data for the MI datasets assessment using different classifiers.

Dataset	**LDA**		**SVM**		**KNN**		**Gaussian**	
	Original	Synthetic	Original	Synthetic	Original	Synthetic	Original	Synthetic
1	80.45	82.50	79.00	**83.13**	81.89	**83.13**	78.44	81.25
2	59.11	63.13	61.56	63.13	54.67	63.13	61.11	**63.75**
3	52.22	**61.25**	51.78	60.63	43.44	60.63	56.56	60.00
4	78.38	67.36	77.63	79.17	74.50	**81.94**	70.13	79.17
5	60.00	65.28	63.00	65.97	**67.75**	66.67	52.75	58.33
6	64.75	65.63	61.88	65.63	56.13	64.38	64.50	**68.75**
7	60.05	**65.83**	62.83	65.00	65.33	63.33	51.83	65.00
8	79.88	**80.71**	78.13	80.71	69.63	80.00	54.00	**80.71**
9	91.00	**93.13**	91.38	93.13	91.00	**93.13**	90.63	91.25
10	71.63	70.63	70.63	69.38	71.50	**72.50**	71.13	**72.50**
11	82.88	**85.00**	83.25	84.38	83.00	84.38	81.00	84.38
12	78.17	77.50	76.17	**78.33**	70.17	**78.33**	69.00	77.50
13	61.63	67.36	59.38	66.67	62.50	67.36	60.88	**70.14**
Avg	70.78	**72.71**	70.51	**73.48**	68.58	**73.76**	66.30	**73.29**

Table 3.2 : Comparison of the MI artificial data performances obtained by the SNN and different generative models.

Dataset	VAE	DCGAN	W-GAN	cc-GAN	SNN
1	50.00	43.75	54.17	50.00	67.36
2	50.00	45.83	50.00	50.00	65.28
3	50.00	50.00	49.17	59.17	65.83
4	65.71	48.57	50.00	76.40	80.71
5	91.25	88.75	50.00	50.00	93.13
6	51.25	65.00	46.88	50.00	70.63
7	83.13	83.13	83.13	82.50	85.00
8	50.00	55.56	50.00	40.00	67.36
Avg	61.42	60.07	54.17	57.26	74.41

3.5 Discussion

Understanding how chaotic neural activity reorganises to allow humans to perform a wide range of activities, such as walking, running, and speech, remains a topic of interest in the neuroscience community. Previous studies have trained models to produce such behaviour using different learning methods, such as FORCE, in both ANNs and spiking networks (Sussillo and Abbott 2009; Nicola and Clopath 2017; DePasquale et al. 2018). These enforced behaviours are periodic in nature, and training using non-stationary signals, such as EEG, is challenging, especially if the algorithm requires a large hyperparameter search space. Also, EEG signals vary for the same stimulus, i.e. no two EEG samples produced by the human brain are the same although they retain their prominent biomarker (e.g., ERD/ERS rhythm for MI and high power at a flickering stimulus frequency in SSVEP). Since EEG signals represents an accumulation of potentials of a spiking neuron, a primary focus of this study was understanding how the SNN's activity is organised to form EEG signals and, in turn, generate different samples while retaining the necessary biomarker. Therefore, this study developed a procedure with feedforward SNN and surrogate

gradient descent to reconstruct the EEG template in a supervised fashion and used neural perturbation to generate synthetic EEG signals. The proposed model was successfully applied for MI and SSVEP reconstruction, artificial data generation, and validation of the synthetic EEG through classification metrics. Additionally, the approach was compatible with other neuron models such as QIF and EIF at a computational cost (see figure 3.9-3.10). To the best of our knowledge, this is the first study to generate synthetic EEG signals using an SNN.

As previously stated, the primary aim of generating synthetic data from a machine learning perspective is to better train a classifier. As shown in Table 3.1, synthetic data can be utilised to enhance BCI performance, especially when the baseline performance of the dataset is low. Although the performance increment was not consistent among all datasets here, the proposed approach yielded a significant increase in performance for certain datasets.

In the field of machine learning, the current state-of-the-art model for data augmentation is the GAN and its variants. However, to generate artificial data, the GAN requires a huge amount of training samples, which we find to be counter-intuitive. Also, existing EEG-based GAN studies normalise the signal from 0 to 1 or -1 to 1 and often fail with EEG data at their original scales. In contrast, the proposed method needs only a few (one or two) samples to generatw artificial data and can handle both normalised and non-normalised EEG signals. To this end, we compared generative models and GAN variants, such as VAE, W-GAN, DCGA), and cc-WGAN, with SNN for MI data generation and validation tests. Previous studies usually mixed the samples of original and artificial data for classification enhancement, often failing to perform *validation-b*. According to table 3.2, we observed that the GAN generated data failed in this validation check with a below chance level. The reasons for this could vary, e.g. the random noise in the GAN generated data improved the performance by chance or the limited amount of data (the GAN was trained independently for each dataset containing approximately 180 trials) failed to capture the MI biomarker. Contrarily, the proposed SNN approach passed this validation check and delivered a close to baseline or improved performance. Another

(A)



(B)

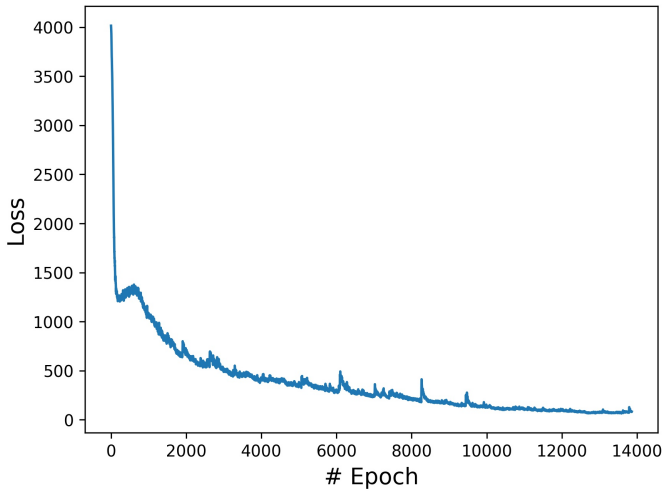

Figure 3.9 : **(A)** The reconstruction (orange line) of 12 Hz and 15 Hz SSVEP EEG signals using the QIF neuron model-based SNN based on original template signal (blue line). **(B)** The decrease in loss during the training period.

major reason for this could have been that since the SNN generate data based on a template signal, the artificial trials with a varying distribution retrained the MI

(A)



(B)

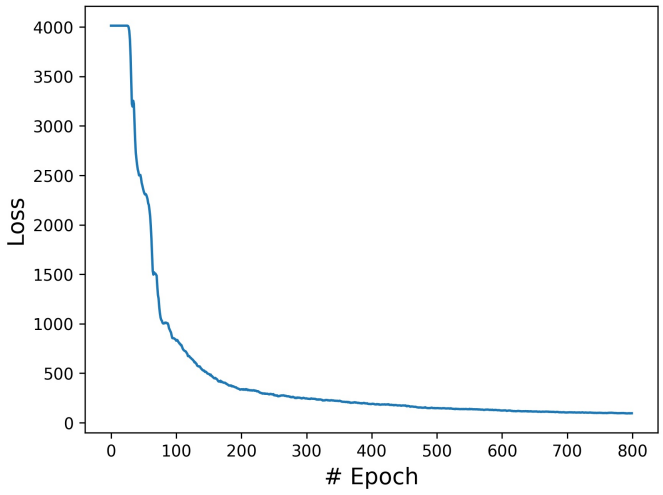

Figure 3.10 : **(A)** The reconstruction (orange line) of 12 Hz and 15 Hz SSVEP EEG signals using the EIF neuron model-based SNN based on the original template signal (blue line). **(B)** The decrease in loss during the training period.

biomarker, and it in turn was able to make the classifier extract better features. And, since GAN accounts for the whole dataset used for training, the artifacts and

noise present in the data could have led to the generation of improper samples. This hypothesis could be explored in the future to fine tune the GAN and SNN training samples. Also, theoretically huge number of artificial samples could generated depending on the properties of perturbation layer.

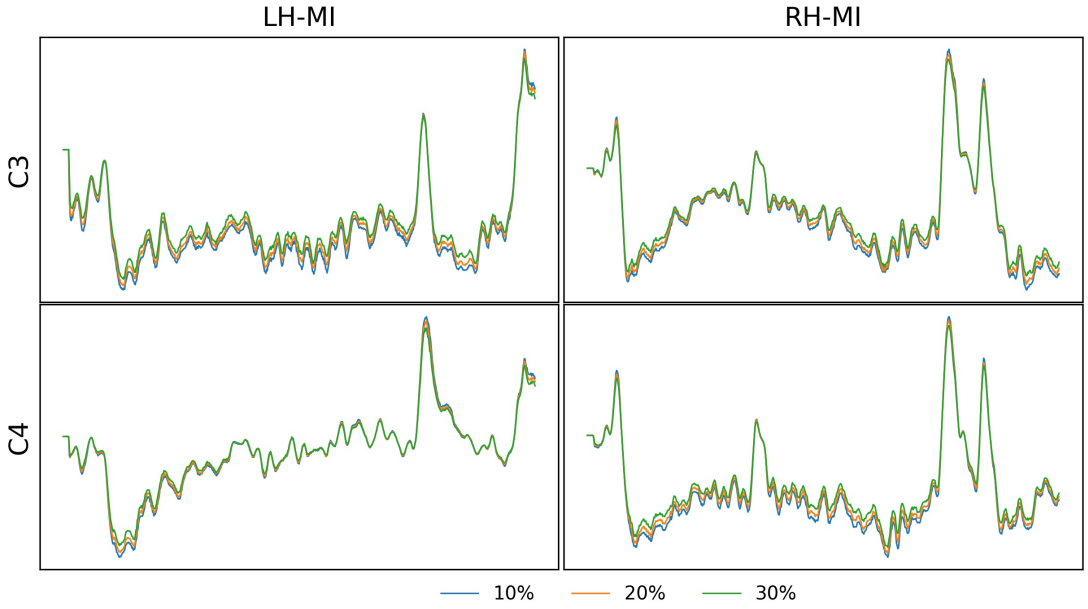

Figure 3.11 : The robustness of the SNN model with random disconnection of synapses for MI reconstruction.

In agreement with previous studies, interestingly, we observed a reorganisation of neural activity (i.e. spike train) concerning the output signal. For example, the SSVEP signal at a defined frequency was slightly oscillatory (like a sine or cosine wave), which was reflected in the periodic spiking activity of certain neurons in the output layer (see figure 3.6B). We further tested the proposed model for robustness by randomly clipping synapses and found that the overall signal trend was maintained despite the 30% reduction in synapses (see figure 3.11).

According to Dale's law, a neuron is only either excitatory or inhibitory (Capano et al. 2015). However, this constraint was omitted from this study for simplicity, although it would be ideal to enforce non-stationary behaviour, such as in EEG, to SNNs to maintain Dale's law in the future. Additionally, the current study, being

focused on MI and SSVEP data, considered only a few channels. However, the model was tested for reconstruction of different number of channels such as 4, 6, and 8 but the models limitation towards full set of channels is to be tested in future studies. Other minor BCI related concepts such as fatigue, attention, and other physiological factors distribute their features across a range of EEG channels. Therefore, another future direction of this study could be to test the limits of the model for BCI performance under the influence of physiological factors. Also, one limitation of this model is that it works for fewer classes and as such complex architecture need to be explored to generating many class data in the future direction. The SNN training process is considerably slow on CPU/GPU machines and such in future direction the ability of SNN signal generation on neuromorphic hardware can be explored for faster training.

Chapter 4

Spike-based EEG Representation

4.1 Abstract

A BCI relying on an EEG based neuroimaging mode has shown promise for real-world usage due to its portability and optional selectivity of fewer channels for compactness. However, noise and artifacts often limit the capacity of BCI systems, especially for event-related potentials such as P300 and ERN, whose biomarkers are present in short time segments at the time-series level. Contrary to EEG, invasive recording is less prone to noise but requires a tedious surgical procedure. Meanwhile, an EEG signal is the result of aggregation of neuronal spiking information underneath the scalp surface, and transforming the relevant BCI task's EEG signal to a spike representation could potentially help improve the BCI performance. In this study, we designed an approach using an SNN trained using surrogate gradient descent to generate task-related multi-channel EEG template signals of all classes. The trained model was in turn leveraged to obtain the latent spike representation for each EEG sample. Comparing the classification performance of the EEG signals and their spike representation, the proposed approach enhanced the performance of the ERN datasets with Naive Bayes and for the P300 dataset, the accuracy was improved using xGboost. In addition, the principal component analysis and correlation metrics were evaluated on both EEG signals and their spikerepresentation to identify the reason for such improvement.

4.2 Background

Rapid developments in EEG acquisition devices have enabled them to be user-friendly and portable and transit data wirelessly. In parallel, advances have been made towards bridging the gap between laboratory settings and real-world usage

by enhancing EEG-based BCI system's performance. To this end, studies have focused on the development of novel machine learning methods and feature extraction techniques to improve the BCI system performance. In particular, deep learning studies have shown promising results in this regard (Lawhern et al. 2018; Manor and Geva 2015). For example, Lawhern et al. (2018) introduced EEGNet based on a convolution neural network and has shown improved performance on various BCI modalities. However, a few shortcomings need to be accounted for to yield complete advantage of such a deep learning model e.g. the availability of a large sample of training data, more EEG channels, and fine-tuned model parameters. For example, Lawhern et al. (2018) used approximately 2000 samples for P300 classification, more than 6000 samples from Manor and Geva (2015) for RSVP classification, and more than 10000 samples by Ma et al. (2021). In practice, EEG data collections require a tedious experimental setup and are often time-consuming for a user to record huge datasets. Additionally, the noise and artifacts distort the recorded sample leading to lesser usable data for testing novel algorithms. Alternatively, classical techniques can be executed with fewer data samples but lack efficient feature representation. Previously, in table 1.1, we showcased how invasive methods provide additional advantages (much higher resolution and better signal quality) over EEG systems but at the cost of inconvenience and surgical requirement. However, EEG signals recorded over the scalp surface are the collective information of multiple neuronal action potentials underneath the surface. We hypothesise that extracting spiking information from EEG signals could potentially help advance the BCI performance. Additionally, the BCI performance enhancing techniques largely focus on EEG signal and its derivatives such as power spectrum, wavelet transform (Sadiq et al. 2019), component analysis (Chiappa and Barber 2006) etc. As depicted in figure 1.4, transforming EEG signal to spike representation could open new avenues for advancing BCI systems.

A model that naturally accommodates spiking information is an SNN mimicking the properties of the biological neural circuit, and such SNNs have been gaining traction in the field of machine learning (Woźniak et al. 2020; Bellec et al. 2018a).

For example, Bellec et al. (2018a) leveraged the adaptive properties of spiking neurons to obtain long short term memory (LSTM) equivalent performance. Similarly, a few studies have demonstrated the efficiency of SNNs in speech recognition (Wu et al. 2020), objection detection (Kim et al. 2020), and language modelling (Woźniak et al. 2020). Also, SNNs have been examined for their ability to classify different EEG signals. For example, Antelis et al. (2020) encoded MI-based EEG signals to spiking data to assess the classification performance of SNNs. Apart from BCI applications, a few EEG-based studies have shown that SNNs can also be adopted as classifiers for emotion recognition (Luo et al. 2020), seizure detection (Ghosh-Dastidar and Adeli 2009), the understanding of functional connectivity changes due to mindfullness training (Doborjeh et al. 2019), and depression (Shah et al. 2019). These mentioned studies assumed SNNs to be a classifier as a standard notion similar to ANNs, where the input (such as an EEG signal) is provided to the network and outputs a class label.

In addition to classification, our previously mentioned research problem (see chapter 3) showed that SNN can be adopted as a generator model to efficiently generate artificial EEG signals to tackle the data augmentation problem of MI-based BCI systems and improved the performance (Singanamalla and Lin 2021). In continuation of our previous work, we believe that reverse engineering SNNs to extract spiking information from EEG signals could provide additional features and improve BCI system performance. Similar to our previous work, the developed SNN was trained to produce task-relevant multi-channel EEG template signals. However, a major difference in this study was that instead of using a trained model to create artificial samples, the model was used to extract spike representations of the EEG samples, and this spike representation was evaluated against the baseline EEG classification performance. Major bottleneck issues for the practical outdoor usage of a BCI system are the noise, artifacts, and fewer channels (for compactness). These particularly affect the BCI paradigms (such as P300 and ERN) that depend on time-series data as features. Until now, the P300 and ERN studies still depend on segments of time-series data from multiple channels as a feature vector

for performance enhancement. For example, Liu et al. (2018) used 667 ms of EEG segments from event onset of 64 channels as input to convolution neural network (CNN), 1000 ms of 16 channel data with SVM (Karimi et al. 2019) and deep belief networks (Cortez et al. 2020), 800 ms of 32 channel data with SVM & CNN (Lee et al. 2020), 400 ms of 17 channel data with LDA (Vařeka and Ladouce 2021), and 1000 ms of 8 channel data with convolution recurrent neural network (CRNN) (Sahay and Brinton 2021). Table 4.1, showcases a summary of the list of P300 studies and their adopted features. Also, these studies selected many channels for classification purposes. Therefore, for this study, two different BCI modalities, P300 and ERN, were primarily focused on for performance enhancement with spike representation time-series data. In addition, considering the above-mentioned bottleneck issues, datasets with limited channels and fewer samples were considered to evaluate the proposed approach. Based on the results, we observed that the proposed approach could potentially improve the BCI performance. This study further explored the reasoning as to why there was a performance enhancement due to the spike representation.

Table 4.1 : A brief list of recent P300 studies and their advised features and number of channels for classification.

Study	**Feature**	**Channels**
Liu et al. (2018)	time-series	64
Karimi et al. (2019)	time-series	16
Cortez et al. (2020)	time-series	16
Lee et al. (2020)	time-series	32
Shukla et al. (2021)	Wavelet transform	17
Cruz et al. (2021)	Spatial filters	12
Vařeka and Ladouce (2021)	time-series	17
Sahay and Brinton (2021)	time-series	8

4.3 Methods

4.3.1 SNN Architecture

A recurrent based SNN model (RSNN), in which each node is based on a simplified LIF model (equation 2.5-2.6), was used in this chapter for producing EEG signals. Similar to Singanamalla and Lin (2021) (Chapter 3), since the source spiking information that generated desired the EEG signal was often not available, the input layers generated spike trains adhering to the Poisson distribution with a firing rate of 10 Hz. These spike trains were then processed via the RSNN population. Since the EEG signal was continuous, contrary to the spike trains (a discrete time series), a double exponential synaptic filter (see equation 2.11-2.12) was applied to the neural activity of the RSNN to smoothen the spike trains, denoted as a latent layer. The filtered spike trains were then weighted averaged to produce multi-channel EEG signals. An overview of the proposed architecture is depicted in figure 4.1. The proposed architecture comprised a different number of nodes (or neurons) in each layer as follows: 50 for the input layer, 100 for the RSNN, 100 for the latent layer, and two for the output layer. The model was built using *pytorch*, a popular Python-based deep learning library, and the weight connections between all layers and recurrent weights within the RSNN were trained using surrogate gradient descent (see section 2.3) with the *Adam* optimiser.

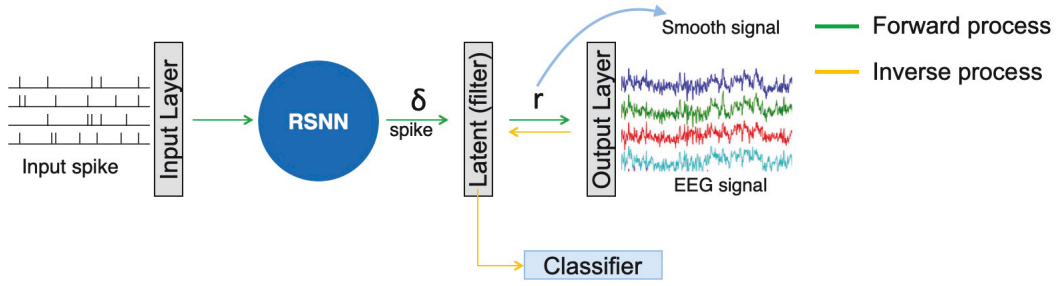

Figure 4.1 : The RSNN model executing two stages: 1) the forward process in which the SNN generated template EEG signals and 2) the inverse process in which the non-template signals were transformed to spike representations for classification.

In a given EEG dataset, no two samples are the same for a defined stimulus.

So, training the model for each EEG sample independently to obtain latent information (i.e. the spike representation of the EEG sample) would be computationally demanding. Therefore, a representative EEG signal, called the template EEG, was initially obtained from a given dataset for the training process. As suggested in Singanamalla and Lin (2021) (Chapter 3), a classifier was trained and tested with a dataset, and the sample with the highest probability of being categorised correctly into its respective class was considered the EEG template. And, only the test sample is used for SNN template reconstruction purpose and the rest of the samples were used for evaluation.

The model was implemented in a two-stage process comprising the *forward process* and *inverse process*. In the *forward process*, the model was trained using surrogate gradient descent to reproduce the multi-channel EEG templates of a given dataset. Following this, the *inverse process* transformed each of the non-template signals (i.e. samples other than those of the template in a given dataset) to their spike representations by equation 4.1 in which the pseudo-inverse of the trained weights (connecting the latent layer to the output layer) was multiplied by the EEG samples.

$$r_j = W_f^{-1} * EEG_j \tag{4.1}$$

where W_f is the trained weight matrix from the latent layer to EEG signal output.

4.3.2 EEG Processing

Two types of ERP signals, ERP and P300, were considered for this study. The datasets are publicly available from Van Veen et al. (2019) and Kappenman et al. (2021). A standard EEG processing pipeline containing bandpass filtering between 0.5- to 45 Hz, epoch extraction, and channel selection were applied to each of the datasets. For both the ERN and P300 datasets, 20 subject datasets were considered. A template EEG signal was extracted (as mentioned in Section 4.3.1) for each subject dataset independently and smoothed using a moving average window. This template was later utilised to train the SNN model.

4.3.3 Classification

For the ERN and P300 signals, the EEG time series data were considered the features for classification. The most predominantly used classifiers for both ERN and P300 include SVM, Gaussian classifiers, and tree-based algorithms (Ventouras et al. 2011; Chavarriaga et al. 2014; Sarraf et al. 2021). Therefore, this study adopted these classifiers to assess the baseline EEG classification accuracy. For a fair comparison, the spike representations (with both LIF-based SNN) of the EEG signals were classified with the same classifiers. A 5x10 fold cross-validation (CV) was applied for each subject dataset and the overall performance of the given subject dataset was the average of all folds. To test the significance of the performance improvement with spike representations, a two-sided Wilcoxon signed-rank test was performed on the classification accuracies obtained from each classifier independently. Refer to Section 4.4.2 for the outcomes of the classification and significance test results.

4.3.4 Explainability

Based on the classification results (see Section 4.4.2), we observed that the performance was enhanced above the baseline by transforming the EEG signals to spike representations. Debugging the reasoning behind such accuracy enhancements could aid in understanding the neural origins of EEG signals and why EEG signals are often ineffective compared to invasive electrode recordings. Principal component analysis (PCA) was applied to the EEG data and the corresponding spike representations to estimate the variance explanation ratio. This assisted in exploring whether the proposed approach was able to extract novel features (or more independent variables). In addition, we compared the confusion matrix analysis and correlation properties to explore the attributes of the spike transformed data.

4.3.5 Contrastive learning

The spike representations achieved with an SNN depend on the similarity of the original and the reconstructed EEG signals. In section 4.3.1, this fitness function or similarity was based on the MSE loss function between the original and reconstructed signal. In recent studies from deep learning, a category of methods called

Representation learning gained attention due to their ability in providing meaningful information from the data (Le-Khac et al. 2020; Bengio et al. 2013). Under this, contrastive learning methods showcased significant improvements towards classification performance.

The role of contrastive learning is to increase the similarity between positive samples and decrease the similarity between a positive & negative sample. The contrastive learning methods were adopted into different training processes such as supervised, unsupervised, and reinforcement learning. For example, Mohsenvand et al. (2020) introduced a contrastive learning framework, SeqCLR, and enhanced the performance of different EEG benchmark datasets such as SEED, TUH, and SleepEDF. Similarly, the contrastive learning variants were applied to other EEG-based tasks such as MI (Han et al. 2021), stroke detection (Fawaz et al. 2020), and obtain subject-invariant representations (Shen et al. 2021). Recently, Khosla et al. (2020) introduced supervised contrastive learning in which a sample is considered positive or negative based on its label. As such, they achieved significant improvement in various image datasets. Considering such contrastive property during SNN training could potentially further enhance the classification accuracy. Therefore, we added a similarity loss function between the latent representation of two different classes, as shown in equation 4.2, to the MSE loss function of the SNN template training procedure to validate our hypothesis.

$$\mathcal{L} = u^T \cdot v \tag{4.2}$$

where u and v are the linearised spike representation of the target and non-target template signals respectively.

4.4 Results

4.4.1 SNN Training

For each subject dataset, a new instance of the model (LIF-based SNN) was trained to generate a set of EEG template signals. In the case of the ERN and P300 datasets, this set comprised two template signals (one from each class denoted as

target and non-target). Accordingly, two Poisson spike trains (at 10 Hz rate) were initialised to act as input signals to the SNN model. For some subjects as shown in figure 4.2A and figure 4.3A, the model was able to reproduce these template EEG signals for both the P300 and ERN signals. Also, it could be observed that the RSNN activity was rearranged during the training process for both the ERN (see figure4.2B) and P300 EEG signals (see figure 4.3B).

(A)

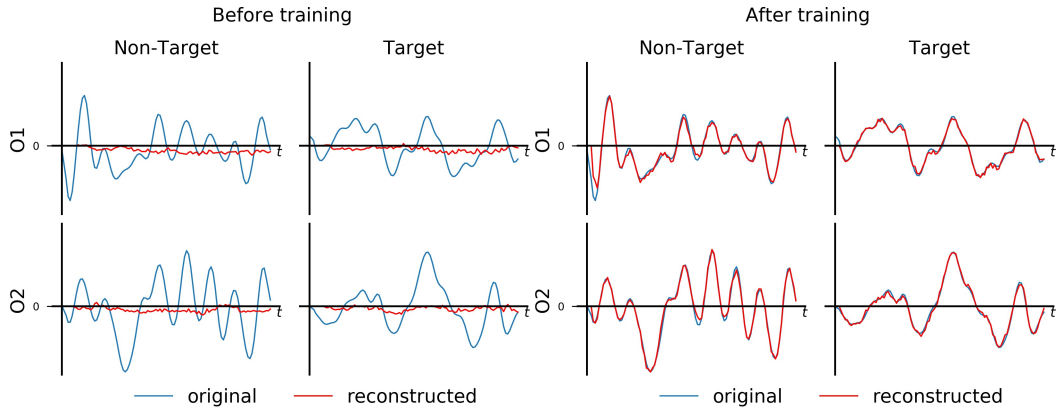

(B)



(C)

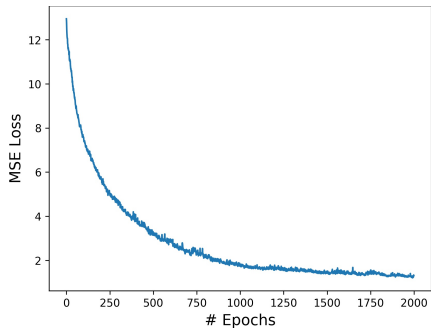

Figure 4.2 : The SNN model training for P300 signal showcasing the **(A)** signal reconstruction, **(B)** spike trains of RSNN activity, and **(C)** MSE loss.

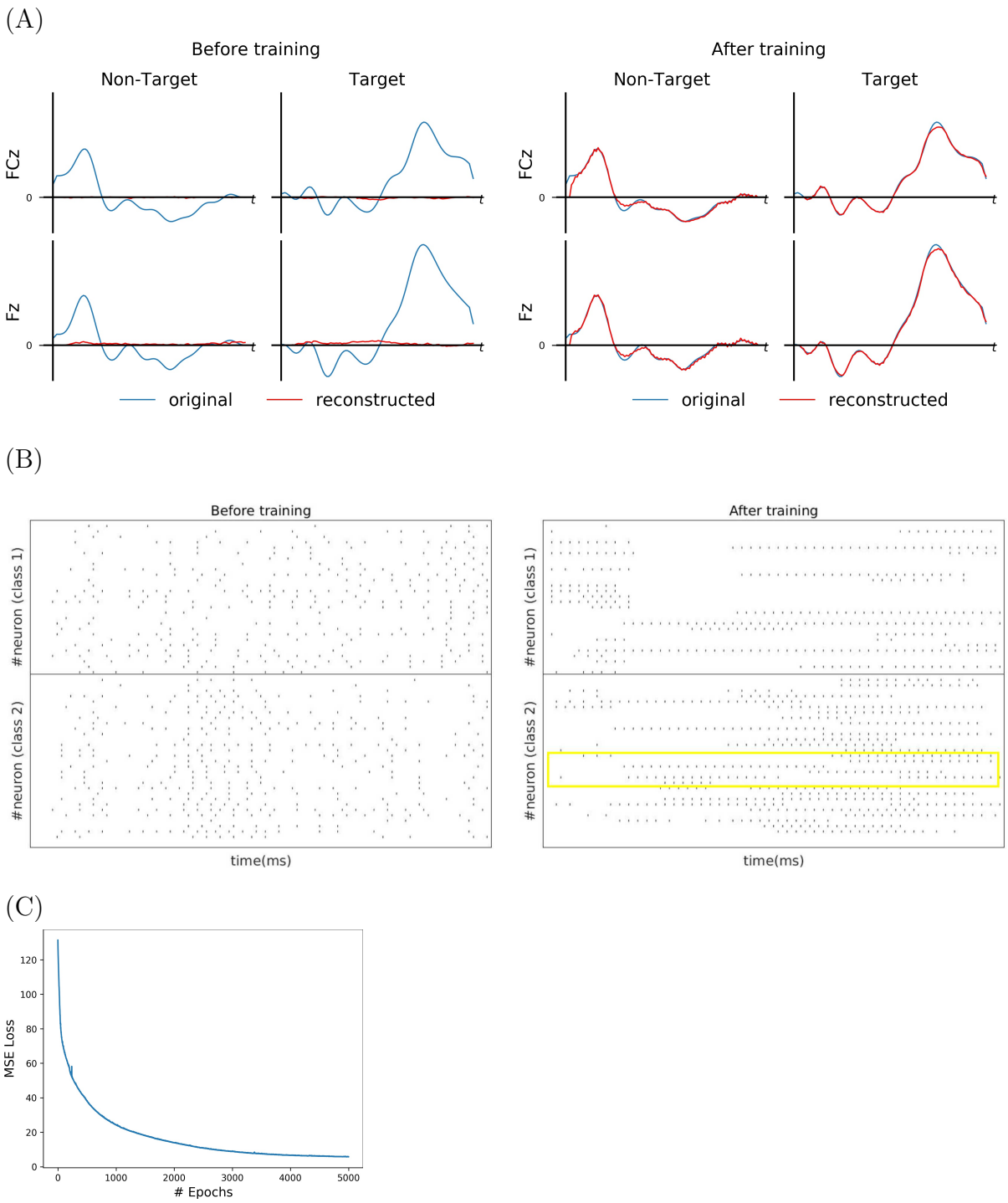

Figure 4.3 : The SNN model training for the ERN signal showcasing the **(A)** signal reconstruction, **(B)** spike trains of RSNN activity, and **(C)** MSE loss.

Since the objective of the model was to reproduce a time series signal (i.e. the EEG template), an MSE loss function was adopted as a cost function. From figure 4.2C and figure 4.3C, it could be observed that this loss converged quickly for both the P300 and ERN EEG signal generations. Since P300 is a binary class (target and non-target class) system, we obtained two EEG templates, one for each class.

4.4.2 Classification

P300

In the P300 analysis, 20 subject datasets from an open source repository by Van Veen et al. (2019) were considered for this study. The datasets were pre-processed according to the pipeline mentioned in Section 4.3.2. As previously mentioned, due to the limits of practicality, only two channels that contributed to the P300 bio-marker, FCz and Fz, were considered for the process. To extract the template signal from a given subjects' dataset, all samples in the dataset were used for both training and testing with the SVM classifier. The sample that obtained the highest probability of being correctly categorised into its class was considered as the template signal.

After training the model to generate this EEG template, each of the remaining samples in the data (i.e. non-template) were converted to its spike representations through equation 4.1. Then, different classifiers such as SVM, Naive Bayes (NVB), and xGboost were used to compare the performance of EEG signals (baseline performance) and their respective spike-representation signals. For each subject, the classification accuracy represented the average of a 5x10 fold CV, in which each fold was executed with 90%of the randomly selected samples as the training set and the remaining percentage as the testing set. As shown in Table 4.2, using xGboost, spike representations of the EEG signals has obtained an average accuracy of 69.56% and exceeded the baseline performance (EEG signal classification accuracy) of 67.73%. Here, the column name LIF represent the performance of spike-representation obtained via LIF-based SNN.

In addition, a few subjects (such as S13 and S19) showcased significant improve-

ment from the baseline performance by up to 5%-7%. A one-sided Wilcoxon-signed rank test was applied between the accuracies obtained from the EEG signals and their spike representations from each classifier separately. This statistical significance analysis resulted in a p-value < 0.05 for all classifiers.

Table 4.2 : Comparison of the classification performance of the P300 based EEG signals and their spike representations by the SNN using different classifiers.

Dataset	**SVM**		**NVB**		**xGboost**	
	EEG	LIF	EEG	LIF	EEG	LIF
S1	69.39	75.39	76.03	77.52	71.02	71.61
S2	69.70	70.63	71.36	72.78	68.47	68.05
S3	66.69	70.91	69.42	70.36	67.99	71.37
S4	72.94	77.96	82.18	84.20	83.09	83.27
S5	58.66	62.96	62.78	63.24	61.24	65.04
S6	70.50	74.89	66.31	71.58	69.57	71.91
S7	61.14	67.80	67.16	67.70	66.88	66.19
S8	70.50	74.81	66.31	71.42	69.57	71.91
S9	67.54	69.29	70.32	69.99	72.60	71.89
S10	57.33	58.59	58.91	61.22	59.63	58.35
S11	62.29	63.75	58.38	63.40	65.62	66.41
S12	81.69	82.95	76.26	83.21	84.86	86.23
S13	57.90	60.01	60.43	60.96	55.88	62.66
S14	54.77	57.01	56.98	57.99	57.83	59.66
S15	62.82	63.40	64.28	66.79	63.94	62.71
S16	64.18	69.81	66.57	71.16	67.22	69.70
S17	67.16	68.01	64.99	65.33	70.84	74.06
S18	60.95	68.26	65.00	66.83	64.60	68.95
S19	69.89	69.18	72.44	71.50	68.65	73.70
S20	59.24	63.41	64.58	63.20	65.08	67.48
Avg	65.26	68.45	67.04	69.02	67.73	**69.56**

ERN

The SNN model training process for ERN was similar to the P300 except that the channels selected for this dataset were Pz and Oz. In total, 20 subjects' datasets were considered to assess the spike-representation competency for this BCI mode. Similar to the P300 assessment in Section 4.4.2, the template signal for each subject was extracted based on the probability (obtained by SVM) of each sample being categorised into its respective class. The classification performance of each ERN signal and its spike representation was evaluated using SVM, NVB, and xGboost classifiers. As shown in Table 4.3, with NVB, the spike representations of the EEG signals obtained an accuracy of 82.27% and exceeded the baseline (EEG) performance of 79.22%.

In addition, a few subjects (such as S15) showed a significant increase (up to 7%) with spike representations. Similar to P300, the statistical significance analysis for ERN using the one-sided Wilcoxon signed-rank test has also resulted in a p-value $<$ 0.05 for all classifiers.

To further assess the impact of the SNN on performance improvement, we have transformed the ERN signal to a high dimensional signal (in equation 4.1) in two ways as a controlled study via 1) using a random weight matrix (of normal distribution equivalent to the initialised SNN weights) and 2) using a liquid state machines (LSM; based on LIF) in which all RSNN related weight matrices (feedforward and recurrent) were fixed, except for the output layer weights that converted filtered signal r to an EEG signal during the model training process. The performance of the transformed signal with these two approaches was estimated using NVB, as it obtained the best performance previously. As shown in Table 4.4, the average performance with random weight was 80.70% (p-value = 0.287 with one-sided Wilcoxon test), and that with the LSM was 81.83% (p-value = 0.74). The effect of the SNN's trained weights onthe performance was not significantly higher than that of these control methods but provided an additional edge in the average performance.

Table 4.3 : Comparison of the classification performance of the ERN based EEG signals and their spike representations by the SNN using different classifiers.

Dataset	**SVM**		**NVB**		**xGboost**	
	EEG	LIF	EEG	LIF	EEG	LIF
S1	69.45	67.56	77.73	80.21	74.44	74.27
S2	92.83	93.00	91.83	91.83	80.67	82.00
S3	77.25	76.39	75.00	78.44	70.92	81.69
S4	86.52	86.12	88.73	89.44	86.05	89.51
S5	70.22	72.02	76.15	76.95	79.06	75.10
S6	81.67	86.33	91.67	93.67	69.67	73.33
S7	81.51	82.80	72.60	76.18	78.98	85.36
S8	69.30	72.78	63.78	58.53	64.68	74.23
S9	78.00	76.52	80.43	83.76	78.81	78.81
S10	87.29	86.73	88.27	90.52	90.41	89.61
S11	77.87	80.00	84.00	86.00	85.60	83.07
S12	67.00	73.67	76.33	75.33	53.33	80.67
S13	87.60	88.76	90.96	91.36	90.96	88.78
S14	81.09	81.71	87.56	89.02	90.64	87.80
S15	84.30	91.30	83.10	90.60	80.80	89.60
S16	55.00	61.00	59.00	63.67	63.67	60.67
S17	77.00	80.00	73.00	95.00	90.00	90.00
S18	79.87	79.60	79.76	82.02	81.60	79.60
S19	71.38	72.77	76.77	78.62	78.15	82.92
S20	80.04	85.63	67.81	74.27	74.32	80.83
Avg	77.76	79.73	79.22	**82.27**	78.14	81.39

4.4.3 Confusion Matrix

From tables 4.2-4.3, it could be observed that spike representations could improve the classification performance. However, the classification metric alone did

Table 4.4 : Comparison of the classification performance of the ERN dataset via NVB for the transformed signal with random weight and LSM.

Dataset	**Random-W**	**LSM**
S1	79.35	82.12
S2	91.83	89.17
S3	77.56	77.25
S4	89.86	88.71
S5	76.81	76.81
S6	93.00	93.67
S7	74.36	76.40
S8	61.56	59.20
S9	82.00	81.24
S10	89.33	91.88
S11	85.60	86.27
S12	70.33	72.33
S13	91.33	92.15
S14	87.96	90.29
S15	90.50	89.70
S16	70.79	72.38
S17	60.00	62.00
S18	85.00	94.00
S19	82.02	82.22
S20	76.62	78.92
Avg	80.79	81.84

not provide enough details on the model performance. Therefore, a confusion matrix analysis with the xGboost classifier was performed on a select subject from both the ERN and P300 datasets that had significant improvement over the baseline performance. Based on figure 4.4, we found that for ERN, the proposed approach increased both the true positive and false negative results. This indicated that the

spike representation was able to account for the patterns of both the target and non-target samples and improved their detection rate. Similar behaviour was identified for the P300 dataset as well (see figure 4.5).

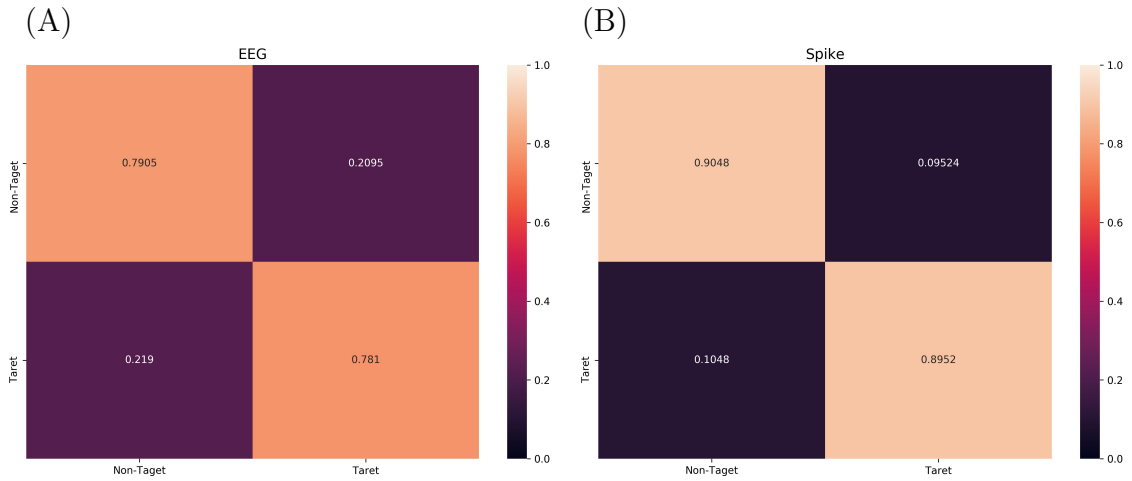

Figure 4.4 : Confusion matrix analysis of the **(A)** EEG signals and **(B)** spike representation of the ERN dataset.

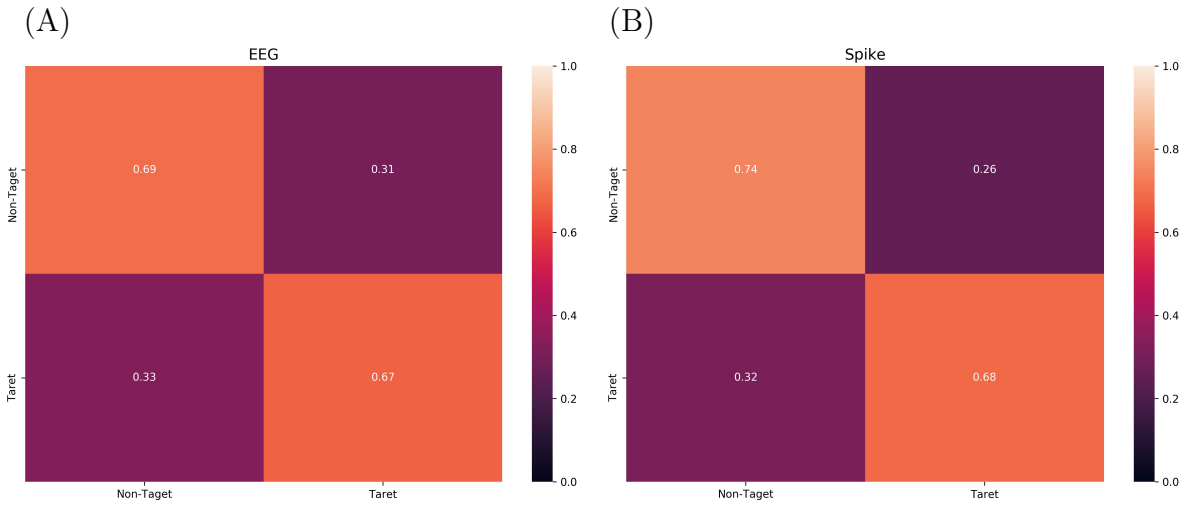

Figure 4.5 : Confusion matrix analysis of the **(A)** EEG signals and **(B)** spike representations of the P300 dataset.

4.4.4 Explainability

Though the EEG signals and their spike representations were directly analogous, the spike representations of the data were able to provide better performance. Exploring the reason behind the performance enhancement could help further improve the credibility of BCI systems. To this end, PCA and correlation measures were applied to both the EEG signals and their spike representations data to assess the internal factor that led to the performance enhancement.

Variance explanation analysis

Commonly, not all variables in a dataset are useful to provide meaningful information. Variance explanation analysis is often used to measure the ratio of information represented by principal components. In other words, it helps to identify the fraction of data variability contributed by a given set of independent variables (features). In this study, we intended to explore whether the spike representations of EEG signals provided additional information to improve the accuracy. Using PCA, we analysed this metric on the EEG signal and its spike-representation. As shown in figure 4.6, it could be observed that for a given dataset from ERN, the spike representation (red line) required more components than the EEG signal (blue line) to explain 75% (black line) of the variability in the data. This could imply that the proposed method was able to extract more unique independent features from the spike representation of the data and that this could, in turn, enable the classifier to induce better classification. Similarly, figure 4.7 showcases a similar observation for the P300 datasets.

Correlation analysis

To further understand the reason for the performance enhancement, we analysed the similarity among the EEG samples and their respective spike representations. To this end, the correlation between all samples of a given ERN dataset was estimated using Pearson's correlation technique. figure 4.8, showcases the correlation matrices for all EEG samples and all spike representation samples and the difference between these two matrices (the Spike-EEG sub-plot). Each pixel represents the correlation

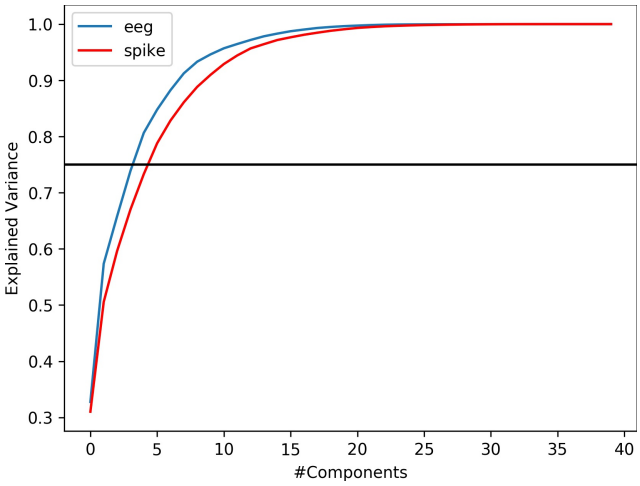

Figure 4.6 : The PCA-based variance explanation of the EEG signal (blue line) and its corresponding spike representation (red line) for the ERN dataset.

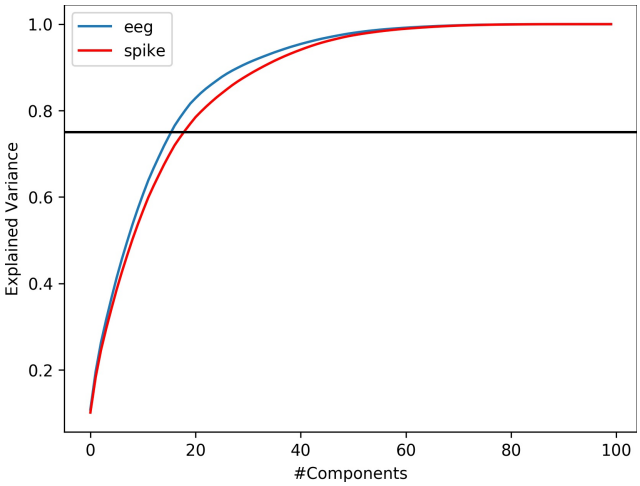

Figure 4.7 : The PCA based variance explanation of the EEG signal (blue line) and its corresponding spike representation (red line) for the P300 dataset (S13).

between any two samples. It could be deduced from the Spike-EEG plot that the correlation among the spike representation samples was slightly higher than that among the EEG samples. This could imply that the proposed approach tended to enhance the similarity among the samples of a given class (i.e. target and non-target classes) and that this in turn increased the performance. A similar increase in correlation for the P300 dataset is shown in figure 4.9.

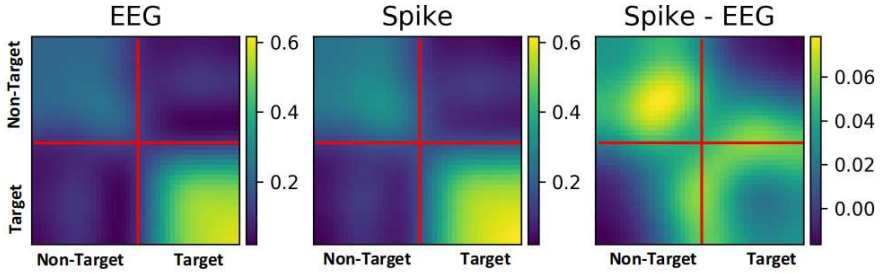

Figure 4.8 : The Pearson's correlation among all samples in the ERN dataset for both the EEG signal and its spike representation.

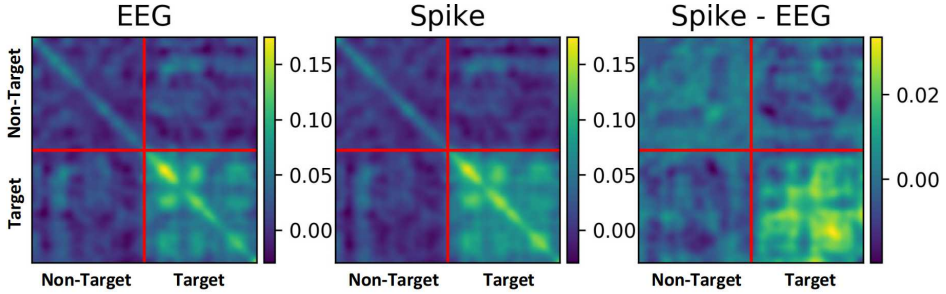

Figure 4.9 : The Pearson's correlation among all samples in the P300 dataset for both the EEG signal and its spike representation.

4.4.5 Node Prioritisation

For both the ERN and P300, their prominent bio-marker (feature) can be found directly through their time-series signal. However, each subject's EEG template is unique, and it is possible for the template to even contain noise and information irrelevant to the biomarker. Therefore, the number of nodes in an RSNN required to generate an EEG template may vary depending on the complexity (i.e. variance) of the signal. As a result, we hypothesise that not all nodes in an RSNN may contain reliable information and that considering only a few nodes' activities (referred to as node prioritisation) could further improve the classification performance. In this study, the nodes with weights (from the latent layer and output layer) that fell outside the $\mu \pm 1.5 * \sigma$ range were assumed to be major contributors of EEG signals, and as such, only these nodes' activity was considered from spike representation of the EEG data. Here, μ and σ represent the mean and standard deviation of

the weight distribution obtained after training the model. Also, it was possible that such prioritisation would not be ideal for all subjects. For this reason, we compared different modes: a) node-prioritisation (NP) and b) threshold-based node prioritisation (TNP). For the threshold-based approach, we estimated the variance of the EEG template signal from each subject and considered the median value (from all variances) as a threshold for determining whether to apply NP for a given subject dataset. In other words, NP was applied to the subject data whose template signals had higher variance. As shown in Table 4.5, for ERN, the two mentioned prioritisation modes improved the performance by a minor fraction compared to the performance of the original spike representation (WNP). A similar observation was seen for the P300 dataset as well (see table 4.6).

4.4.6 Contrastive Learning

Spike representation extraction process with the procedure established in Section 4.4.1 was implemented with the addition of contrastive loss function (see equation 4.2) during the training process. Since xGboost and NVB showed the best performance with P300 and ERN, respectively, spike representation obtained through contrastive learning was evaluated with these classifiers. As shown in table 4.7–4.8, the average performance slightly increased in comparison to the values from table 4.1 and 4.2, indicating that the contrastive learning provided a minor edge in performance enhancement.

4.5 Discussion

Often, EEG signals are noisy and affect the performance of BCI systems. In addition, ERP-based BCI modalities such as ERN and P300 explicitly rely on the time-series segment of a signal to identify the biomarkers. As such, they are often susceptible to noise and artifacts. Broadly, an EEG signal is the result of an accumulation of neural spiking information beneath the scalp surface. Theoretically, though invasive recording is less prone to noise and contains robust information compared to EEG, it requires complex surgical effort. Extracting such spiking information responsible for an ERP could potentially help in understanding the internal processes

Table 4.5 : Comparison of the classification performance of the spike representation of the ERN datasets with xGboost under different prioritisation conditions.

Dataset	**WNP**	**NP**	**TNP**
S1	74.27	74.82	74.27
S2	82.00	83.67	82.00
S3	81.69	81.47	81.47
S4	89.51	90.10	90.10
S5	75.10	75.51	75.51
S6	73.33	73.67	73.33
S7	85.36	83.44	83.44
S8	74.23	69.76	69.76
S9	78.81	76.76	78.81
S10	89.61	88.41	89.61
S11	83.07	83.20	83.07
S12	80.67	84.33	84.33
S13	88.78	89.96	88.78
S14	87.80	90.84	90.84
S15	89.60	84.80	84.80
S16	60.67	81.19	81.19
S17	90.00	64.00	90.00
S18	79.60	90.00	90.00
S19	82.92	81.29	82.92
S20	80.83	84.00	80.83
Avg	81.39	81.56	**82.75**

of BCI relevant activity and in turn improve the BCI performance. Therefore, this study designed an approach based on SNN to generate relevant EEG signals (such as ERN and P300) and in turn extract their spike representations from the latent layer. Such latent spike-representation can be assumed to be an amalgamation of spiking information from differen sources. These spike representations were assessed

Table 4.6 : Comparison of the classification performance of the spike representation of the P300 datasets with xGboost under different prioritisation conditions.

Dataset	**WNP**	**NP**	**TNP**
S1	71.61	71.84	71.84
S2	68.05	66.04	66.04
S3	71.37	71.93	71.93
S4	83.27	84.58	83.27
S5	65.04	65.00	65.04
S6	71.91	72.93	71.91
S7	66.19	66.98	66.98
S8	71.91	72.14	71.91
S9	71.89	73.01	71.89
S10	58.35	60.58	60.58
S11	66.41	66.69	66.69
S12	86.23	87.19	86.23
S13	62.66	63.90	62.66
S14	59.66	60.07	60.07
S15	62.71	64.38	62.71
S16	69.70	71.90	71.90
S17	74.06	72.50	74.06
S18	68.95	69.04	69.04
S19	73.70	72.85	72.85
S20	67.48	64.83	67.48
Avg	69.56	**69.92**	69.75

towards BCI performance enhancements. As shown in Section 4.4.2, the proposed approach was able to reorganize the spiking activity (see figure 4.2B) and generate both ERN and P300 template signals.

Using 5x10 fold CV metric with different standardised classifiers such as SVM,

Table 4.7 : Comparison of classification performance of P300 dataset via xGboost for transformed signal with constrastive learning.

Dataset	**Constrastive**
S1	72.41
S2	65.25
S3	72.47
S4	84.20
S5	62.88
S6	71.27
S7	67.45
S8	70.26
S9	73.11
S10	60.27
S11	67.74
S12	86.85
S13	61.26
S14	59.70
S15	64.43
S16	71.66
S17	74.16
S18	69.29
S19	73.70
S20	66.65
Avg	69.75

NVB, and xGboost, the spike representation obtained from the LIF-based model showed an enhanced average BCI performance compared to the baseline performance and a significant enhancement for certain datasets. Aside from ERN and P300, the model was also tested with non-ERP signals such as MI, and we observed similar performance enhancement with the spike representation compared to the baseline

Table 4.8 : Comparison of classification performance of ERN dataset via NVB for transformed signal with constrastive learning.

Dataset	**Constrastive**
S1	80.73
S2	91.67
S3	78.67
S4	90.00
S5	76.74
S6	96.33
S7	74.78
S8	61.30
S9	83.14
S10	90.39
S11	86.00
S12	73.67
S13	92.15
S14	90.49
S15	88.70
S16	71.13
S17	64.33
S18	95.00
S19	82.38
S20	78.92
Avg	82.33

performance (see table 4.9).

In addition to classification, inferring the reason behind such performance improvement using PCA and correlation analysis showcased that the proposed approach was able to extract more independent eigenvectors (features) and increased

Table 4.9 : Comparison of the classification performance of an MI EEG signal and its spike representation using MLP classifier.

Dataset	**EEG**	**LIF**
S1	99.41	98.24
S2	59.41	63.53
S3	81.76	88.24
S4	48.75	61.86
S5	68.13	80.63
S6	60.63	57.50
S7	61.88	59.38
S8	65.00	65.83
S9	52.50	54.17
S10	53.75	56.25
S11	76.25	78.75
S12	63.33	63.33
S13	73.33	77.50
S14	60.50	62.50
S15	64.38	73.75
S16	65.00	68.13
Avg.	65.88	**69.35**

within-class correlation and that it facilitated the classifiers to better categorise the samples. To further validate the impact of the SNN's trained weights, we also compared the performance of transformed signals obtained with random weight and LSM and found that the SNN's weights provided an additional edge in performance enhancement. A current limitation of this study is that threshold estimation requires information on many datasets for NP. However, this technique offers advantages in terms of faster inference in edge devices, as the prioritisation enables profound node reduction. As a proof of concept, this also suggests that novel techniques such as pruning (Li et al. 2019) and deep rewiring (Bellec et al. 2017) could be desired

approaches for future direction.

Here, the template signal extraction was based on the assumption that a given stimulus should ideally produce similar neural activity over repeated trials (Mainen and Sejnowski 1995). However, it could be plausible for a template containing irrelevant information to influence the spike representation too. Therefore, the future direction of this work includes the derivation of a clean template signal so that the spike representation could be more robust. Also, since the BCI modalities tested in this chapter have feature on time-series, combining EEG feature and spike-feature could be redundant and as such many not provide additional accuracy

Chapter 5

Burst Spiking Neural Unit

5.1 Abstract

In the last decade, different properties of SNNs were explored to assess their utility towards machine intelligence. However, the bursting phenomenon was often ignored due to the complexity of the relevant spiking neuron model for deep learning computations. Recently, a simplified spiking model called spiking neural unit (SNU) was originated and has shown competing performance on various benchmark tests. Inspired by this, we introduce a simple spiking model, Burst Spiking Neural Unit (BSNU) to accommodate burst patterns to SNU and to explore the effects of bursting. This research problem explores the utility of bursts towards enhancing the spike-representation of EEG signals. Also, the model is validated in various machine learning benchmark tasks across multiple domains including image, text, audio, and radar datasets. BSNU resulted in enhanced performance of P300 and ERN performance. Also, for the majority of these benchmark tasks, BSNU outperformed SNU and in addition, BSNU showcased better reproducibility in a few tasks. These results indicate that the new spiking neuron model with bursting property has the potential in advancing spike-based machine intelligence.

5.2 Background

Enabling SNNs to perform on par with their artificial counterparts on different machine learning benchmark tasks has been a challenging problem. To address this, the past decade has seen a rise in different credit assignment solutions for SNNs, such as surrogate gradient descent, e-prop, and force (Nicola and Clopath 2017; Neftci et al. 2019; Bellec et al. 2020). The introduction of gradient-based optimisation significantly has improved SNNs performance. On a different note, a

few studies have explored the different properties of spiking neuron models such as heterogeneity, adaptive threshold, and time constants as learning parameters to achieve unprecedented improvements in performance (Shaban et al. 2021; Perez-Nieves et al. 2021). For example, a neural adaptation or adaptive threshold which enables a neuron to increase its membrane threshold after a spike event has been shown to absorb longer neural time scales and in turn enhance SNN performance (Bellec et al. 2018b). The human brain is heterogeneous and changing a model's parameter can result in different behaviours. Accordingly, Perez-Nieves et al. (2021) showcased that by inducing heterogeneity via having a different membrane and synaptic constants for each LIF neuron in the model, the accuracy of an SNN can be increased.

Bursting, a phenomenon with a successive high frequency of spikes, is commonly observed in pyramidal neurons of the cortex, thalamus, hippocampus, etc. It is known to increase the possibility of post-synaptic spikes and be involved in various cognitive tasks such as reward-based learning (Daniel and Pollmann 2014; Lin and Nicolelis 2008), and working memory (Gordleeva et al. 2021). Many studies have also shown that bursting is influential on the reliability of information transfer, improved signal-to-noise ratio, sensory processing, and parallel coding (Zeldenrust et al. 2018; Oswald et al. 2004). In the field of computational neuroscience, some studies have shown its utility in plasticity and information processing. For example, Park et al. (2019) showed that bursting could improve the inference speed and reduce the energy consumption of SNNs. Additionally, as bursting was influential in plasticity, Payeur et al. (2021) developed a burst dependent plasticity rule to enable online learning in hierarchical circuits that resulted in an approximated gradient-based loss function. However, the bursting property largely remains unexplored regarding its role in machine intelligence. Therefore, this study aimed to explore the role of bursting in various machine learning tasks to validate its significance and its ability to induce better spike representations of EEG signals.

Recently, Woźniak et al. (2020) developed a new and simple spiking neuron model called SNU, whose computations are recursive in nature and unify with a recurrent

artificial neuron such as LSTM. Additionally, depending on the choice of activation functions in the model, it can also be utilized as an artificial or spiking neuron. An SNU-based SNNs was shown to achieve performance on par with their ANN counterparts on a variety of tasks such as image recognition, language modelling, and music prediction. This model has also been shown to be efficient with precision issues of hardware implementation. Existing bursting models tend to be complex for computations with gradient descent based optimisation. Therefore, inspired by the simplistic nature of the SNU model and its potency in hardware implementation, we introduced a novel spiking neuron model, BSNU, computed in a recursive fashion similar to the SNU model, to accommodate both tonic spiking and bursting patterns under a constant current. To this end, the BSNU and SNU performances were evaluated with various benchmark tests across multiple domains that included image, audio, text, and radar inputs.

5.3 Methods

5.3.1 Spiking Neural Unit model

The temporal dynamics of the SNU model is described according to equation 5.1. This abstract model is based on the structure of the LIF model.

$$\mathbf{s}_t = g\left(W\mathbf{x}_t + l(\tau) \odot \mathbf{s}_{t-1} \odot (1 - \mathbf{y}_{t-1})\right) \tag{5.1}$$

where s_t represents the membrane voltage at time t, $l(\tau)$ acts as the decay factor with the previous time step's state s_{t-1}, x_t is the input information, W is the weight variable, and $\odot$ represents the element-wise multiplication. When a neuron's membrane voltage exceeds the threshold b, i.e. $s_t b$, a spike is produced and is represented by y_t.

$$\mathbf{y}_t = h\left(\mathbf{s}_t - b\right) \tag{5.2}$$

Depending on the choice of activation functions (g, h), the SNU can act as a spiking neuron or artificial neuron. In this study, we focused on SNN and as such, g and h were the *relu* and *step* activation functions, respectively.

5.3.2 BSNU Model

To build a simplistic computational model like the SNU with bursting properties, we take the essence of the computations from the adaptive exponential LIF model (AdEx) whose dynamics are described in equation 5.3-5.4.

$$\tau_m \frac{\mathrm{d}u}{\mathrm{d}t} = -\left(u - u_{\text{rest}}\right) + \Delta_T \exp\left(\frac{u - \vartheta_{rh}}{\Delta_T}\right) - Rw + RI(t) \tag{5.3}$$

$$\tau_w \frac{\mathrm{d}w}{\mathrm{d}t} = a\left(u - u_{\text{rest}}\right) - w + b\tau_w \sum_{t^{(f)}} \delta\left(t - t^{(f)}\right) \tag{5.4}$$

Here, u describes the membrane voltage dynamics with a nonlinear exponential activation term. This dynamics is coupled to the adaptive current variable w. δ is the spike train (with t^f representing the time of spike occurrence) that increases the adaptive current by a fixed factor b.

Similar to the AdEx model, we introduced analogous sub-threshold dynamics to the SNU to accommodate burst patterns. This resulted in the formation of the BSNU model whose dynamics are described according to equation 5.5.

$$\begin{aligned} \mathbf{s}_t &= g\left(W\mathbf{x}_t + l(\tau) \odot \left(\mathbf{s}_{t-1} - \mathbf{u}_{t-1}\right) \odot \left(1 - \mathbf{y}_{t-1}\right)\right) \\ \mathbf{u}_t &= g\left(a * s_{t-1} - \mathbf{u}_t + p * y_{t-1}\right) \end{aligned} \tag{5.5}$$

where, s_t represents the voltage dynamics, u_t mimics the sub-threshold dynamics, with a and p acting as abstract constants. This model produces two type of patterns: (1) doublet and (2) tonic spiking. A higher value of p induces bursts (doublets), and a lower value induces tonic spiking. Table 5.1 contains the list of parameter values used in all the models. Figure 5.1 depicts the behaviour of the SNU and BSNU model (producing tonic and doublet burst pattern in a black bounding box for different p value) under the influence of constant input current of $x_t = 0.3$.

The SNN architecture based on the SNU and BSNU was trained in a supervised fashion using surrogate gradient descent, in which the *step* activation function for spike estimation during forward propagation was replaced with the *sigmoid* function during backward propagation. Refer to Section 2.3 for more details on the training process of the SNN.

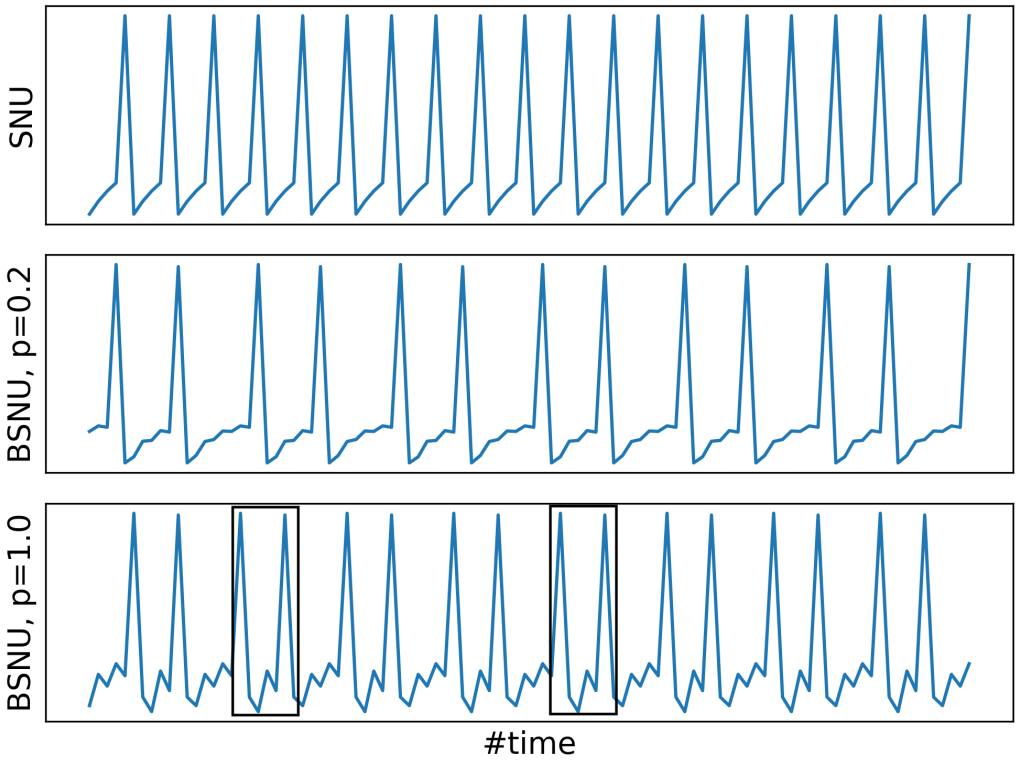

Figure 5.1 : The firing pattern of the SNU and BSNU model under constant input current.

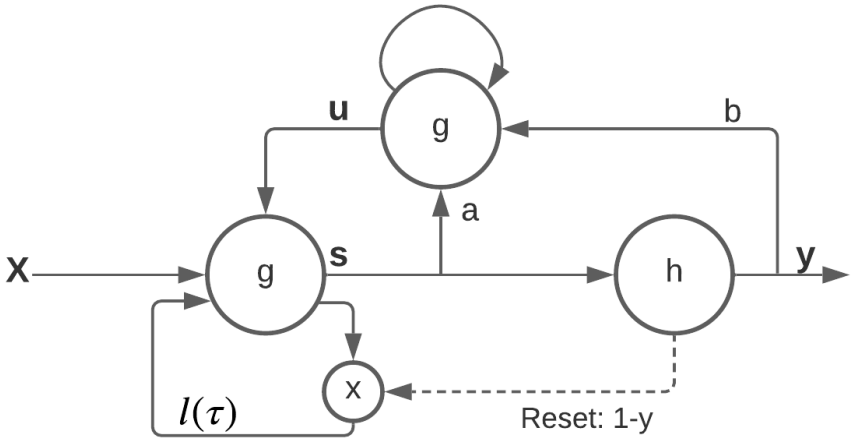

Figure 5.2 : The BSNU model flow diagram mimicking the structure by ref Woźniak et al. (2020).

Table 5.1 : List of SNU and BSNU model parameters.

Parameter	value
1. $l(\tau)$	0.8
2. b	1
3. a	0.2
4. p	[0,1]

5.4 Results

5.4.1 BSNU Validation

The performance of the SNN based on the SNU and BSNU was compared with open source datasets for benchmark tasks across multiple domains commonly used in AI such as image, audio, text, and radar domains, as shown in the following sections. For BSNU-based SNNs, only the first layer (or sensory layer) comprised BSNU neurons, where each neuron has a randomly assigned p value (to control the burst property), while the remaining layers are based on SNU neurons. However, for SNU-based SNN models, all layers contain SNU units only. Here, for each task, both the SNU and BSNU based SNNs were compared with the same structure i.e. the same numbers of neurons and layers, and seeding was also used to instill the same weight initialisation for both models.

Image

The performance of the SNU and BSNU based SNNs were compared on some image-based benchmark datasets such as MNIST (10 classes), KMNIST (10 classes), EMNIST (13 classes), and CIFAR10 (10 classes). A three layered feedforward architecture was used for training (in a supervised fashion with 10 seeds) with all datasets, except for CIFAR, for which we adopted a convolution based LeNet-5 architecture. For all the datasets except for CIFAR10, the images were linearised and converted to a spike train of 20 time steps for the forward processing in all models

and datasets. Since CIFAR10 classification was based on convolution styled SNN, the three dimensional input structure is maintained but was converted to spike trains of 20 time-steps. Figure 5.3A-D (where A:= MNIST, B:= EMNIST, C:= KMNIST, and D:= CIFAR10) shows that for most of the datasets, the BSNU exceeded the SNU's classification performance.

Audio

For the audio based classification assessment, we used the Heidelberg spiking dataset (SHD) (Cramer et al. 2020), which was created using an inner ear model specifically for the SNNs performance evaluation. From the dataset, we extracted 10 classes of German digits and processed them in a forward fashion, by which the number of SNN time steps was equal to the time points of the samples. Figure 5.4 shows that the average performance (of 10 seeds) of the BSNU outperformed that of the SNU.

Radar

In the past decade, radar-based gesture recognition gained attention for edge deep learning applications. As such, it received interest for low-power and energy-efficient algorithms such as SNNs. Therefore, we tested the ability of the BSNU based SNN in classifying a processed Soli dataset containing 12 classes from Safa et al. (2021). Similar to the audio-based classification, the number of SNN time steps here was equal to the time points of the input signal. Figure 5.5 showcases that the BSNU achieved enhanced average performance (of 10 seeds) over the SNU.

Text

Finally, another popular domain commonly studied in AI applications is text. In this study, we further compared the SNU and BSNU with two different text-based applications: language translation and sentiment analysis. Regarding this domain, we implemented a softer version (non-spiking) of the models by setting both g and h to the $leaky\,relu$ activation function. For the language translation, we used a two-layered Seq2Seq architecture and Multi30K dataset (a multilingual

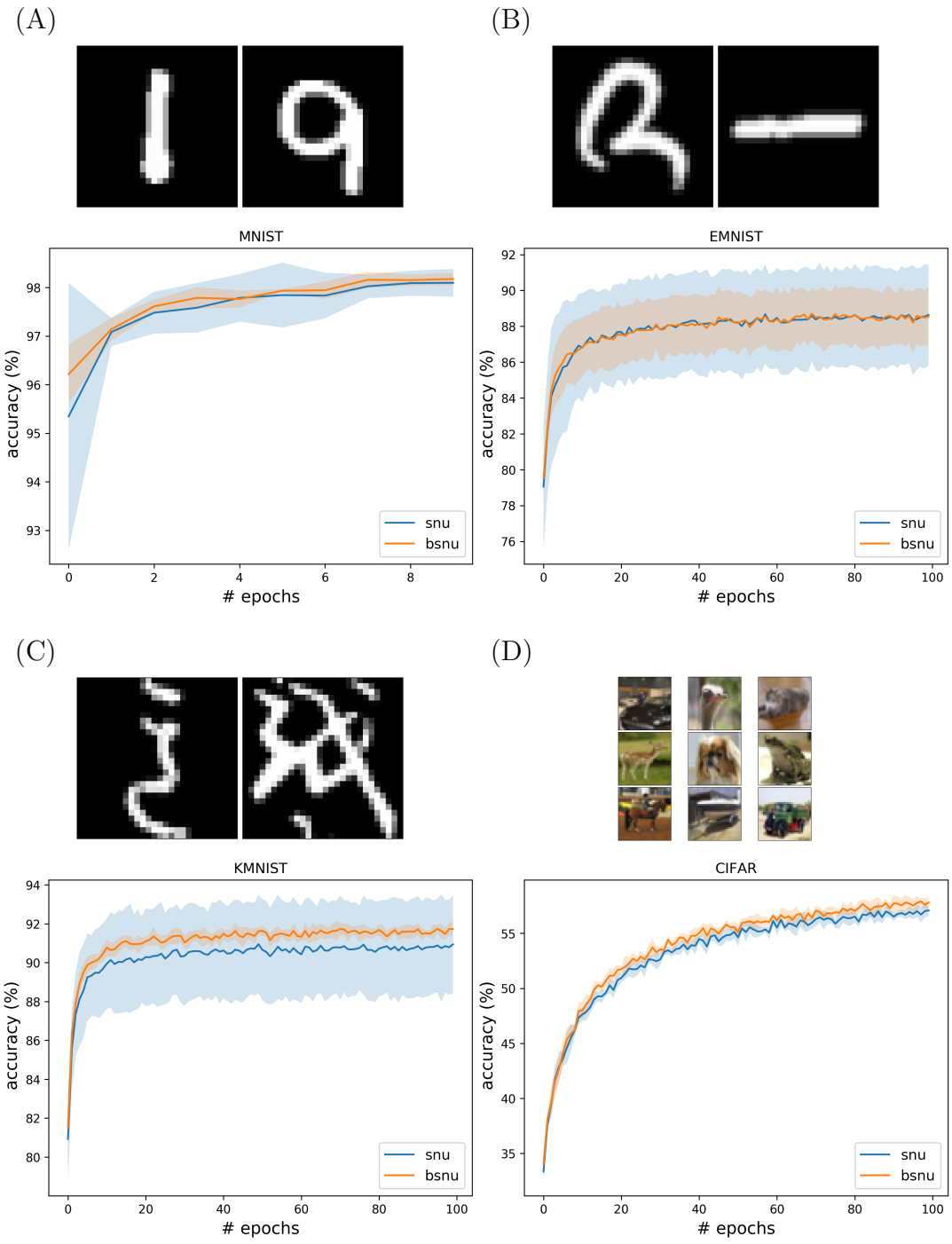

Figure 5.3 : Comparing the classification performance of the SNU and BSNU based SNN for image domain datasets. The top inset of each plot showcases a sample image, and the bottom image displays the average classification performance of multiple seeds.

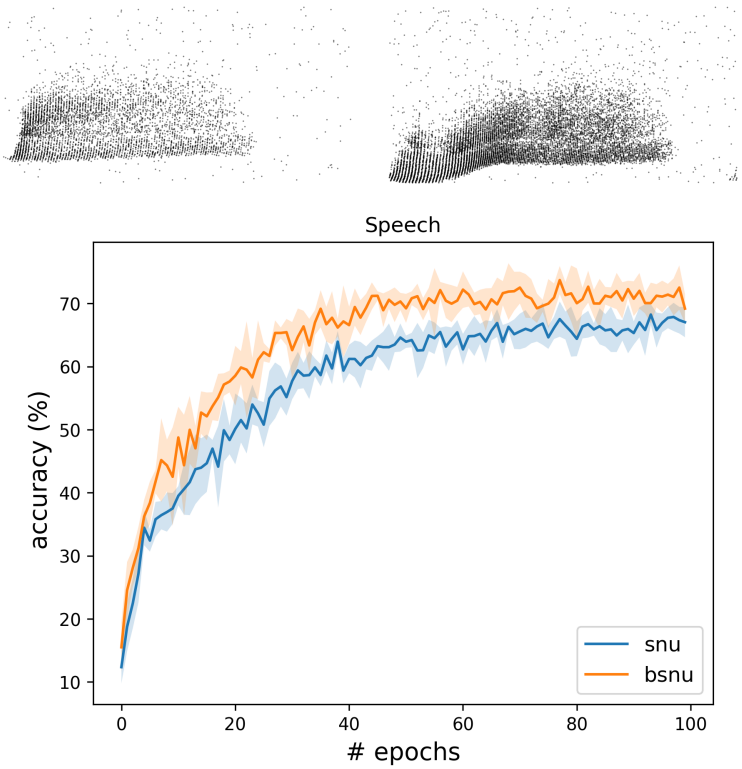

Figure 5.4 : Comparing the classification performance of the SNU and BSNU based SNN on an SHD audio dataset containing German digits.

dataset with English to German translation) in which the sentences were restricted to 23 words, where each word embedding acted as the input of one time step. Similarly, for sentient analysis (2 classes) was performed with the softer versions of the models on the MR Movie Reviews dataset using one layered recurrent structure. For this dataset, each sentence was restricted to 32 words. Figure 5.6A–B showcases that in both of the text-based applications, the BSNU resulted in a better average performance (of 10 seeds) over the SNU.

5.4.2 EEG Classification

An SNU and BSNU based SNN architecture similar to figure 4.1 was instantiated and trained in a similar fashion of *forward process* and *inverse process* (mentioned in Section 4.3.1) to reconstruct the P300 and MI template signals. However, to enable a better fit of the EEG signal, in addition to the EEG pre-processing steps, the

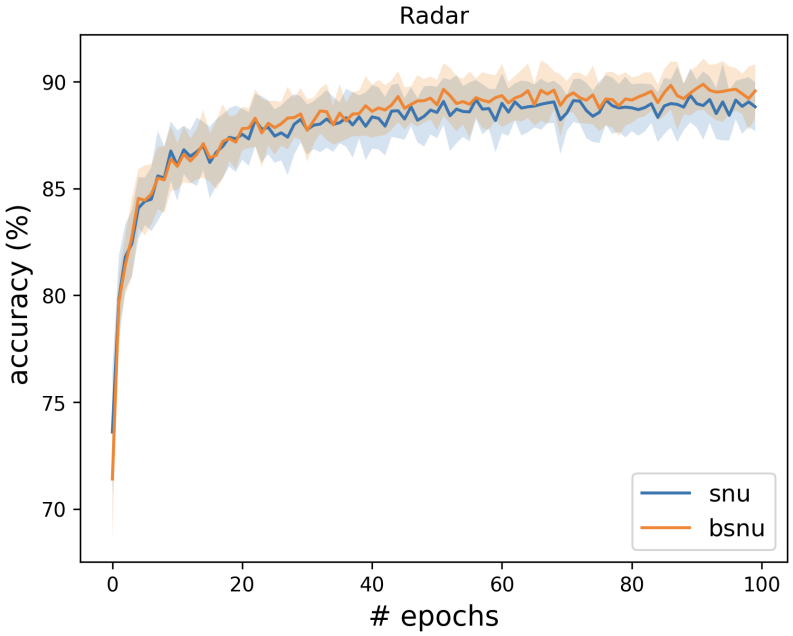

Figure 5.5 : The Soli radar's gesture recognition performance with the SNU and BSNU based SNN.

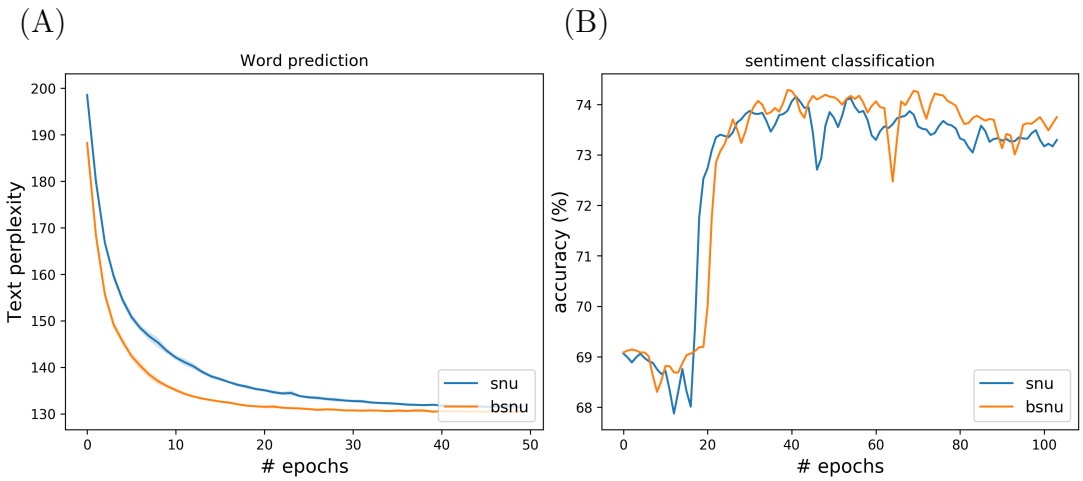

Figure 5.6 : The text domain analysis with a softer version of the BSNU model for (**A**) language translation and (**B**) sentiment analysis.

template signals were normalised from -1 to 1. After template fitting, the trained weights were then used to transform the non-template signals of a given dataset according to equation 4.1. However, these non-template signals were not normalised

during transformation. Since the P300 dataset resulted in better performance with xGboost previously (from table 4.2), the capability of the SNU- and BSNU-based SNN was evaluated using the same classifier.

Table 5.2 : The P300 classification performance comparison of the spike representations obtained by the SNU and BSNU based SNN with xGboost and a 5x10 fold CV.

Dataset	**SNU**	**BSNU**
S1	71.09	70.24
S2	67.56	67.51
S3	71.23	71.74
S4	82.34	83.65
S5	63.54	64.26
S6	71.00	72.85
S7	66.99	67.29
S8	71.12	72.22
S9	72.39	71.35
S10	59.14	61.88
S11	65.58	66.70
S12	85.55	85.86
S13	59.46	62.05
S14	59.82	59.33
S15	62.02	63.64
S16	70.02	70.62
S17	73.36	74.07
S18	68.73	69.13
S19	72.87	74.20
S20	66.96	68.67
Avg.	69.04	**69.86**

As shown in table 5.2, the BSNU-based SNN resulted in a better average performance of 69.89% in comparison to the SNU-based SNN with 69.05%. Similarly, the model comparison was made for the MI-EEG datasets using the MLP and bagging classifier. The BNSU-based SNN produced a better average classification performance of 67.82%, whereas the SNU-based SNN had a performance of 67.36% with the bagging classifiers.

Table 5.3 : Performance of the MI-EEG spike representations of the SNU and BSNU using the MLP and bagging classifier. For each dataset, a 5x10 fold CV was applied.

Dataset	**MLP**		**Bagging**	
	SNU	BSNU	SNU	BSNU
S1	59.84	58.46	55.37	59.00
S2	61.30	61.82	56.30	57.74
S3	69.32	67.53	70.35	69.90
S4	82.63	81.75	71.00	69.00
S5	75.00	75.17	68.33	70.67
S6	57.33	57.50	60.33	59.33
S7	53.29	54.71	60.00	61.43
S8	51.38	52.38	65.25	66.50
S9	62.88	64.38	60.50	60.13
S10	49.38	49.63	73.13	72.13
S11	60.38	59.13	56.50	55.63
S12	83.88	83.38	81.63	82.50
S13	98.13	97.88	97.00	97.75
Avg	66.52	66.44	67.36	**67.82**

5.5 Discussion

In this research problem, we introduced a simplified spiking neuron model with bursting property, i.e. BSNU, and explored its ability in enhancing the spike representation with P300 and MI datasets. Both the MI and P300 BSNU-based SNNs

resulted in better performance compared to the SNU-based SNN. Also, to validate the BSNU model's advantages, different benchmark AI tasks across different domains of data commonly used in the real world, such as image, audio, radar and text domains were verified. For the majority of these tasks, the BSNU-based SNNs outperformed the SNU-based SNNs. In addition, for a few tasks, such as the image-based tasks, the BSNU resulted in better reproducibility, i.e. a low standard deviation of accuracies from multiple seeds, indicating that it was sometimes agnostic to weight initialisation. Another advantage of the BSNU was that it did not require additional trainable parameters over the SNU, and this illustrated that the performance improvement was primarily due to the addition of the bursting property of the burst model. A plausible reason for such enhancement could be the ability of bursting to have a stronger effect on post-synaptic neurons than a single spike and a better signal-to-noise ratio. These results concluded that the proposed model with bursting property has prospects in advancing spike-based machine intelligence. However, all the tests were explored with simple architectures and require further exploration with complex tasks and architectures in the future directions.

Chapter 6

Conclusion

This thesis explored the capability of SNN to advance different BCI paradigms. For better performance, EEG-based BCI systems often require a huge number of samples to leverage advanced learning algorithms. However, generic EEG recordings are usually short, and among them, some recorded samples are rejected due to noise and artifacts. To overcome these shortcomings, some novel strategies include data augmentation, and feature extraction techniques. A major portion of BCI paradigms are implemented with EEG devices due to their portability and compactness despite the drawback of loss of spatial resolution and noise. The invasive recording are although better in these aspects, it requires surgical methods to obtain population level activity. Also, the conventional norm of BCI systems is to apply the above mentioned methods to EEG signals and it's derivation such as power spectrum, and wavelet transform. But, the EEG signal changes are coupled with underlying spiking activity (Snyder and Smith 2015). Therefore, in this thesis, we explored the possibility of reverse engineering EEG signals to spike representations using an SNN, which is the most biologically inspired network model, to address these challenges from the different directions of BCI perspectives, data generation, and SNN properties. These challenges were organised into three research problems, each with a dedicated chapter (Chapters 3–5).

Chapter 3 detailed the problem of data augmentation, i.e. the generation of synthetic EEG signals using SNN. We showed that SNNs can be leveraged to generate synthetic MI and SSVEP signals while retaining biomarkers with small samples, unlike DNN based generative models (such as GAN) that require huge samples. This showcased the major advantage of our approach, as data augmentation methods are generally required when there are insufficient data, which is counter-intuitive

since a DNN model still requires a large dataset. Also, we showcased that with the *validation-a* test from Section 3.4.3, the artificial data were able to successfully classify original data; existing studies often ignore this validation test and mixed the artificial and original samples for performance assessment. Since a major reason for generating artificial data is enhancement of the classification performance, we assessed the same with the SNN generated synthetic MI data using cross-validation in which the artificial samples were appended to the original samples in each fold. From Section 3.4.4 we have shown that the MI performance was improved significantly with the artificial data. In addition, we compared with DNN-based generative algorithms and demonstrated that the proposed SNN-based approach has outperformed these deep generative models. To the best of our knowledge, this chapter is the first study that illustrated the ability of SNN for EEG data augmentation.

Chapter 4 explored the SNN's ability to obtain novel features from EEG signals. A majority of the previous ERP studies such as P300 and ERN solely rely on the time series data as a feature for classification. We hypothesised that the spike representations of these EEG signals should have better resolution, and as such, able to provide additional features to induce higher classification performance. To this end, we trained the SNN to initially reconstruct EEG template signals similar to those of the previous problem, and the trained model was used to transform EEG signals to approximated high-dimensional spike representations. Different classifiers such as NVB, xGboost, and SVM were implemented to compare different EEG signals (of different BCI paradigms) and their spike representations. P300, ERN, and MI resulted in significantly enhanced performance with the spike representations. In addition, we explored reasons for such improvements using PCA and correlation metrics. Using PCA's variance of explanation analysis, we observed that spike representation indeed extracted additional features that led to the performance enhancement. Additionally, from the Pearson's correlation analysis that was measured among all samples, we observed an increased correlation among the samples from the same category for spike representation than the EEG signals. This implies that our approach apart from extracting additional features, it has also increased the

similarity of samples from a given class. Representation learning from the field of DNN provided additional hints on improving the latent representation. Inspired by these, we have shown that the inclusion of contrastive learning loss during the SNN training process provided a minor edge in further enhancing the classification performance by spike representations.

Chapter 5 discussed the influence of inherent properties of spiking neurons towards AI advancements. Different properties such as adaptive threshold and heterogeneity were often explored for enhancing the SNN-based AI capabilities. We assumed that such properties could potentially improve the spike representation of EEG signals. However, the busting property, a common feature of pyramidal neurons in the cortex is often ignored due to its complex model format. However, the bursting property is known for its role in memory encoding, efficiency in signal transmission, and low signal-to-noise ratio. A recent study introduced a novel simplified spiking neuron model called SNU from the essence of LIF's dynamics. Inspired by its characteristics, we developed a novel spiking model with bursting property, BSNU. Based on the bursting role in information processing, we hypothesised that the BSNU-based SNN could also improve the spike representation of EEG signals. Therefore, in this chapter, we explored this model's ability on a wide range of benchmark tasks initially and explored its ability for improving the spike representation. The BSNU-based SNN of various architecture styles were validated and compared with SNU-based SNNs on different benchmark AI tasks across domains such as text, image, audio, and radar domains. In a majority of these tasks, the BSNU showed enhanced classification performance, and were also showed to be better at reproducability. This indicated the bursting property could indeed help enhance AI capabilities. Similar to chapter 4, we trained the BSNU and SNU-based SNN on the EEG signals of P300 and MI to obtain spike representations. The BSNU-based spike representation produced enhanced performance in comparison to SNU-based spike-representation. This implies that the bursting property of the SNN played a role in advancing the BCI systems.

Overall, the research problems of this thesis were aimed to establish a new line

of study to unfold the neural activity from EEG signals without the explicit requirement of invasive recordings. However, a current limitation of this thesis is that each BCI paradigm adopted had only two classes i.e. left-hand and right-hand motor activity for MI, target/non-target classes for P300, and target/on-target classes for ERN. It is unclear on the SNNs performance for datasets with higher number of classes, which could be a future direction of this work. Also, for the reasons of portability and few channel systems, we only considered two EEG channels for all problems. Expanding the current work to high-dense EEG systems for clinical purposes could be beneficial. Additionally, the time-series of the spike representations were directly considered as the input to a classifier in the case of P300 and ERN, as is the custom of these BCI paradigms. However, signal processing and feature extraction methods such as wavelet transform, power spectrum,and signal components could be considered on the spike representation as a future direction.

In addition, complex architectures can be explored in future direction to test the model limits with number of classes and channels. Adaptive BCIs often focus on algorithms to accommodate changes in the user's physiological state and exploring its spike-based changes could potentially help improve the adaptive algorithms too in future research.

Bibliography

Aghaei, A. S., Mahanta, M. S. & Plataniotis, K. N., 2015, 'Separable common spatio-spectral patterns for motor imagery bci systems', *IEEE Transactions on Biomedical Engineering*, vol. 63, no. 1, pp. 15–29.

Alemi, A., Machens, C., Deneve, S. & Slotine, J.-J., 2018, 'Learning nonlinear dynamics in efficient, balanced spiking networks using local plasticity rules', *Proceedings of the AAAI Conference on Artificial Intelligence*, , vol. 32.

Altaheri, H., Muhammad, G., Alsulaiman, M., Amin, S. U., Altuwaijri, G. A., Abdul, W., Bencherif, M. A. & Faisal, M., 2021, 'Deep learning techniques for classification of electroencephalogram (eeg) motor imagery (mi) signals: a review', *Neural Computing and Applications*, pp. 1–42.

Alzhrani, W., Doborjeh, M., Doborjeh, Z. & Kasabov, N., 2021, 'Emotion recognition and understanding using eeg data in a brain-inspired spiking neural network architecture', *2021 International Joint Conference on Neural Networks (IJCNN)*, IEEE, pp. 1–9.

An, Y., Lam, H. K. & Ling, S. H., 2022, 'Auto-denoising for eeg signals using generative adversarial network', *Sensors*, vol. 22, no. 5, p. 1750.

Anicet Zanini, R. & Luna Colombini, E., 2020, 'Parkinson's disease emg data augmentation and simulation with dcgans and style transfer', *Sensors*, vol. 20, no. 9, p. 2605.

Antelis, J. M., Falcón, L. E. et al., 2020, 'Spiking neural networks applied to the classification of motor tasks in eeg signals', *Neural networks*, vol. 122, pp. 130–143.

Arsalan, M., Chmurski, M., Santra, A., El-Masry, M., Weigel, R. & Issakov, V., 2021, 'Resource efficient gesture sensing based on fmcw radar using spiking neural

networks', *2021 IEEE MTT-S International Microwave Symposium (IMS)*, IEEE, pp. 78–81.

Arvaneh, M., Robertson, I. H. & Ward, T. E., 2019, 'A p300-based brain-computer interface for improving attention', *Frontiers in human neuroscience*, p. 524.

Aznan, N. K. N., Atapour-Abarghouei, A., Bonner, S., Connolly, J., Moubayed, N. A. & Breckon, T., 2019, 'Simulating brain signals: Creating synthetic eeg data via neural-based generative models for improved ssvep classification', *arXiv preprint arXiv:1901.07429*.

Behrenbeck, J., Tayeb, Z., Bhiri, C., Richter, C., Rhodes, O., Kasabov, N., Espinosa-Ramos, J. I., Furber, S., Cheng, G. & Conradt, J., 2019, 'Classification and regression of spatio-temporal signals using neucube and its realization on spinnaker neuromorphic hardware', *Journal of neural engineering*, vol. 16, no. 2, p. 026014.

Bellec, G., Kappel, D., Maass, W. & Legenstein, R., 2017, 'Deep rewiring: Training very sparse deep networks', *arXiv preprint arXiv:1711.05136*.

Bellec, G., Salaj, D., Subramoney, A., Legenstein, R. & Maass, W., 2018a, 'Long short-term memory and learning-to-learn in networks of spiking neurons', *arXiv preprint arXiv:1803.09574*.

Bellec, G., Salaj, D., Subramoney, A., Legenstein, R. & Maass, W., 2018b, 'Long short-term memory and learning-to-learn in networks of spiking neurons', Bengio, S., Wallach, H., Larochelle, H., Grauman, K., Cesa-Bianchi, N. & Garnett, R. (eds.) *Advances in Neural Information Processing Systems*, , vol. 31Curran Associates, Inc.

Bellec, G., Scherr, F., Subramoney, A., Hajek, E., Salaj, D., Legenstein, R. & Maass, W., 2020, 'A solution to the learning dilemma for recurrent networks of spiking neurons', *Nature communications*, vol. 11, no. 1, pp. 1–15.

Bengio, Y., Courville, A. & Vincent, P., 2013, 'Representation learning: A review and new perspectives', *IEEE transactions on pattern analysis and machine intelligence*, vol. 35, no. 8, pp. 1798–1828.

Bi, L., Lian, J., Jie, K., Lai, R. & Liu, Y., 2014, 'A speed and direction-based cursor control system with p300 and ssvep', *Biomedical Signal Processing and Control*, vol. 14, pp. 126–133.

Bing, Z., Meschede, C., Huang, K., Chen, G., Rohrbein, F., Akl, M. & Knoll, A., 2018, 'End to end learning of spiking neural network based on r-stdp for a lane keeping vehicle', *2018 IEEE International Conference on Robotics and Automation (ICRA)*, IEEE, pp. 4725–4732.

Budhraja, S., Bhattacharya, B. S., Durrant, S., Doborjeh, Z., Doborjeh, M. & Kasabov, N., 2020, 'Sleep stage classification using neucube on spinnaker: a preliminary study', *2020 International Joint Conference on Neural Networks (IJCNN)*, IEEE, pp. 1–8.

Capano, V., Herrmann, H. J. & De Arcangelis, L., 2015, 'Optimal percentage of inhibitory synapses in multi-task learning', *Scientific reports*, vol. 5, p. 9895.

Carino-Escobar, R., Cantillo-Negrete, J., Vazquez, R. A. & Gutierrez-Martinez, J., 2016, 'Spiking neural networks trained with particle swarm optimization for motor imagery classification', *International Conference on Swarm Intelligence*, Springer, pp. 245–252.

Chavarriaga, R., Sobolewski, A. & Millán, J. d. R., 2014, 'Errare machinale est: the use of error-related potentials in brain-machine interfaces', *Frontiers in neuroscience*, vol. 8, p. 208.

Cheng, X., Hao, Y., Xu, J. & Xu, B., 2020, 'Lisnn: Improving spiking neural networks with lateral interactions for robust object recognition.', *IJCAI*, pp. 1519–1525.

Chiappa, S. & Barber, D., 2006, 'Eeg classification using generative independent component analysis', *Neurocomputing*, vol. 69, no. 7-9, pp. 769–777.

Chiarelli, A. M., Croce, P., Merla, A. & Zappasodi, F., 2018, 'Deep learning for hybrid eeg-fnirs brain–computer interface: application to motor imagery classification', *Journal of neural engineering*, vol. 15, no. 3, p. 036028.

Churchland, M. M., Cunningham, J. P., Kaufman, M. T., Foster, J. D., Nuyujukian, P., Ryu, S. I. & Shenoy, K. V., 2012, 'Neural population dynamics during reaching', *Nature*, vol. 487, no. 7405, p. 51.

Cinel, C., Valeriani, D. & Poli, R., 2019, 'Neurotechnologies for human cognitive augmentation: current state of the art and future prospects', *Frontiers in human neuroscience*, p. 13.

Corley, I. A. & Huang, Y., 2018, 'Deep eeg super-resolution: Upsampling eeg spatial resolution with generative adversarial networks', *2018 IEEE EMBS International Conference on Biomedical & Health Informatics (BHI)*, IEEE, pp. 100–103.

Cortez, S. A., Flores, C. & Andreu-Perez, J., 2020, 'Single-trial p300 classification using deep belief networks for a bci system', *2020 IEEE XXVII International Conference on Electronics, Electrical Engineering and Computing (INTERCON)*, IEEE, pp. 1–4.

Cramer, B., Stradmann, Y., Schemmel, J. & Zenke, F., 2020, 'The heidelberg spiking data sets for the systematic evaluation of spiking neural networks', *IEEE Transactions on Neural Networks and Learning Systems*.

Cruz, A., Pires, G., Lopes, A., Carona, C. & Nunes, U. J., 2021, 'A self-paced bci with a collaborative controller for highly reliable wheelchair driving: Experimental tests with physically disabled individuals', *IEEE Transactions on Human-Machine Systems*, vol. 51, no. 2, pp. 109–119.

Dagdevir, E. & Tokmakci, M., 2021, 'Truncation thresholds based empirical mode decomposition approach for classification performance of motor imagery bci systems', *Chaos, Solitons & Fractals*, vol. 152, p. 111450.

Daniel, R. & Pollmann, S., 2014, 'A universal role of the ventral striatum in reward-based learning: evidence from human studies', *Neurobiology of learning and memory*, vol. 114, pp. 90–100.

Degenhart, A. D., Eles, J., Dum, R., Mischel, J. L., Smalianchuk, I., Endler, B., Ashmore, R. C., Tyler-Kabara, E. C., Hatsopoulos, N. G., Wang, W. et al., 2016,

'Histological evaluation of a chronically-implanted electrocorticographic electrode grid in a non-human primate', *Journal of neural engineering*, vol. 13, no. 4, p. 046019.

DePasquale, B., Cueva, C. J., Rajan, K., Abbott, L. et al., 2018, 'full-force: A target-based method for training recurrent networks', *PloS one*, vol. 13, no. 2, p. e0191527.

Diehl, P. U., Neil, D., Binas, J., Cook, M., Liu, S.-C. & Pfeiffer, M., 2015, 'Fast-classifying, high-accuracy spiking deep networks through weight and threshold balancing', *2015 International Joint Conference on Neural Networks (IJCNN)*, IEEE, pp. 1–8.

Dinarès-Ferran, J., Ortner, R., Guger, C. & Solé-Casals, J., 2018, 'A new method to generate artificial frames using the empirical mode decomposition for an eeg-based motor imagery bci', *Frontiers in neuroscience*, vol. 12, p. 308.

Doborjeh, M. G., Wang, G. Y., Kasabov, N. K., Kydd, R. & Russell, B., 2015, 'A spiking neural network methodology and system for learning and comparative analysis of eeg data from healthy versus addiction treated versus addiction not treated subjects', *IEEE transactions on biomedical engineering*, vol. 63, no. 9, pp. 1830–1841.

Doborjeh, Z., Doborjeh, M., Taylor, T., Kasabov, N., Wang, G. Y., Siegert, R. & Sumich, A., 2019, 'Spiking neural network modelling approach reveals how mindfulness training rewires the brain', *Scientific reports*, vol. 9, no. 1, pp. 1–15.

Fawaz, S., Sim, K. S. & Tan, S. C., 2020, 'Encoding rich frequencies for classification of stroke patients eeg signals', *IEEE Access*, vol. 8, pp. 135811–135820.

Ferré, P., Mamalet, F. & Thorpe, S. J., 2018, 'Unsupervised feature learning with winner-takes-all based stdp', *Frontiers in computational neuroscience*, vol. 12, p. 24.

Freudenburg, Z. V., Branco, M. P., Leinders, S., Vijgh, B. H., Pels, E. G., Denison, T., Berg, L. H., Miller, K. J., Aarnoutse, E. J., Ramsey, N. F. et al., 2019,

'Sensorimotor ecog signal features for bci control: a comparison between people with locked-in syndrome and able-bodied controls', *Frontiers in neuroscience*, p. 1058.

Gerstner, W., Kistler, W. M., Naud, R. & Paninski, L., 2014, *Neuronal dynamics: From single neurons to networks and models of cognition*, Cambridge University Press.

Ghosh-Dastidar, S. & Adeli, H., 2009, 'A new supervised learning algorithm for multiple spiking neural networks with application in epilepsy and seizure detection', *Neural networks*, vol. 22, no. 10, pp. 1419–1431.

Gilra, A. & Gerstner, W., 2017, 'Predicting non-linear dynamics by stable local learning in a recurrent spiking neural network', *Elife*, vol. 6, p. e28295.

Golany, T., Lavee, G., Yarden, S. T. & Radinsky, K., 2020, 'Improving ecg classification using generative adversarial networks', *Proceedings of the AAAI Conference on Artificial Intelligence*, , vol. 34pp. 13280–13285.

Gordleeva, S. Y., Tsybina, Y. A., Krivonosov, M. I., Ivanchenko, M. V., Zaikin, A. A., Kazantsev, V. B. & Gorban, A. N., 2021, 'Modelling working memory in spiking neuron network accompanied by astrocytes', *Frontiers in Cellular Neuroscience*, vol. 15, p. 86.

Guger, C., Allison, B. Z. & Müller-Putz, G. R., 2015, 'Brain-computer interface research: A state-of-the-art summary 4', *Brain-Computer Interface Research*, Springer, pp. 1–8.

Gutierrez, G. J. & Denève, S., 2019, 'Population adaptation in efficient balanced networks', *Elife*, vol. 8, p. e46926.

Han, J., Gu, X. & Lo, B., 2021, 'Semi-supervised contrastive learning for generalizable motor imagery eeg classification', *2021 IEEE 17th International Conference on Wearable and Implantable Body Sensor Networks (BSN)*, IEEE, pp. 1–4.

Hartmann, K. G., Schirrmeister, R. T. & Ball, T., 2018, 'Eeg-gan: Generative adversarial networks for electroencephalograhic (eeg) brain signals', *arXiv preprint arXiv:1806.01875*.

Holm, N. S., Puthusserypady, S. et al., 2019, 'An improved five class mi based bci scheme for drone control using filter bank csp', *2019 7th International Winter Conference on Brain-Computer Interface (BCI)*, IEEE, pp. 1–6.

Hwang, H.-J., Kwon, K. & Im, C.-H., 2009, 'Neurofeedback-based motor imagery training for brain–computer interface (bci)', *Journal of neuroscience methods*, vol. 179, no. 1, pp. 150–156.

Ingrosso, A. & Abbott, L., 2019, 'Training dynamically balanced excitatory-inhibitory networks', *PloS one*, vol. 14, no. 8, p. e0220547.

Ioannides, G., Kourouklides, I. & Astolfi, A., 2022, 'Spatiotemporal dynamics in spiking recurrent neural networks using modified-full-force on eeg signals', *Scientific Reports*, vol. 12, no. 1, pp. 1–20.

Iqbal, T. & Ali, H., 2018, 'Generative adversarial network for medical images (mi-gan)', *Journal of medical systems*, vol. 42, no. 11, pp. 1–11.

Izhikevich, E. M., 2003, 'Simple model of spiking neurons', *IEEE Transactions on neural networks*, vol. 14, no. 6, pp. 1569–1572.

Jiao, Y., Deng, Y., Luo, Y. & Lu, B.-L., 2020, 'Driver sleepiness detection from eeg and eog signals using gan and lstm networks', *Neurocomputing*, vol. 408, pp. 100–111.

Jolivet, R., Timothy, J. & Gerstner, W., 2003, 'The spike response model: a framework to predict neuronal spike trains', *Artificial neural networks and neural information processing—ICANN/ICONIP 2003*, Springer, pp. 846–853.

Jordan, J., Weidel, P. & Morrison, A., 2019, 'A closed-loop toolchain for neural network simulations of learning autonomous agents', *Frontiers in computational neuroscience*, vol. 13, p. 46.

Jubien, G., Schaeffer, M.-C., Bonnet, S. & Aksenova, T., 2019, 'Decoding of finger activation from ecog data: a comparative study', *2019 International Joint Conference on Neural Networks (IJCNN)*, IEEE, pp. 1–8.

Kappenman, E. S., Farrens, J. L., Zhang, W., Stewart, A. X. & Luck, S. J., 2021, 'Erp core: An open resource for human event-related potential research', *NeuroImage*, vol. 225, p. 117465.

Karimi, S. A., Mijani, A., Talebian, M. & Mirzakuchaki, S., 2019, 'Comparison of the p300 detection accuracy related to the bci speller and image recognition scenarios', *arXiv preprint arXiv:1912.11371*.

Kasabov, N. K., 2014, 'Neucube: A spiking neural network architecture for mapping, learning and understanding of spatio-temporal brain data', *Neural Networks*, vol. 52, pp. 62–76.

Kerdels, J. & Peters, G., 2018, 'A grid cell inspired model of cortical column function.', *IJCCI*, pp. 204–210.

Khorshidtalab, A. & Salami, M. J. E., 2011, 'Eeg signal classification for real-time brain-computer interface applications: A review', *2011 4th International Conference on Mechatronics (ICOM)*, IEEE, pp. 1–7.

Khosla, P., Teterwak, P., Wang, C., Sarna, A., Tian, Y., Isola, P., Maschinot, A., Liu, C. & Krishnan, D., 2020, 'Supervised contrastive learning', *Advances in Neural Information Processing Systems*, vol. 33, pp. 18661–18673.

Kim, C. M. & Chow, C. C., 2018, 'Learning recurrent dynamics in spiking networks', *Elife*, vol. 7, p. e37124.

Kim, C. M. & Chow, C. C., 2021, 'Training spiking neural networks in the strong coupling regime', *Neural Computation*, vol. 33, no. 5, pp. 1199–1233.

Kim, R., Li, Y. & Sejnowski, T. J., 2019, 'Simple framework for constructing functional spiking recurrent neural networks', *Proceedings of the national academy of sciences*, vol. 116, no. 45, pp. 22811–22820.

Kim, R. & Sejnowski, T. J., 2021, 'Strong inhibitory signaling underlies stable temporal dynamics and working memory in spiking neural networks', *Nature Neuroscience*, vol. 24, no. 1, pp. 129–139.

Kim, S., Park, S., Na, B. & Yoon, S., 2020, 'Spiking-yolo: Spiking neural network for energy-efficient object detection', *Proceedings of the AAAI Conference on Artificial Intelligence*, , vol. 34pp. 11270–11277.

Kingma, D. P. & Ba, J., 2014, 'Adam: A method for stochastic optimization', *arXiv preprint arXiv:1412.6980*.

Ko, L.-W., Lu, Y.-C., Bustince, H., Chang, Y.-C., Chang, Y., Ferandez, J., Wang, Y.-K., Sanz, J. A., Dimuro, G. P. & Lin, C.-T., 2019, 'Multimodal fuzzy fusion for enhancing the motor-imagery-based brain computer interface', *IEEE Computational Intelligence Magazine*, vol. 14, no. 1, pp. 96–106.

Ko, L.-W., Ranga, S., Komarov, O. & Chen, C.-C., 2017, 'Development of single-channel hybrid bci system using motor imagery and ssvep', *Journal of healthcare engineering*, vol. 2017.

Kumarasinghe, K., Kasabov, N. & Taylor, D., 2020, 'Deep learning and deep knowledge representation in spiking neural networks for brain-computer interfaces', *Neural Networks*, vol. 121, pp. 169–185.

Kuśmierz, Ł., Isomura, T. & Toyoizumi, T., 2017, 'Learning with three factors: modulating hebbian plasticity with errors', *Current opinion in neurobiology*, vol. 46, pp. 170–177.

Kwak, N.-S., Müller, K.-R. & Lee, S.-W., 2015, 'A lower limb exoskeleton control system based on steady state visual evoked potentials', *Journal of neural engineering*, vol. 12, no. 5, p. 056009.

Lansdell, B., Milovanovic, I., Mellema, C., Fetz, E. E., Fairhall, A. L. & Moritz, C. T., 2019, 'Reconfiguring motor circuits for a joint manual and bci task', *IEEE Transactions on Neural Systems and Rehabilitation Engineering*, vol. 28, no. 1, pp. 248–257.

Lawhern, V. J., Solon, A. J., Waytowich, N. R., Gordon, S. M., Hung, C. P. & Lance, B. J., 2018, 'Eegnet: a compact convolutional neural network for eeg-based brain–computer interfaces', *Journal of neural engineering*, vol. 15, no. 5, p. 056013.

Le-Khac, P. H., Healy, G. & Smeaton, A. F., 2020, 'Contrastive representation learning: A framework and review', *IEEE Access*, vol. 8, pp. 193907–193934.

Lee, J. H., Delbruck, T. & Pfeiffer, M., 2016, 'Training deep spiking neural networks using backpropagation', *Frontiers in neuroscience*, vol. 10, p. 508.

Lee, T., Kim, M. & Kim, S.-P., 2020, 'Data augmentation effects using borderline-smote on classification of a p300-based bci', *2020 8th International Winter Conference on Brain-Computer Interface (BCI)*, IEEE, pp. 1–4.

Li, L., Zhu, J. & Sun, M.-T., 2019, 'Deep learning based method for pruning deep neural networks', *2019 IEEE International Conference on Multimedia & Expo Workshops (ICMEW)*, IEEE, pp. 312–317.

Li, M.-a., Zhang, C. & Yang, J.-F., 2010, 'An eeg-based method for detecting drowsy driving state', *2010 Seventh International Conference on Fuzzy Systems and Knowledge Discovery*, , vol. 5IEEE, pp. 2164–2167.

Lin, G., Zhang, J. & Liu, Y., 2020, 'Single shot reversible gan for bcg artifact removal in simultaneous eeg-fmri', *arXiv preprint arXiv:2011.01710*.

Lin, S.-C. & Nicolelis, M. A., 2008, 'Neuronal ensemble bursting in the basal forebrain encodes salience irrespective of valence', *Neuron*, vol. 59, no. 1, pp. 138–149.

Liu, M., Wu, W., Gu, Z., Yu, Z., Qi, F. & Li, Y., 2018, 'Deep learning based on batch normalization for p300 signal detection', *Neurocomputing*, vol. 275, pp. 288–297.

Lotte, F., 2011, 'Generating artificial eeg signals to reduce bci calibration time', *5th International Brain-Computer Interface Workshop*, pp. 176–179.

Luo, Y., Fu, Q., Xie, J., Qin, Y., Wu, G., Liu, J., Jiang, F., Cao, Y. & Ding, X., 2020, 'Eeg-based emotion classification using spiking neural networks', *IEEE Access*, vol. 8, pp. 46007–46016.

Luo, Y. & Lu, B.-L., 2018, 'Eeg data augmentation for emotion recognition using a conditional wasserstein gan', *2018 40th annual international conference of the IEEE engineering in medicine and biology society (EMBC)*, IEEE, pp. 2535–2538.

Ma, R., Yu, T., Zhong, X., Yu, Z. L., Li, Y. & Gu, Z., 2021, 'Capsule network for erp detection in brain-computer interface', *IEEE Transactions on Neural Systems and Rehabilitation Engineering*, vol. 29, pp. 718–730.

Maass, W., 1997, 'Networks of spiking neurons: the third generation of neural network models', *Neural networks*, vol. 10, no. 9, pp. 1659–1671.

Mainen, Z. F. & Sejnowski, T. J., 1995, 'Reliability of spike timing in neocortical neurons', *Science*, vol. 268, no. 5216, pp. 1503–1506.

Manor, R. & Geva, A. B., 2015, 'Convolutional neural network for multi-category rapid serial visual presentation bci', *Frontiers in computational neuroscience*, vol. 9, p. 146.

Mashford, B. S., Yepes, A. J., Kiral-Kornek, I., Tang, J. & Harrer, S., 2017, 'Neural-network-based analysis of eeg data using the neuromorphic truenorth chip for brain-machine interfaces', *IBM Journal of Research and Development*, vol. 61, no. 2/3, pp. 7–1.

Miah, A. S. M., Mouly, M. A., Debnath, C., Shin, J. & Sadakatul Bari, S., 2021, 'Event-related potential classification based on eeg data using xdwan with mdm and knn', *International Conference on Computing Science, Communication and Security*, Springer, pp. 112–126.

Mika, S., Ratsch, G., Weston, J., Scholkopf, B. & Mullers, K.-R., 1999, 'Fisher discriminant analysis with kernels', *Neural networks for signal processing IX: Proceedings of the 1999 IEEE signal processing society workshop (cat. no. 98th8468)*, Ieee, pp. 41–48.

Milekovic, T., Sarma, A. A., Bacher, D., Simeral, J. D., Saab, J., Pandarinath, C., Sorice, B. L., Blabe, C., Oakley, E. M., Tringale, K. R. et al., 2018, 'Stable long-term bci-enabled communication in als and locked-in syndrome using lfp signals', *Journal of neurophysiology*, vol. 120, no. 7, pp. 343–360.

Mishuhina, V. & Jiang, X., 2018, 'Feature weighting and regularization of common spatial patterns in eeg-based motor imagery bci', *IEEE Signal Processing Letters*, vol. 25, no. 6, pp. 783–787.

Mohdiwale, S., Sahu, M., Sinha, G. & Bhateja, V., 2020, 'Statistical wavelets with harmony search-based optimal feature selection of eeg signals for motor imagery classification', *IEEE Sensors Journal*, vol. 21, no. 13, pp. 14263–14271.

Mohsenvand, M. N., Izadi, M. R. & Maes, P., 2020, 'Contrastive representation learning for electroencephalogram classification', *Machine Learning for Health*, PMLR, pp. 238–253.

Muddapu, V. R., Mandali, A., Chakravarthy, V. S. & Ramaswamy, S., 2019, 'A computational model of loss of dopaminergic cells in parkinson's disease due to glutamate-induced excitotoxicity', *Frontiers in neural circuits*, vol. 13, p. 11.

Mudgal, S. K., Sharma, S. K., Chaturvedi, J. & Sharma, A., 2020, 'Brain computer interface advancement in neurosciences: Applications and issues', *Interdisciplinary Neurosurgery*, vol. 20, p. 100694.

Müller, S. M. T., Bastos-Filho, T. F. & Sarcinelli-Filho, M., 2011, 'Using a ssvep-bci to command a robotic wheelchair', *2011 IEEE International Symposium on Industrial Electronics*, IEEE, pp. 957–962.

Nakanishi, M., Wang, Y., Wang, Y.-T., Mitsukura, Y. & Jung, T.-P., 2014, 'A high-speed brain speller using steady-state visual evoked potentials', *International journal of neural systems*, vol. 24, no. 06, p. 1450019.

Nakra, A. & Duhan, M., 2020, 'Feature extraction and dimensionality reduction techniques with their advantages and disadvantages for eeg-based bci system: A review.', *IUP Journal of Computer Sciences*, vol. 14, no. 1.

Nawrot, M. P., Boucsein, C., Molina, V. R., Riehle, A., Aertsen, A. & Rotter, S., 2008, 'Measurement of variability dynamics in cortical spike trains', *Journal of neuroscience methods*, vol. 169, no. 2, pp. 374–390.

Neftci, E. O., Mostafa, H. & Zenke, F., 2019, 'Surrogate gradient learning in spiking neural networks: Bringing the power of gradient-based optimization to spiking neural networks', *IEEE Signal Processing Magazine*, vol. 36, no. 6, pp. 51–63.

Nicola, W. & Clopath, C., 2017, 'Supervised learning in spiking neural networks with force training', *Nature communications*, vol. 8, no. 1, p. 2208.

Nicola, W. & Clopath, C., 2019, 'A diversity of interneurons and hebbian plasticity facilitate rapid compressible learning in the hippocampus', *Nature Neuroscience*, vol. 22, no. 7, pp. 1168–1181.

Nunes, R. V., Reyes, M. B. & De Camargo, R. Y., 2019, 'Evaluation of connectivity estimates using spiking neuronal network models', *Biological cybernetics*, vol. 113, no. 3, pp. 309–320.

Oswald, A.-M. M., Chacron, M. J., Doiron, B., Bastian, J. & Maler, L., 2004, 'Parallel processing of sensory input by bursts and isolated spikes', *Journal of Neuroscience*, vol. 24, no. 18, pp. 4351–4362.

Panicker, R. C., Puthusserypady, S. & Sun, Y., 2011, 'An asynchronous p300 bci with ssvep-based control state detection', *IEEE Transactions on Biomedical Engineering*, vol. 58, no. 6, pp. 1781–1788.

Panwar, S., Rad, P., Jung, T.-P. & Huang, Y., 2020, 'Modeling eeg data distribution with a wasserstein generative adversarial network to predict rsvp events', *IEEE Transactions on Neural Systems and Rehabilitation Engineering*, vol. 28, no. 8, pp. 1720–1730.

Panwar, S., Rad, P., Quarles, J. & Huang, Y., 2019, 'Generating eeg signals of an rsvp experiment by a class conditioned wasserstein generative adversarial network', *2019 IEEE International Conference on Systems, Man and Cybernetics (SMC)*, IEEE, pp. 1304–1310.

Park, S., Kim, S., Choe, H. & Yoon, S., 2019, 'Fast and efficient information transmission with burst spikes in deep spiking neural networks', *2019 56th ACM/IEEE Design Automation Conference (DAC)*, IEEE, pp. 1–6.

Parra, L. C., Spence, C. D., Gerson, A. D. & Sajda, P., 2003, 'Response error correction-a demonstration of improved human-machine performance using real-time eeg monitoring', *IEEE transactions on neural systems and rehabilitation engineering*, vol. 11, no. 2, pp. 173–177.

Payeur, A., Guerguiev, J., Zenke, F., Richards, B. A. & Naud, R., 2021, 'Burst-dependent synaptic plasticity can coordinate learning in hierarchical circuits', *Nature neuroscience*, pp. 1–10.

Pena, R. F., Zaks, M. A. & Roque, A. C., 2018, 'Dynamics of spontaneous activity in random networks with multiple neuron subtypes and synaptic noise', *Journal of computational neuroscience*, vol. 45, no. 1, pp. 1–28.

Perez-Nieves, N., Leung, V. C., Dragotti, P. L. & Goodman, D. F., 2021, 'Neural heterogeneity promotes robust learning', *bioRxiv*, pp. 2020–12.

Reshmi, G. & Amal, A., 2013, 'Design of a bci system for piloting a wheelchair using five class mi based eeg', *2013 Third International Conference on Advances in Computing and Communications*, IEEE, pp. 25–28.

Rothschild, R. M., 2010, 'Neuroengineering tools/applications for bidirectional interfaces, brain–computer interfaces, and neuroprosthetic implants–a review of recent progress', *Frontiers in neuroengineering*, vol. 3, p. 112.

Rueckauer, B., Lungu, I.-A., Hu, Y., Pfeiffer, M. & Liu, S.-C., 2017, 'Conversion of continuous-valued deep networks to efficient event-driven networks for image classification', *Frontiers in neuroscience*, vol. 11, p. 682.

Sadiq, M. T., Yu, X., Yuan, Z., Fan, Z., Rehman, A. U., Li, G. & Xiao, G., 2019, 'Motor imagery eeg signals classification based on mode amplitude and frequency components using empirical wavelet transform', *Ieee Access*, vol. 7, pp. 127678–127692.

Saduanov, B., Tokmurzina, D., Kunanbayev, K. & Abibullaev, B., 2020, 'Design and optimization of a real-time asynchronous bci control strategy for robotic manipulator assistance', *2020 8th International Winter Conference on Brain-Computer Interface (BCI)*, IEEE, pp. 1–5.

Safa, A., Bourdoux, A., Ocket, I., Catthoor, F. & Gielen, G. G., 2021, 'A 2-μj, 12-class, 91% accuracy spiking neural network approach for radar gesture recognition', *arXiv preprint arXiv:2108.02669*.

Sahay, R. & Brinton, C. G., 2021, 'Robust subject-independent p300 waveform classification via signal pre-processing and deep learning', *IEEE Access*, vol. 9, pp. 87579–87591.

Santhanam, G., Ryu, S. I., Byron, M. Y., Afshar, A. & Shenoy, K. V., 2006, 'A high-performance brain–computer interface', *nature*, vol. 442, no. 7099, p. 195.

Sarraf, J., Pattnaik, P. et al., 2021, 'A study of classification techniques on p300 speller dataset', *Materials Today: Proceedings*.

Schwemmer, M. A., Skomrock, N. D., Sederberg, P. B., Ting, J. E., Sharma, G., Bockbrader, M. A. & Friedenberg, D. A., 2018, 'Meeting brain–computer interface user performance expectations using a deep neural network decoding framework', *Nature medicine*, vol. 24, no. 11, p. 1669.

Shaban, A., Bezugam, S. S. & Suri, M., 2021, 'An adaptive threshold neuron for recurrent spiking neural networks with nanodevice hardware implementation', *Nature Communications*, vol. 12, no. 1, pp. 1–11.

Shah, D., Wang, G. Y., Doborjeh, M., Doborjeh, Z. & Kasabov, N., 2019, 'Deep learning of eeg data in the neucube brain-inspired spiking neural network architecture for a better understanding of depression', *International Conference on Neural Information Processing*, Springer, pp. 195–206.

Shahid, S., Sinha, R. K. & Prasad, G., 2010, 'Mu and beta rhythm modulations in motor imagery related post-stroke eeg: a study under bci framework for post-stroke rehabilitation', *Bmc Neuroscience*, vol. 11, no. S1, p. P127.

Shen, X., Liu, X., Hu, X., Zhang, D. & Song, S., 2021, 'Contrastive learning of subject-invariant eeg representations for cross-subject emotion recognition', *arXiv preprint arXiv:2109.09559*.

Shukla, P. K., Chaurasiya, R. K. & Verma, S., 2021, 'Performance improvement of p300-based home appliances control classification using convolution neural network', *Biomedical Signal Processing and Control*, vol. 63, p. 102220.

Singanamalla, S. K. R. & Lin, C.-T., 2021, 'Spiking neural network for augmenting electroencephalographic data for brain computer interfaces', *Frontiers in neuroscience*, vol. 15, p. 248.

Snyder, A. C. & Smith, M. A., 2015, 'Stimulus-dependent spiking relationships with the eeg', *Journal of neurophysiology*, vol. 114, no. 3, pp. 1468–1482.

Sossa, H., Antelis, J. M., Falcón, L. E. et al., 2019, 'Motor imagery task classification in eeg signals with spiking neural network', *Mexican Conference on Pattern Recognition*, Springer, pp. 14–24.

Stam, C. J., Jones, B., Nolte, G., Breakspear, M. & Scheltens, P., 2007, 'Small-world networks and functional connectivity in alzheimer's disease', *Cerebral cortex*, vol. 17, no. 1, pp. 92–99.

Sukenik, N., Vinogradov, O., Weinreb, E., Segal, M., Levina, A. & Moses, E., 2021, 'Neuronal circuits overcome imbalance in excitation and inhibition by adjusting connection numbers', *Proceedings of the National Academy of Sciences*, vol. 118, no. 12.

Sussillo, D. & Abbott, L. F., 2009, 'Generating coherent patterns of activity from chaotic neural networks', *Neuron*, vol. 63, no. 4, pp. 544–557.

Tamura, H. & Tanaka, G., 2021a, 'partial-force: A fast and robust online training method for recurrent neural networks', *2021 International Joint Conference on Neural Networks (IJCNN)*, IEEE, pp. 1–8.

Tamura, H. & Tanaka, G., 2021b, 'Transfer-rls method and transfer-force learning for simple and fast training of reservoir computing models', *Neural Networks*, vol. 143, pp. 550–563.

Tan, C., Šarlija, M. & Kasabov, N., 2020, 'Spiking neural networks: Background, recent development and the neucube architecture', *Neural Processing Letters*, vol. 52, no. 2, pp. 1675–1701.

Tan, C., Šarlija, M. & Kasabov, N., 2021, 'Neurosense: Short-term emotion recognition and understanding based on spiking neural network modelling of spatio-temporal eeg patterns', *Neurocomputing*, vol. 434, pp. 137–148.

Tang, Y.-B., Oh, S., Tang, Y.-X., Xiao, J. & Summers, R. M., 2019, 'Ct-realistic data augmentation using generative adversarial network for robust lymph node segmentation', *Medical Imaging 2019: Computer-Aided Diagnosis*, , vol. 10950SPIE, pp. 976–981.

Tangermann, M., Müller, K.-R., Aertsen, A., Birbaumer, N., Braun, C., Brunner, C., Leeb, R., Mehring, C., Miller, K. J., Mueller-Putz, G. et al., 2012, 'Review of the bci competition iv', *Frontiers in neuroscience*, vol. 6, p. 55.

Thomas, E., Fruitet, J. & Clerc, M., 2012, 'Investigating brief motor imagery for an erd/ers based bci', *2012 Annual International Conference of the IEEE Engineering in Medicine and Biology Society*, IEEE, pp. 2929–2932.

Thomas, K. P., Guan, C., Lau, C. T., Vinod, A. P. & Ang, K. K., 2009, 'A new discriminative common spatial pattern method for motor imagery brain–computer interfaces', *IEEE Transactions on Biomedical Engineering*, vol. 56, no. 11, pp. 2730–2733.

Thomas, K. P., Vinod, A. & Guan, C., 2013, 'Enhancement of attention and cognitive skills using eeg based neurofeedback game', *2013 6th International IEEE/EMBS Conference on Neural Engineering (NER)*, IEEE, pp. 21–24.

Truong, N. D., Zhou, L. & Kavehei, O., 2019, 'Semi-supervised seizure prediction with generative adversarial networks', *2019 41st Annual International Conference*

of the IEEE Engineering in Medicine and Biology Society (EMBC), IEEE, pp. 2369–2372.

Van Veen, G. F. P., Barachant, A., Andreev, A., Cattan, G., Coelho Rodrigues, P. L. & Congedo, M., 2019, 'Building Brain Invaders: EEG data of an experimental validation', <https://doi.org/10.5281/zenodo.2649069>.

Vařeka, L. & Ladouce, S., 2021, 'Prediction of navigational decisions in the real-world: a visual p300 event-related potentials brain-computer interface', *International Journal of Human–Computer Interaction*, vol. 37, no. 14, pp. 1375–1389.

Varsehi, H. & Firoozabadi, S. M. P., 2021, 'An eeg channel selection method for motor imagery based brain–computer interface and neurofeedback using granger causality', *Neural Networks*, vol. 133, pp. 193–206.

Vasilev, I., Slater, D., Spacagna, G., Roelants, P. & Zocca, V., 2019, *Python Deep Learning: Exploring deep learning techniques and neural network architectures with Pytorch, Keras, and TensorFlow*, Packt Publishing Ltd.

Ventouras, E. M., Asvestas, P., Karanasiou, I. & Matsopoulos, G. K., 2011, 'Classification of error-related negativity (ern) and positivity (pe) potentials using knn and support vector machines', *Computers in biology and medicine*, vol. 41, no. 2, pp. 98–109.

Vishwakarma, R., Khwaja, H., Samant, V., Gaude, P., Gambhir, M. & Aswale, S., 2020, 'Eeg signals analysis and classification for bci systems: A review', *2020 International Conference on Emerging Trends in Information Technology and Engineering (ic-ETITE)*, IEEE, pp. 1–6.

Wang, L., Gu, Y., Zhao, G. & Chen, A., 2020, 'Error-related negativity and error awareness in a go/no-go task', *Scientific Reports*, vol. 10, no. 1, pp. 1–12.

Wang, Y., Chen, X., Gao, X. & Gao, S., 2016, 'A benchmark dataset for ssvep-based brain–computer interfaces', *IEEE Transactions on Neural Systems and Rehabilitation Engineering*, vol. 25, no. 10, pp. 1746–1752.

Wang, Y., Gao, S. & Gao, X., 2006, 'Common spatial pattern method for channel selelction in motor imagery based brain-computer interface', *2005 IEEE Engineering in Medicine and Biology 27th Annual Conference*, IEEE, pp. 5392–5395.

Wierzgała, P., Zapała, D., Wojcik, G. M. & Masiak, J., 2018, 'Most popular signal processing methods in motor-imagery bci: a review and meta-analysis', *Frontiers in neuroinformatics*, vol. 12, p. 78.

Willett, F. R., Avansino, D. T., Hochberg, L. R., Henderson, J. M. & Shenoy, K. V., 2021, 'High-performance brain-to-text communication via handwriting', *Nature*, vol. 593, no. 7858, pp. 249–254.

Wolpaw, J. R., Birbaumer, N., Heetderks, W. J., McFarland, D. J., Peckham, P. H., Schalk, G., Donchin, E., Quatrano, L. A., Robinson, C. J., Vaughan, T. M. et al., 2000, 'Brain-computer interface technology: a review of the first international meeting', *IEEE transactions on rehabilitation engineering*, vol. 8, no. 2, pp. 164–173.

Woźniak, S., Pantazi, A., Bohnstingl, T. & Eleftheriou, E., 2020, 'Deep learning incorporating biologically inspired neural dynamics and in-memory computing', *Nature Machine Intelligence*, vol. 2, no. 6, pp. 325–336.

Wu, J., Yılmaz, E., Zhang, M., Li, H. & Tan, K. C., 2020, 'Deep spiking neural networks for large vocabulary automatic speech recognition', *Frontiers in neuroscience*, vol. 14, p. 199.

Xia, J., Marks, T. D., Goard, M. J. & Wessel, R., 2021, 'Stable representation of a naturalistic movie emerges from episodic activity with gain variability', *Nature communications*, vol. 12, no. 1, pp. 1–15.

Xu, W., Wang, J. & Yan, X., 2021, 'Advances in memristor-based neural networks', *Frontiers in Nanotechnology*, vol. 3.

Xygonakis, I., Athanasiou, A., Pandria, N., Kugiumtzis, D. & Bamidis, P. D., 2018, 'Decoding motor imagery through common spatial pattern filters at the eeg source space', *Computational intelligence and neuroscience*, vol. 2018.

Yeom, S.-K., Fazli, S., Müller, K.-R. & Lee, S.-W., 2014, 'An efficient erp-based brain-computer interface using random set presentation and face familiarity', *PloS one*, vol. 9, no. 11, p. e111157.

Zeldenrust, F., Wadman, W. J. & Englitz, B., 2018, 'Neural coding with bursts—current state and future perspectives', *Frontiers in computational neuroscience*, vol. 12, p. 48.

Zenke, F. & Ganguli, S., 2018, 'Superspike: supervised learning in multilayer spiking neural networks', *Neural computation*, vol. 30, no. 6, pp. 1514–1541.

Zhai, J., Zhang, S., Chen, J. & He, Q., 2018, 'Autoencoder and its various variants', *2018 IEEE International Conference on Systems, Man, and Cybernetics (SMC)*, IEEE, pp. 415–419.

Zhang, A., Su, L., Zhang, Y., Fu, Y., Wu, L. & Liang, S., 2022, 'Eeg data augmentation for emotion recognition with a multiple generator conditional wasserstein gan', *Complex & Intelligent Systems*, vol. 8, no. 4, pp. 3059–3071.

Zhang, J., Yan, C. & Gong, X., 2017, 'Deep convolutional neural network for decoding motor imagery based brain computer interface', *2017 IEEE International Conference on Signal Processing, Communications and Computing (ICSPCC)*, IEEE, pp. 1–5.

Zhang, Y., Chen, W., Lin, C.-L., Chu, J. & Meng, F., 2018, 'Research on command confirmation unit based on motor imagery eeg signal decoding feedback in brain-computer interface', *2018 15th International Conference on Control, Automation, Robotics and Vision (ICARCV)*, IEEE, pp. 1923–1928.

Zhang, Y., Zhou, G., Jin, J., Wang, M., Wang, X. & Cichocki, A., 2013a, 'L1-regularized multiway canonical correlation analysis for ssvep-based bci', *IEEE transactions on neural systems and rehabilitation engineering*, vol. 21, no. 6, pp. 887–896.

Zhang, Y., Zhou, G., Zhao, Q., Jin, J., Wang, X. & Cichocki, A., 2013b, 'Spatial-temporal discriminant analysis for erp-based brain-computer interface', *IEEE*

Transactions on Neural Systems and Rehabilitation Engineering, vol. 21, no. 2, pp. 233–243.

Zhang, Z., Duan, F., Sole-Casals, J., Dinares-Ferran, J., Cichocki, A., Yang, Z. & Sun, Z., 2019, 'A novel deep learning approach with data augmentation to classify motor imagery signals', *IEEE Access*, vol. 7, pp. 15945–15954.